Variability and potential predictability of Elbe river streamflow and their relationship to global teleconnection patterns

Dissertation
vorgelegt von
Monica Ionita **aus Bukarest, Rumänien**

zur Erlangung des Doktorgrades
Dr. rer. nat.

Fachbereich Physik und Elektrotechnik,
Universität Bremen

1. Gutachter:	Prof. Dr. Gerrit Lohmann
2. Gutachter:	Prof. Dr. Reiner Schlitzer
Eingereicht am:	14.04.2009

Contents

Zusammenfassung iv

Abstract vi

Chapter 1. Introduction and research questions **1**

1.1 Introduction ……. 1

1.2 Study area – Elbe river basin …….. 2

1.3 Research questions …….. 4

1.4 Thesis outline …….. 5

Chapter 2. The climate system and its teleconnection patterns **7**

2.1 The climate system components ……. 7

2.2 Global teleconnection patterns ……... 8

2.2.1 North Atlantic Oscillation ……. 9

2.2.2 Arctic Oscillation ……... 11

2.2.3 The East Atlantic Pattern ……... 12

2.2.4 The East Atlantic / Western Russia Pattern ……. 13

2.2.5 The Scandinavian Pattern ……. 14

2.2.6 The Polar / Eurasia Pattern …….. 15

2.2.7 El Niño – Southern Oscillation …….. 16

2.2.8 Pacific Decadal Oscillation …… 17

Chapter 3. Extreme events in Elbe's river catchment area and their associated circulation patterns **20**

3.1 Introduction ……. 20

3.2 Data and methods …… 21

3.2.1 Data description …….. 21

3.2.2 Methodology ……... 22

3.2.2.a Peak over Threshold …….. 22

3.2.2.b Return levels …….. 23
3.2.2.c K-means cluster analysis ……... 24
3.3 Application of the General Pareto Distribution to seasonal Elbe river discharge ……. 25
3.4 Circulation patterns associated with extreme river discharge events .. 28
3.4.1 Winter circulation pattern …… 28
3.4.2 Spring circulation patterns ……... 30
3.4.3 Summer circulation patterns …… 31
3.4.4 Autumn circulation patterns …… 33
3.5 Discussions ……. 35
3.6 Conclusions ……. 36

Chapter 4. Prediciton of spring Elbe discharge based on stable teleconnections with winter global temperature 37
4.1 Introduction ……. 37
4.2 Data and methodology …… 38
4.2.1 Data sets description …… 38
4.2.2 Stability criteria and stability maps ……. 40
4.2.3 Model evaluation ……. 41
4.3 Stable teleconnections of the Elbe streamflow ……... 42
4.3.1 Sea surface temperature ……..…… 42
4.3.2 Surface temperature over land ……. 45
4.3.3 Precipitation ……. 48
4.3.4 Combination of indices …… 48
4.4 Potential predictability …… 51
4.5 Discussions and conclusions ……... 53

Chapter 5. Decadal variability of the Elbe river flow 55
5.1 Introduction ……..…… 55
5.2 Data sets description ……... 56
5.3 Methodology ……... 56
5.3.1 Singular Spectrum Analysis …… 56
5.4 Relation with precipitation and temperature over land ……... 59

5.5 Relation with sea surface temperature and sea level pressure …… 61
5.5.1 Relationship with global Sea Surface Temperature ……. 61
5.5.2 Connection with global Sea Level Pressure …… 63
5.6 Singular Spectrum Analysis ……... 65
5.7 Bandpass – filter analysis ……... 67
5.8 Discussion and conclusions …… 69

Chapter 6. The influence of large scale atmospheric circulation on the variability of salinity at Helgoland Roads station 71
6.1 Introduction ……. 71
6.2 Data ……. 72
6.3 The dominant pattern of variability in the salinity, Elbe river discharge and precipitation time series ……... 73
6.4 The relationship between salinity and large-scale atmospheric circulation ……... 76
6.5 Summary and conclusions …….. 80

Chapter 7. Conclusions and outlook 81
7.1 General summary……... 81
7.2 Conclusions and outlook ……... 84

Appendix A – Empirical Orthogonal Function Analysis 86
Appendix B – Software 90
References 91
Acknowledgements

Zusammenfassung

Die Bestimmung von Variabilität und Vorhersagbarkeit der Abflussmengen von Oberflächengewässern ist für viele Gesellschaften von entscheidender Bedeutung, denn sie kämpfen mit verschiedenen hydrologischen Risiken in Verbindung mit Überschwemmungen, Dürren und der Süßwasserversorgung. Diese Untersuchung ist eine der ersten, die die Variabilität und die potentielle Vorhersagbarkeit des Strömungsflusses der Elbe sowie deren Verbindung mit globalen Telekonnektionsmustern von einer synoptischen Skala bis hin zu einer dekadischen Zeitskala auswertet.

Im ersten Teil der Dissertation werden Extremereignisse im Einzugsgebiet der Elbe und damit verbundene Hauptzirkulationsmuster auf saisonalen Zeitskalen analysiert. Um festzustellen, welcher Schwellenwert ein Extremereignis definiert und um die Daten in eine Verteilung der Extremwerte einzupassen, haben wir die „Peak over Threshold"-Methode in Verbindung mit der verallgemeinerten Pareto-Verteilung (GPD) benutzt. Der Verlauf des täglichen Strömungsflusses der Elbe wird durch die GPD statistisch gut modelliert. Die Ergebnisse zeigen, dass die Zeitserien für Winter, Frühjahr und Herbst normales *tail*-Verhalten haben, während die Verteilung für den Sommer ein *heavy-tail*-Verhalten aufweist, da im Sommer mehr Extremereignisse auftreten als in den anderen Jahreszeiten. „Composite-Maps" der Meeresspiegeldruck-Anomalie für die Tage, an denen der Grenzwert überschritten wird, unterscheiden sich stark von einer Jahreszeit zur anderen und sind in einer Clusteranalyse zusammengefasst.
Es konnten vier deutliche Zirkulationsmuster für jede spezifische Jahreszeit identifiziert werden. Im Winter konnten die meisten extremen Abflussereignisse mit einem Dipolmuster in Verbindung gebracht werden. Dieses Muster weist ein starkes negatives Zentrum über Mitteleuropa auf, welches sich bis in den Südatlantik erstreckt, sowie ein starkes positives Zentrum über dem nördlichen Teil des Atlantiks. Ein solches Muster begünstigt eine nordöstliche Zirkulation.
Im Sommer werden Extremereignisse durch ein einer Blockade ähnlichem Muster über dem Atlantik sowie durch eine zyklonale Zirkulation über dem südlichen Teil Europas, die feuchte Luft von der Ostsee über den nördlichen Teil Deutschlands transportiert, ausgelöst. Diese Ergebnisse deuten darauf hin, dass größere Überflutungen im Einzugsgebiet der Elbe durch das Auftreten saisonal spezifischer Zirkulationsmuster ausgelöst werden.

Auch auf saisonalen Zeitskalen wird die Vorhersagbarkeit der Strömungsfluss-Anomalien der Elbe während des Frühjahrs anhand der Meeresoberflächentemperatur (SST) im vorangegangenen Winter, anhand der Temperatur über Land (TT) und anhand von Niederschlagsanomalien (PP) analysiert. Gestützt durch Korrelationsanalysen identifizierten wir verschiedene Regionen, bei denen die Strömungsfluss-Anomalien mit SST-, TT- und PP-Anomalien aus dem vorangegangenen Winter, stabil korreliert sind. Wir zeigen außerdem, dass der Strömungsfluss der Elbe während des Zeitraums 1902-1971 stabil korreliert ist mit: PP-Anomalien aus dem Einzugsgebiet der Elbe aus dem vorherigen Winter, TT-Anomalien aus der Region Schwarzes Meer-Kaspisches Meer, Nordwest-Europa

und Nord-Kanada sowie SST-Anomalien aus dem tropischen Pazifik, dem Indischen Ozean und mehreren Regionen des Nordpazifiks und Nordatlantiks.
Ein Index, basierend auf Winter-SST-, TT- und PP-Anomalien dieser Regionen ist erheblich korreliert mit Frühjahrs-Strömungsfluss-Anomalien während dieser Periode. Basierend auf SST-, TT- und PP-Anomalien aus stabil korrelierten Gebieten, wird ein Vorhersageschema entwickelt und angewandt, um Frühjahrs-Strömungsflussanomalien während der letzten Jahrzehnte vorherzusagen. Die auf unserem statistischen Schema beruhende Vorhersage stellt gegenüber der traditionell zur Vorhersage von Strömungsflüssen benutzten, auf Telekonnektionsindizes basierenden Prognose eine deutliche Verbesserung dar.

Ein weiteres Ziel dieser Dissertation ist die Erforschung der dekadischen Variabilität (>7 Jahre) der jährlichen Strömung der Elbe in Verbindung mit atmosphärischer Zirkulation auf großen Skalen.
Dabei wird die Beziehung von Niederschlag und Temperatur im europäischen Raum sowie globaler Meeresoberflächentemperatur und atmosphärischer Zirkulation über dem Nordatlantik untersucht.
Starke Anomalien des Strömungsflusses der Elbe sind mit einem Tripol ähnlichen Muster im Nordatlantik, negativen SST-Anomalien im mittleren Nordpazifik sowie positiven Anomalien im östlichen und mittleren tropischen Pazifik verbunden. Das auf Meeresniveau (SLP) identifizierte Muster ähnelt dem Muster der Arktischen Oszillation.
Durch Verwenden einer „Singulären-Spektralanalyse“ konnten zwei deutliche dekadische Zeitkomponenten von ~12-13 Jahren und ~20 Jahren identifiziert werden. Diese Ergebnisse haben große Auswirkungen auf die Vorhersage der Entwicklung der Abflussmengen der Elbe auf dekadischen Zeitskalen.

Außerdem wird der Einfluss der atmosphärischen Zirkulation und der Abflussmengen der Elbe auf die Schwankungen der Salinität an der Helgoländer Station (54.12°N, 7.9ºE, Deutschland) im April analysiert. Es wird gezeigt, dass die Abflussanomalien des vorangegangenen Monats der Hauptantrieb für die Salinitätsanomalien sind. Diese Abflussanomalien sind stark mit Niederschlagsanomalien aus dem Einzugsgebiet der Elbe verbunden. Veränderungen hinsichtlich Salinität, Abfluss und Niederschlagsanomalien werden von einem atmosphärischen Wellenzug-Zirkulationsmuster begleitet, das den tropischen Atlantik mit dem nördlichen Teil Europas verbindet sowie von großskaligen Änderungen des Wasserdampftransports über der gesamten Deutschen Bucht. Positive Anomalien der Meeresoberflächentemperatur mit Zentrum in der Karibischen Region und der Nordsee sind mit positiven Salinitätsanomalien und negativen Anomalien von Abfluss und Niederschlag verbunden.

Abstract

Determining the variability and predictability of river discharge is of crucial importance to many societies as they struggle with different hydrological risks related to flooding, drought and fresh water supply. This study is among the first to assess the variability and potential predictability of Elbe river streamflow and their relationship with global teleconnection patterns, from a synoptical scale and extending to decadal time scales.

In the first part of the thesis, extreme events in the Elbe river catchment area and their associated main circulation patterns are analyzed on seasonal timescale. To identify the threshold, which defines an extreme event, and to fit the data to an extreme value distribution we have made use of the Peak over Threshold method associated with generalised Pareto distribution (GPD). The behaviour of Elbe daily streamflow is well statistically modelled by the GPD. The results indicate that for winter, spring and fall the times series have normal tail behaviour, meanwhile for summer the distribution has heavy-tail behaviour, summer being more exposed to the occurrence of extreme events compared to the other seasons. The composite maps of sea level pressure anomalies, corresponding to the days when the discharge was above the threshold differs from one season to another and are grouped in a cluster analysis. Four distinct circulation patterns are identified for each specific season. In winter most of the extreme discharge events are associated with a dipole-like pattern with a strong negative centre over central Europe and extending over the southern part of the Atlantic Ocean and a strong positive centre over the northern part of the Atlantic Ocean. Such pattern favours a north-easterly circulation. In summer, extreme events are triggered by a blocking-like pattern over the Atlantic Ocean and a cyclonic circulation over the southern part of Europe, which carries humid air form the Baltic Sea over the northern part of Germany. These findings imply that major floods in Elbe's catchment area are triggered by the occurrence of seasonal specific circulation patterns.

On seasonal time scales, the predictability of Elbe streamflow anomalies during spring using previous winter sea surface temperature (SST), temperature over land (TT) and precipitation (PP) anomalies is also analyzed. Based on running correlation analysis, we identify several regions where the spring streamflow anomalies are stable correlated with SST, TT and PP anomalies from previous winter. We show that during the period 1902-1971 the Elbe spring streamflow is stable correlated with previous winter PP anomalies from its catchment area, with TT anomalies from the Black Sea-Caspian Sea region, north-western Europe and northern Canada, as well as with SST anomalies from the tropical Pacific, the Indian Ocean and several regions of the North Pacific and the North Atlantic. An index based on winter SST, TT and PP anomalies from these regions is highly significantly correlated with spring streamflow anomalies during this period. Based on SST, TT and PP anomalies from stable correlated regions, a forecast scheme is developed and applied to predict spring streamflow anomalies during the last decades. The prediction based on our statistical scheme represents a marked improvement relative to the forecast based on teleconnection indices which are traditionally used for streamflow prediction.

Another goal of this thesis is to investigate the decadal variability (>7 years) of annual Elbe river flow in connection with large scale atmospheric circulation. The relationship with precipitation (PP) and temperature (TT) in the European sector and global sea surface temperature (SST) and atmospheric circulation over the Northern Hemisphere is investigated. High anomalies of the river flow are associated with a tripole-like pattern in the North Atlantic and with negative SST anomalies in the central North Pacific and positive anomalies in the eastern and central tropical Pacific. The pattern identified in the sea level field (SLP) resembles the Arctic Oscillation pattern. Two distinct decadal time components of ~12-13yr and ~20 yr in the time series were identified by using the Singular Spectral Analysis. These results have implications for predicting the evolution of Elbe river discharge on decadal time scales.

The influence of atmospheric circulation and Elbe river discharge on the variability of April salinity at Helgoland Roads station (54.12°N, 7.9ºE, Germany), is also analyzed. It is shown that the main driver of salinity anomalies is the river discharge anomalies from the previous month. These discharge anomalies are strongly related with precipitation anomalies from the Elbe catchment area. Changes in the salinity, discharge and precipitation anomalies are accompanied by a wave-train atmospheric circulation pattern that connects the tropical Atlantic Ocean and northern part of Europe, as well as with changes in large-scale water vapour transport over the whole German Bight. Positive sea surface temperature anomalies centred in the Caribbean region and the North Sea are associated with positive salinity anomalies and negative anomalies of discharge and precipitation.

Chapter 1

Introduction and research questions

1.1 Introduction

Hydrological variables such as precipitation, river flow, soil moisture or groundwater levels display high spatial and temporal variability. From time to time they take on extremely high values, exerting considerable impacts on ecosystems and human society. Intensified extreme hydrological events have been associated with observed changes in climatic variability. Societies with large populations exist within river watersheds obtaining water for social purposes, agriculture and industrial production. Streamflow forecasting is of great importance to water resources management and flood defense. On the other hand, to be able to improve the skill of the streamflow forecast, one needs to get a better understanding of the streamflow processes. The methods used in streamflow forecasting may fall into two general classes (Wang, 2006):

i) ***Process-driven models***, which treat a streamflow process as the output of a watershed system. These models can also be divided in two groups: a) *rainfall-runoff models*, are the ones that are based on physical facts (Pitman, 1973; Hughes, 2004) and b) *low flow models* – are the ones constituted to predict the flow that may occur in streams in dry seasons (Tallaksen, 1995).

ii) ***Data-driven methods***, which identify the relationship between the inputs and outputs on a mathematical ground, without taking into account the physical mechanism (e.g. regression models, artificial neural networks). These models are more useful in that they can be quite simple and applicable.

Although predictability is an important aspect of the dynamics of hydrological process, this practice has not attracted much the attention of the hydrological community, until recent years (Trigo et al., 2004; Rimbu et al., 2004, 2005). Since the research on predictability is not well understood, there is a lack of well-established methods on how to estimate the predictability of hydrological processes.
Based on the existing literature, two approaches may be distinguished: i) univariate approach, which allows measuring the predictability based on univariate times series analysis techniques (Wang et al., 2004) and ii) multivariate approach, which allows estimating the predictability based on the knowledge of the rainfall-runoff mechanism and/or the teleconnections between the climatic elements and streamflow (Maurer et al., 2003, 2004; Rimbu et al., 2004, 2005).
The availability of water is greatly influenced by climate conditions that vary on seasonal, interannual, and decadal time scales. Characterisation of hydrological variability on climatic timescales and identification of connections to climate forcings provide potential improvement for hydrological forecasts when these forcings are predictable or slowly evolving (Souza and Lall, 2003; Croley, 2003). Evidence from long hydrological records shows that periods with anomalous

hydrological behaviour (Arnell et al., 1993) are associated with persistent climate anomalies.
On seasonal timescales, anomalous atmospheric conditions are often linked with seasonal variations in the rivers streamflow, via variations in precipitation and temperature (Dettinger and Diaz, 2000; Cullen et al., 2002). For example, spring and summer rainfall and temperature anomalies across Europe may be forecasted from prior knowledge of varying boundary conditions such as anomalous sea surface temperature in the North Atlantic (Colman, 1997; Colman and Davey, 1999; Wilby, 2001) and/or the tropical Pacific (Kiladis and Diaz, 1989; Lloyd-Hughes and Saunders, 2002; van Oldenborgh et al., 2000). Spring precipitation over central Europe is higher than the normal average following warm El Niño events combined with lower SSTs west of Ireland (Lloyd-Hughes and Saunders, 2002). Predictability is found to be higher in El Niño-Southern Oscillation (ENSO) extreme years (Branković and Palmer, 2000), implying that at least part of the available skill can be attributed to the forcing from the tropical Pacific Ocean.
Two of the most important phenomena that influence streamflow variability are the North Atlantic Oscillation (NAO) and ENSO (Dettinger and Diaz, 2000; Cullen et al., 2002). The indices of these large-scale climatic patterns are used as predictors for seasonal streamflow anomalies over Europe (Rimbu et al., 2005, Cullen et al., 2002, Trigo et al., 2004). Significant lag-correlations were identified between NAO index and several river streamflow anomalies from the Iberian Peninsula (Trigo et al., 2004) and Tigris-Euphrates streamflow anomalies (Cullen et al., 2002). Rimbu et al. (2004) found significant lag-correlation between NAO and ENSO indices and Danube streamflow. However, the association between NAO and ENSO and streamflow from the Iberian Peninsula (Trigo et al., 2004) and from south-east Europe (Rimbu et al., 2004; Cullen et al., 2002) is non-stationary, i.e. the strength of the correlation between these two phenomena and streamflow anomalies has changed over time. These teleconnection patterns, though dominant on a large scale, often fail to provide forecast skill in individual basins (McCabe and Dettinger, 2002; Grantz et al., 2005). The predictability of precipitation and streamflow from Europe using NAO and ENSO as predictors is limited due to non-stationarity. One way to improve the seasonal forecast for streamflow would be to identify stable predictors.

1.2 Study area - Elbe river basin

The Elbe river rises in the Giant Mountains in Czech Republic at an elevation of 1383m. The Elbe River basin, comprising the Elbe and its tributaries, has a catchment area of 148,268 square kilometres (57,247 sq mi), the fourth largest in Europe (Figure 1.1). The basin spans four countries, with its largest parts in Germany (65.5%) and the Czech Republic (33.7%). Much smaller parts lie in Austria (0.6%) and Poland (0.2%).

Its length is 1094 km, of which 367 km are located in the Czech Republic and 727 km in Germany. The mouth is in the North Sea and the principal tributaries are: Vltava (Moldau), Havel, Saale, Mulde, Eger and Schwarze Elster. The basin covers different geographical regions from middle mountain ranges in the west and south to large lowlands in the central, northern and eastern part of the catchment.

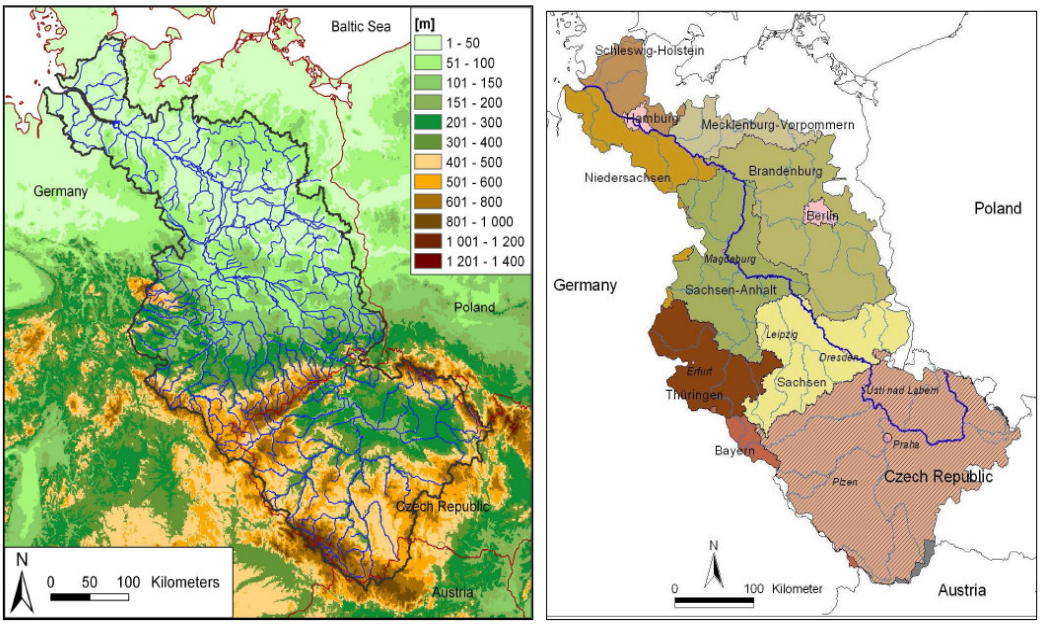

Figure 1.1 Topographical map of Elbe drainage basin and the administrative borders and cities
(Source: NeWater project – Report Nr. 17)

The whole basin is formally partitioned into three main sectors, due to the geomorphologic character: the Upper Elbe (463 km), the Middle Elbe (489 km) and the Lower Elbe (142 km).
From a climatic point of view, the Elbe river basin is located in a transition zone between the maritime and the continental climate. The temperature shows strong intra-annual variability (Figure 1.2) and this influences the evaporation.

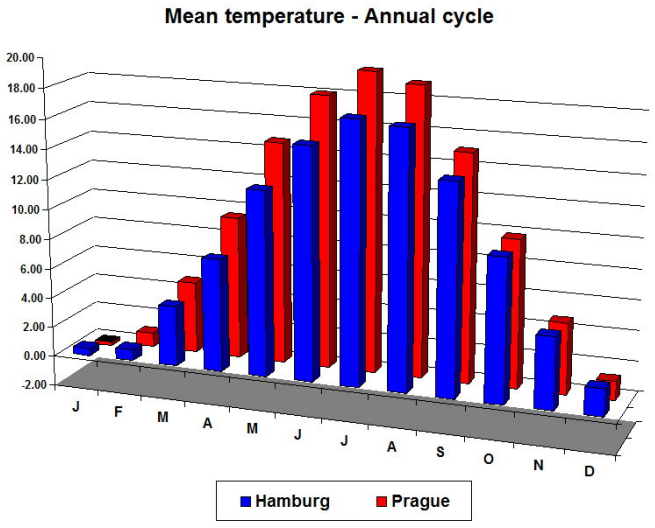

Figure 1.2 Mean temperature annual cycle for Hamburg and Prague (1891 – 2002)

The Elbe river basin is the driest basin in Germany (compared to Rhine, Weser or Danube) due to the low precipitation levels of about 659 mm/year on average. Precipitation is ranging from below 450 mm/year in the central part to 1600 mm/year in the mountain area (Figure 1.3).
The mean annual discharge at the border between the Czech Republic and Germany is approximately 311 m^3/s. At Cuxhaven (Germany), the Elbe discharges into the North Sea. The mean annual discharge at the mouth is around 861 m^3/s.

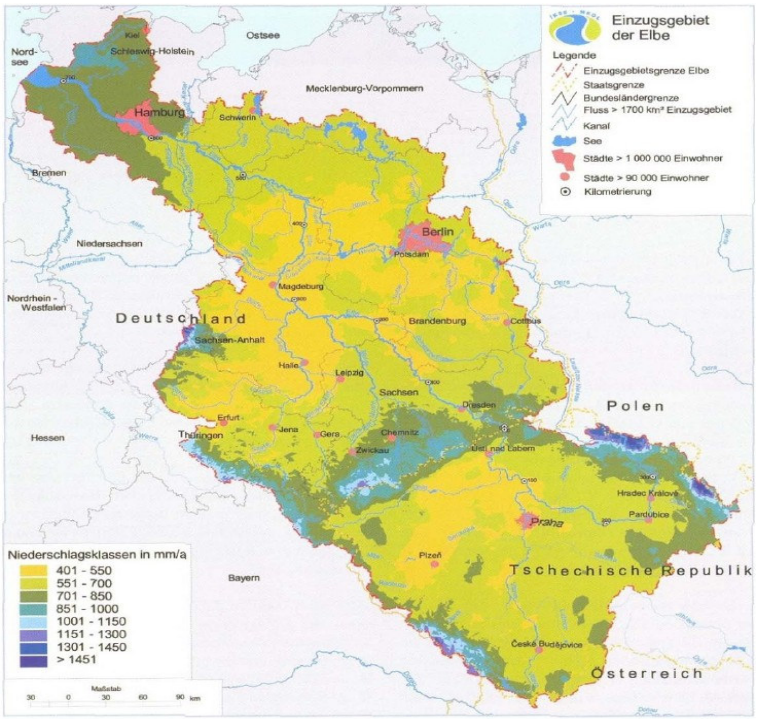

Figure 1.3 Annual mean precipitation in Elbe catchement area
(Source: BfG - Bundesanstalt für Gewässerkunde, ČHMÚ - Tschechisches Hydrometeorologisches Institut, IKSE - Internationale Kommission zum Schutz der Elbe)

1.3 Research questions

Giving the importance of river discharge for the inhabitants of the river basin, it is important to find answers to the following questions:

(i) How important are the seasonal fluctuations in flood frequency analysis?
(ii) Are there special synoptic weather patterns responsible for the occurrence of extreme events in the Elbe river catchement area?
(iii) Can we resolve the problem of non-stationarity by identifying **stable** predictors from several key regions, which can be used for the prediction of Elbe river streamflow?
(iv) Is there any statistically significant relationship between different climatic variables (e.g. sea surface temperature, precipitation) and the seasonal to decadal variability of discharge anomalies?
(v) By applying a simple statistical model is it possible to capture the physical mechanism between the identified predictors and the predictand?

(vi) To which extent is Elbe river streamflow influencing the variability of salinity in the German Bight area?

This thesis is focusing on these questions and determines the variability of Elbe's river discharge on time scales from weeks to decades.

1.4 Thesis outline

The thesis is organized in 4 main chapters (besides the general introduction, the description of the climate system and summary), each addressing a subset of the questions mentioned above. Two chapters are already published, one is under review and the other one is submitted. Due to this fact, each chapter forms a largely independent study with a corresponding introduction as well as a methodology description section. This kind of structure implies a partial overlap of some of the contents between the chapters.

Extreme events in Elbe's river catchment area and their associated circulation patterns, Chapter 3[1]

Between 1998 and 2002, Europe suffered over 100 major damaging floods, including the catastrophic floods along the Danube and Elbe rivers in 2002 (Ulbrich et al., 2003 a, b; Bronstert et al., 1998). Since 1998, floods have caused around 700 fatalities, the displacement of about half a million people and at least € 25 billion in insured economic losses (European Environment Agency, 2003).
In this context, the aim of this chapter is to study the occurrence of extreme discharge events in Elbe's catchment area in relation with different circulation patterns and to statistically model the behaviour of these extremes, by employing the Extreme Value Analysis Theory.

Prediction of spring Elbe discharge based on stable teleconnections with winter global temperature and precipitation, Chapter 4[2]

One of the most difficult issues of hydrology is how to appreciate the seasonal variability of rivers discharge. It has been established that changes in the cycling of water between land, sea and air can have significant impacts on the environment, economy and society through their effects on the water resources and their management (Arnell, 1995, 1999; Arnell and Reynard, 1996). The availability of water is greatly influenced by climate conditions that vary on seasonal, interannual, and decadal time scales.
This chapter describes a forecasting scheme for spring Elbe streamflow based on **stable** lag-correlation with global temperature and precipitation indices. It is shown

[1] This chapter is based on the manuscript: Ionita, M., G. Lohmann, M. Dima and S. Chelcea (2009), Extreme events in Elbe's river catchment area and their associated circulation patterns, submitted to *Tellus A*

[2] This chapter is based on the manuscript: Ionita, M., G. Lohmann and N. Rimbu (2008), Prediction of Elbe discharge based on stable teleconnections with winter global temperature and precipitation, *J. Climate*, **21**, 6215–6226, doi:10.1175/2008JCLI2248.1

that when climate indices from key regions are used together as predictors, the forecast improves compared to the case when they are used separately or when we use predefined teleconnection indices (e.g. NAO, ENSO).

Decadal variability of the Elbe river stramflow, Chapter 5[3]

Water is a vital resource for human beings as well as for the natural ecosystems. The possibility of predicting river flows months and even years in advance is of great interest to regional economies that depend heavily on hydroelectricity and irrigation. This motivated the development of methods for streamflow prediction that use climatic information, such as the El Niño-Southern Oscillation (ENSO) (e.g. Dettinger et al., 2000) and NAO (Rimbu et al., 2005).
The goal of this chapter is to investigate the connection between Elbe river flow and large scale atmospheric circulation and SST at global scale, at decadal time scales. It is important to study the connection between the climate variability and hydrological regime, in order to understand the physical mechanisms that drive hydrological variability. Long-term variability may be of significant importance for the managers of water resources systems for whom the ability to forecast reservoirs inflows is highly desirable.

The influence of large-scale atmospheric circulation on the variability of salinity at Helgoland Roads stations, Chapter 6[4]

The eastern German Bight is a zone of intensive mixing of two water bodies, the North Sea water and the coastal water which is of lower salinity and density. In addition, the water of the river Elbe leads to a strong inhomogeneity in this area which can be seen in the distribution of salinity and nutrients Goedecke (1968). The interannual variability in observed ecological time series is sometimes suspected to be driven by interannual variability in climatic parameters (Fromentin and Planque, 1996).
The goal of this chapter is to investigate the possible relationships between the large-scale atmospheric circulation, Elbe river streamflow and salinity at Helgolan Roads stations. Understanding the causes of salinity variability will: (i) help to reconstruct historical salinities in connection with the atmosphere-ocean dynamics and (ii) allow the study of the variability of other ecological time series (i.e. nutrients) in connection with the large-scale circulation, due to the fact that salinity anomalies are supposed to coincide with observed changes in the ecosystem (Nehring, 1994; Lindeboom et al., 1995).

[3] This chapter is based on the manuscript: Ionita, M., N. Rimbu and G. Lohmann (2008), Decadal variability of Elbe river streamflow, under review in *International Journal of Climatology*.

[4] This chapter is based on the manuscript: Ionita, M., G. Lohmann, N. Rimbu and K. Wiltshire (2008), The influence of large-scale atmospheric circulation on the variability of salinity at Helgoland Roads station, *Tellus*, **60A**, 1103-1108, doi: 10.1111/j.1600-0870.2008.00352.x

Chapter 2

The climate system and its teleconnection patterns

2.1 The climate system

Weather is defined as the set of all the phenomena occurring in a given atmosphere at a given time. Weather phenomena lie in the hydrosphere and troposphere. Weather refers to current activity, as opposed to the term climate, which refers to the average atmospheric conditions over longer periods of time. When used without qualification, "weather" is understood to be the weather of Earth.

Climate in a narrow sense is usually defined as the “average weather”, or more rigorously, as the statistical description in terms of the mean and variability of relevant quantities over a period of time ranging from months to thousands or millions of years (IPCC, 2007). The classical period is 30 years, as defined by the World Meteorological Organization (WMO). These quantities are most often surface variables such as temperature, precipitation, and wind. Climate in a wider sense is the state, including a statistical description, of the climate system.

The time span variability of climate varies from season to season, year to year, decade to decade or on much longer time scales, like the Ice Ages. Climate is determined by the atmospheric circulation and by its interactions with large-scale ocean currents and the land with his features such as albedo, vegetation and soil moisture.

The climate system (Figure 2.1) is an interactive system, consisting of five major components: the atmosphere, the hydrosphere, the cryosphere, the land surface and the biosphere. These components interact on many different scales in both space and time, causing the climate to have a large natural variability; and human influences such as greenhouse-gas emissions add further complexity.

The atmosphere - is a largely homogenous mixture of gases which covers the Earth and helps it from becoming too hot or too cold. Its circulation, the heat (terrestrial radiation) and light (solar radiation) which pass through it, and the processes which go on in it, all affect the climate. The temperature of the atmosphere varies strongly both in the vertical and with latitude. The latter is due to an imbalance in the radiation received over the Earth’s surface throughout the year due to the planet’s orbit and obliquity. The circulation of both the atmosphere and ocean are ultimately derived from this energy imbalance; they act to counter it, in the ratio of about 3:2 respectively.

The hydrosphere - is the component which comprises all liquid surfaces and subterranean water, both fresh water, including rivers, lakes and aquifers, and saline water of the oceans and seas. The oceans cover 361 million square kilometres, or 70% of the surface area of the globe, almost two and a half times the land area. There is a constant exchange of heat, momentum and water between the ocean and the atmosphere. The ocean can absorb and dissipate heat, influencing our climate. Ocean currents transport large amounts of heat and water around the world.

The land surface, including its vegetation and seasonal snow cover, has an important influence on the flow of air over it, the absorption of solar energy, and the water cycle. Vegetation and soils at the *land surface* control how energy received

from the Sun is returned to the atmosphere. Some is returned as long-wave (infrared) radiation, heating the atmosphere as the land surface warms. Some serves to evaporate water, either in the soil or in the leaves of plants, bringing water back into the atmosphere. Because the evaporation of soil moisture requires energy, soil moisture has a strong influence on the surface temperature.

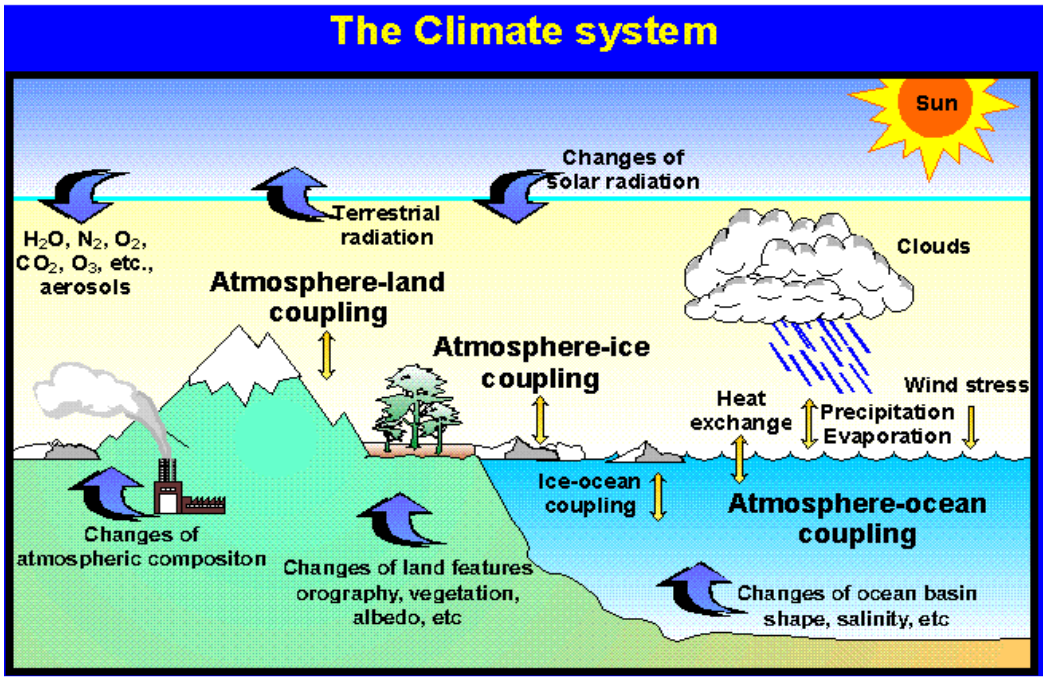

Figure 2.1 The components of the climate system and their interaction (Source: CSIRO Division of Atmospheric Research)

The cryosphere: includes the ice sheets of Greenland and Antarctica, continental glaciers and snow fields, sea ice and permafrost. It is very variable seasonally and derives its importance to the climate system from its high reflectivity (albedo) for solar radiation, its low thermal conductivity, its large thermal inertia and, especially, its critical role in driving deep ocean water circulation. Ice covers about 5.7% of the Earth's surface and contains 2.05% of the Earth's supply of water (the oceans contain 97.25%).

The biosphere: is the part of the Earth, including air, land, surface rocks, and water, within which life occurs. The biota influences the uptake and release of greenhouse gases. Through the photosynthetic process, both marine and terrestrial plants (especially forests) store significant amounts of carbon from carbon dioxide. Thus, the biosphere plays a central role in the carbon cycle, as well as in the budgets of many other gases, such as methane and nitrous oxide.

2.2 Global teleconnection patterns

The global atmospheric circulation has a number of preferred patterns of variability, all of which have expressions in surface climate. Monthly mean surface pressures vary markedly about the long-term mean SLP distribution. This variability occurs in well-defined spatial patterns (Wallace and Gutzler, 1981; Barnston and Livezey,

1987) particularly during the boreal winter over the Northern Hemisphere (NH). Such variations are commonly referred as "teleconnections" in the literature, since they result in simultaneous variations in weather and climate over widely separated points over the earth. Regional climates in different locations may vary out of phase, owing to the action of such teleconnections, which modulate the location and strength of the strom tracks and poleward fluxes of heat, moisture and momentum (Hurrell et al., 2003; Quadrelli and Wallace, 2004; Trenberth et al., 2005b). Such monthly, seasonal and longer-time scales anomalies have direct impacts on humans, as they are often associated with floods, droughts, heat or cold waves and other factors that can directly affect and disrupt agriculture, water supplies, and can modulate the fresh water quality, energy demands and human health.The strength of teleconnections and the way they influence surface climate varies over long time scale.
In sections 2.2.1 – 2.2.8 a short description of every teleconnection pattern used in this study is going to be made.

2.2.1 North Atlantic Oscillation

One of the most prominent patterns that act over the NH and especially over the North Atlantic region and the surrounding continents is the North Atlantic Oscillation (**NAO**). The **NAO** refers to a north-south oscillation in atmospheric mass between the Icelandic Low and the Azores High-pressure centers (Walker and Bliss, 1932). The **NAO** is the dominant pattern of near-surface atmospheric variability over the North Atlantic, accounting for one third of the total variance in monthly SLP in winter. A schematic representation of the spatial signature and climate impacts of **NAO** is given in Figure 2.2. The positive phase (Figure 2.2.a) of this pattern is associated with higher than normal surface pressure south of 55°N combined with a broad region of anomalously low pressure throughout the Arctic and subarctic. Consequently, this phase is associated with stronger-than-average winds across the mid-latitudes of the Atlantic onto Europe, with anomalously southerly flow over the eastern United States and anomalously northerly flows across Greenland, the northern part of Canada and the Mediterranean region and enhanced easterly trade winds over the sub-tropical North Atlantic (CPC, 2005).
During the negative phase, both the Icelandic low and Azores high-pressure systems are weaker-than-normal, so both middle latitude westerlies and the sub-tropical trade winds are also weak (Figure 2.2.b). The negative phase brings higher-than-normal pressure over the polar region and lower-than-normal pressure at about 45° N. The negative phase allows cold air to plunge into the Midwestern United States and western Europe, and storms bring rain to the Mediterranean.

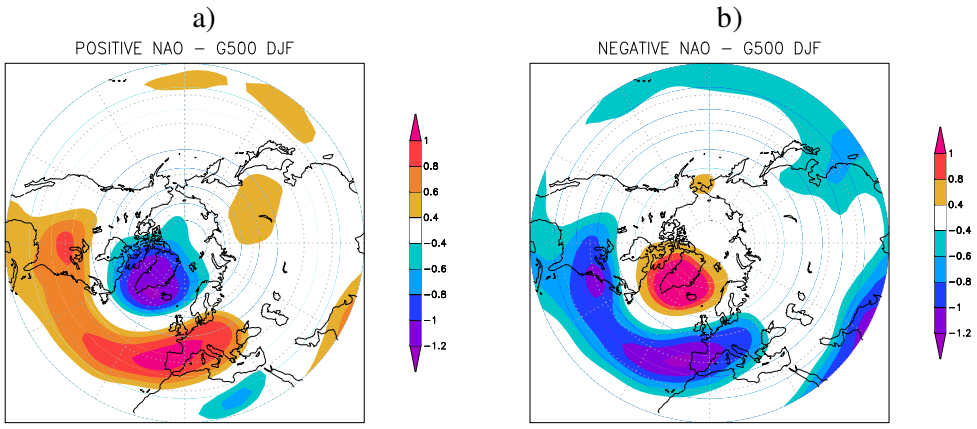

Figure 2.2 The composite map between the normalized NAO index and the normalized geopotential height at 500 mb for DJF: a) the positive phase (NAO Index > +0.75 standard deviation) and b) the negative phase (NAO Index < -0.75 standard deviation)

The NAO exhibits considerable interseasonal and interannual variability, and prolonged periods (several months) of both positive and negative phases of the pattern are common (Figure 2.3). The negative phase of the NAO dominated the circulation from the mid-1950's through the 1978/79 winter (CPC, 2005). During this interval, there were four prominent periods of at least three years each in which the negative phase was dominant and the positive phase was notably absent. An abrupt transition to the positive phases of the NAO then occurred during the 1979/80 winter, with the atmosphere remaining locked into this mode through the 1994/95 winter season. However, the winter 1995/96 was characterized by a return to the strong negative phase of the NAO.

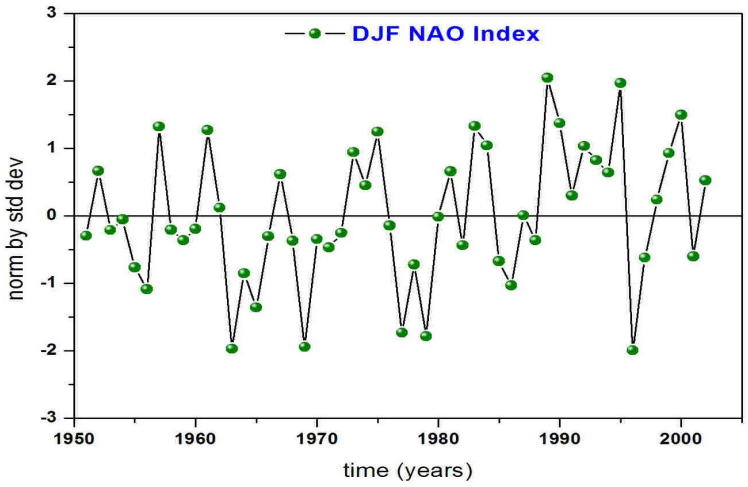

Figure 2.3 The time series of the normalized NAO index for winter (DJF)

2.2.2 Arctic Oscillation

The **Arctic Oscillation** (also referred to as the northern annular mode) is closely related to the **NAO**, with the observed time series correlating at 0.95 for monthly data (Deser, 2000). The **AO** is the dominant mode of variability on interannual time scales in the Northern Hemisphere and exhibits an annular pattern with decreased SLP over the Arctic basin associated with increase SLP at midlatitudes with centres of action in the North Atlantic and North Pacific.
As such, the **AO** essentially encompasses the **NAO** variability but emphasizes the zonally symmetric nature of the hemispheric variability. The oscillation exhibits a "negative phase" with relatively high pressure over the polar region and low pressure at midlatitudes (about 45 degrees North), and a "positive phase" in which the pattern is reversed (Figure 2.4). In the positive phase (Figure 2.4.a), higher pressure at midlatitudes drives ocean storms farther north, and changes in the circulation pattern bring wetter weather to Alaska, Scotland and Scandinavia, as well as drier conditions to the western United States and the Mediterranean. Weather patterns in the negative phase (Figure 2.4.b) are in general "opposite" to those of the positive phase.

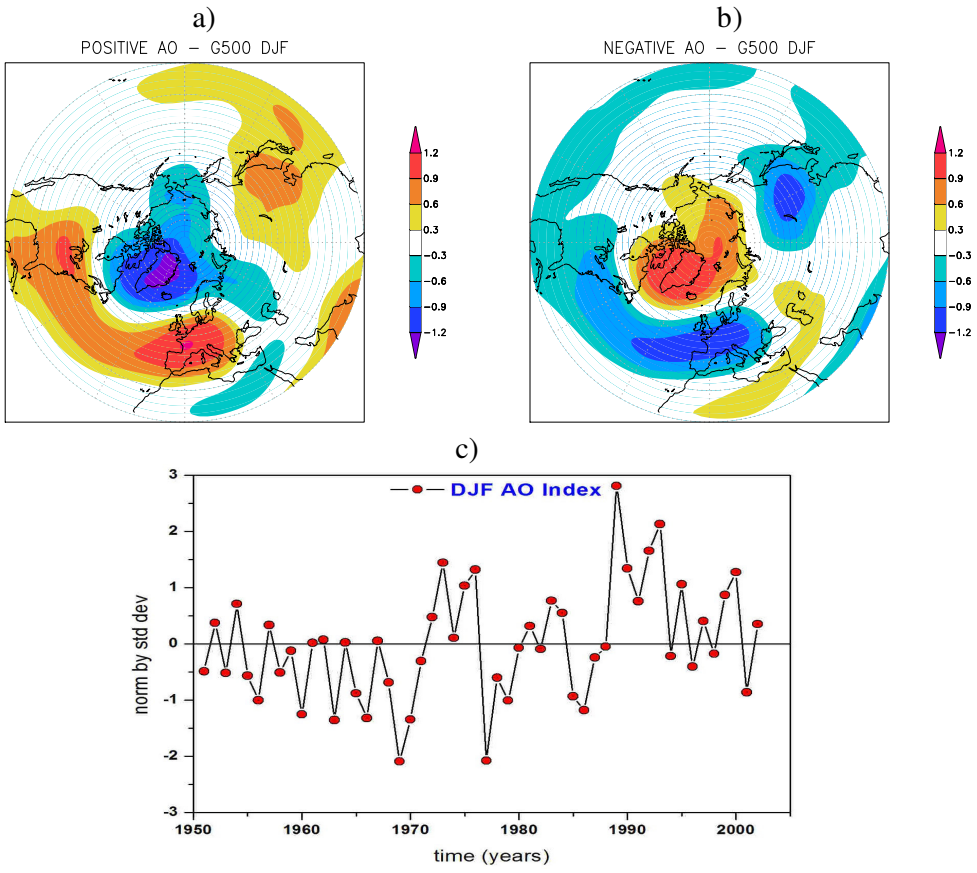

Figure 2.4 The composite map between the normalized AO index and the normalized geopotential height at 500 mb for DJF: a) the positive phase (AO Index > +0.75 standard deviation) and b) the negative phase (AO Index < -0.75 standard deviation);
c) The time series of the normalized AO index for winter (DJF)

2.2.3 The East Atlantic Pattern

The **East Atlantic** (**EA**) pattern is the second prominent mode of low-frequency variability over the North Atlantic region and appears as a leading mode in all months. The **EA** pattern is structurally similar to the **NAO**, and consists of a north-south dipole of anomaly centres spanning the North Atlantic from east to west. The anomaly centres of the **EA** pattern are displaced southeastward to the approximate nodal lines of the **NAO** pattern. For this reason, the **EA** pattern is often interpreted as a "southward shifted" **NAO** pattern. However, the lower-latitude centre contains a strong subtropical link in association with modulations in the subtropical ridge intensity and location. This subtropical link makes the **EA** pattern distinct from its **NAO** counterpart.

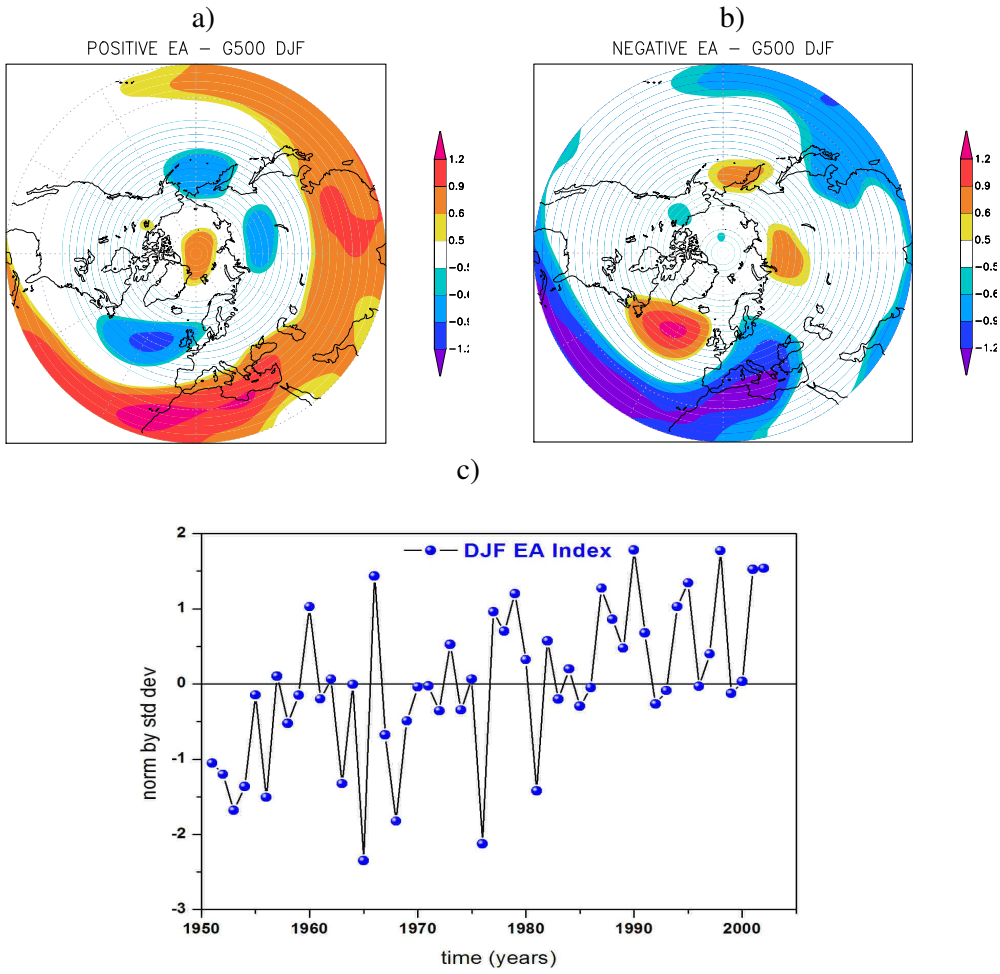

Figure 2.5 The composite map between the normalized EA index and the normalized geopotential height at 500 mb for DJF: a) the positive phase (EA Index > +0.75 standard deviation) and b) the negative phase (EA Index < -0.75 standard deviation); c) The time series of the normalized EA index for winter (DJF)

The positive phase of the **EA** pattern (Figure 2.5.a) is associated with above-average surface temperatures in Europe in all months and with below-average temperatures

over the southern U.S. during January-May and in the north-central U.S. during July-October. It is also associated with above-average precipitation over northern Europe and Scandinavia and with below-average precipitation across southern Europe. In the negative phase (Figure 2.5.b) the weather patterns are in general "opposite" to those of the positive phase.
The **EA** pattern exhibits a strong multi-decadal variability (Figure 2.5.c). The period 1950-1975 was characterized by a very intense negative phase; meanwhile the positive phase occurred during much of the period 1976-2002.

2.2.4 The East Atlantic / Western Russia Pattern

The East Atlantic/ West Russia (EA/WR) pattern is one of three prominent teleconnection patterns that affects Eurasia throughout year. The East Atlantic/ West Russia pattern consists of four main anomaly centres (Figure 2.6). The positive phase (Figure 2.6.a) is associated with positive height anomalies located over Europe and northern China, and negative height anomalies located over the central North Atlantic and north of the Caspian Sea.

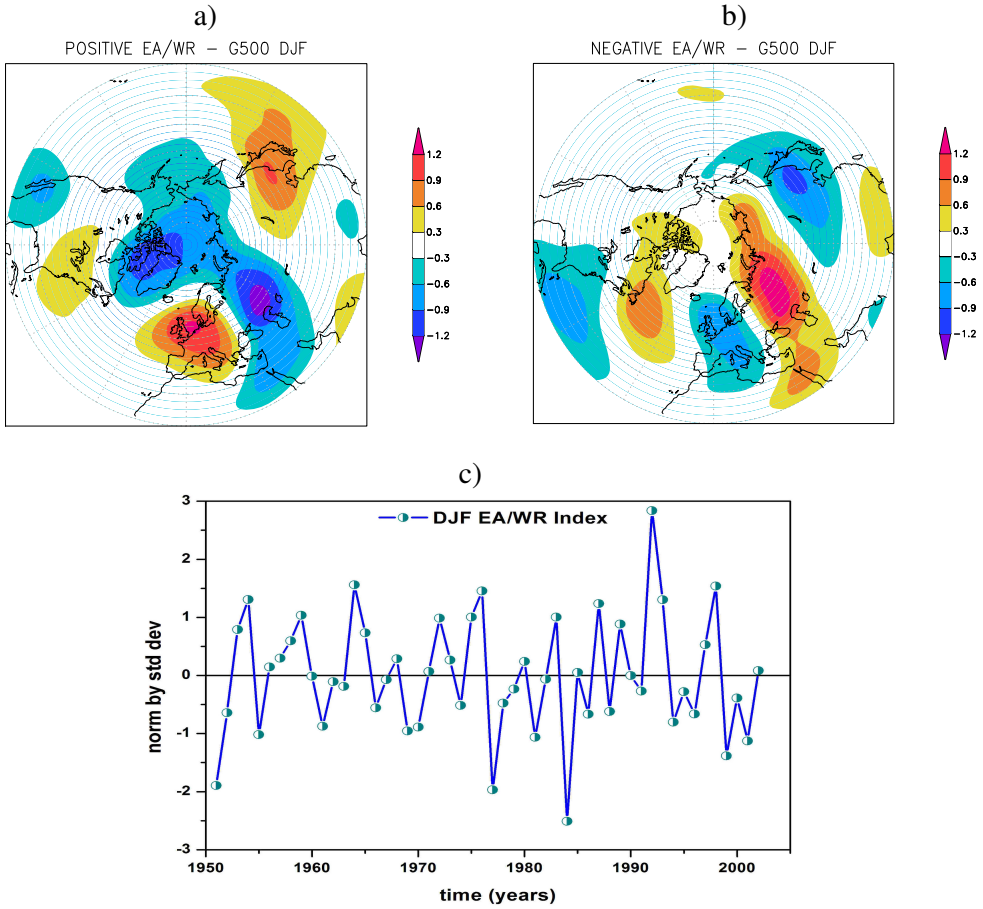

Figure 2.6 The composite map between the normalized EA/WR index and the normalized geopotential height at 500 mb for DJF: a) the positive phase (EA/WR Index > +0.75 standard deviation) and b) the negative phase (EA/WR Index < -0.75 standard deviation); c) The time series of the normalized EA/WR index for winter (DJF)

The surface temperature anomalies associated with the positive phase of the EATL/ WRUS pattern reflect above-average temperatures over eastern Asia, and below-average temperatures over large portions of western Russia and northeastern Africa. The precipitation anomalies reflect generally above-average precipitation in eastern China and below-average precipitation across central Europe (CPC, 2005).

2.2.5 The Scandinavian Pattern

The **Scandinavian** pattern (**SCA**) consists of a primary circulation centre over Scandinavia and two weaker centres of opposite sign over western Europe and eastern Russia/ western Mongolia. The **Scandinavian** pattern has been previously referred to as the Eurasia-1 pattern by Barnston and Livezey (1987).

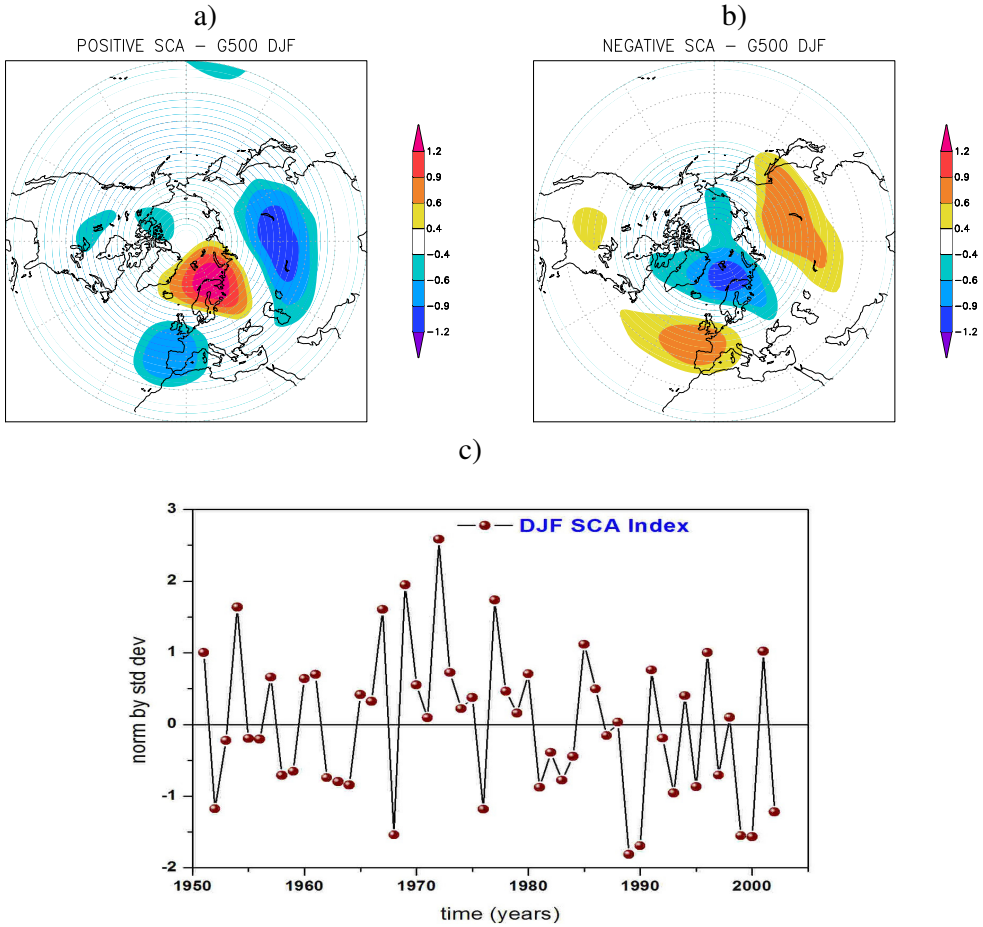

Figure 2.7 The composite map between the normalized SCA index and the normalized geopotential height at 500 mb for DJF: a) the positive phase (SCA Index > +0.75 standard deviation) and b) the negative phase (SCA Index < -0.75 standard deviation); c) The time series of the normalized SCA index for winter (DJF)

The positive phase (Figure 2.7.a) of the Scandinavia pattern is associated with below-average temperatures across central Russia and also over western Europe. It is also associated with above-average precipitation across central and southern Europe and below-average precipitation across Scandinavia (CPC, 2005).

The time series (Figure 2.7.c) for the Scandinavia pattern exhibits relatively large interseasonal, interannual and interdecadal variability. For example, a negative phase of the pattern dominated the circulation from early 1964 through mid-1968 and from mid-1986 through early 1993. Negative phases of the pattern have also been prominent during winter 1988/89, spring 1990, and winter/spring 1991/92. In contrast, positive phases of the pattern were observed during much of 1972, 1976 and 1984.

2.2.6 The Polar/ Eurasia Pattern

The Polar/ Eurasia pattern appears in all seasons. The positive phase (Figure 2.8.a) of this pattern consists of negative height anomalies over the polar region and positive anomalies over northern China and Mongolia. This pattern is associated with fluctuations in the strength of the circumpolar circulation, with the positive phase reflecting an enhanced circumpolar vortex and the negative phase reflecting a weaker than average polar vortex (CPC, 2005).

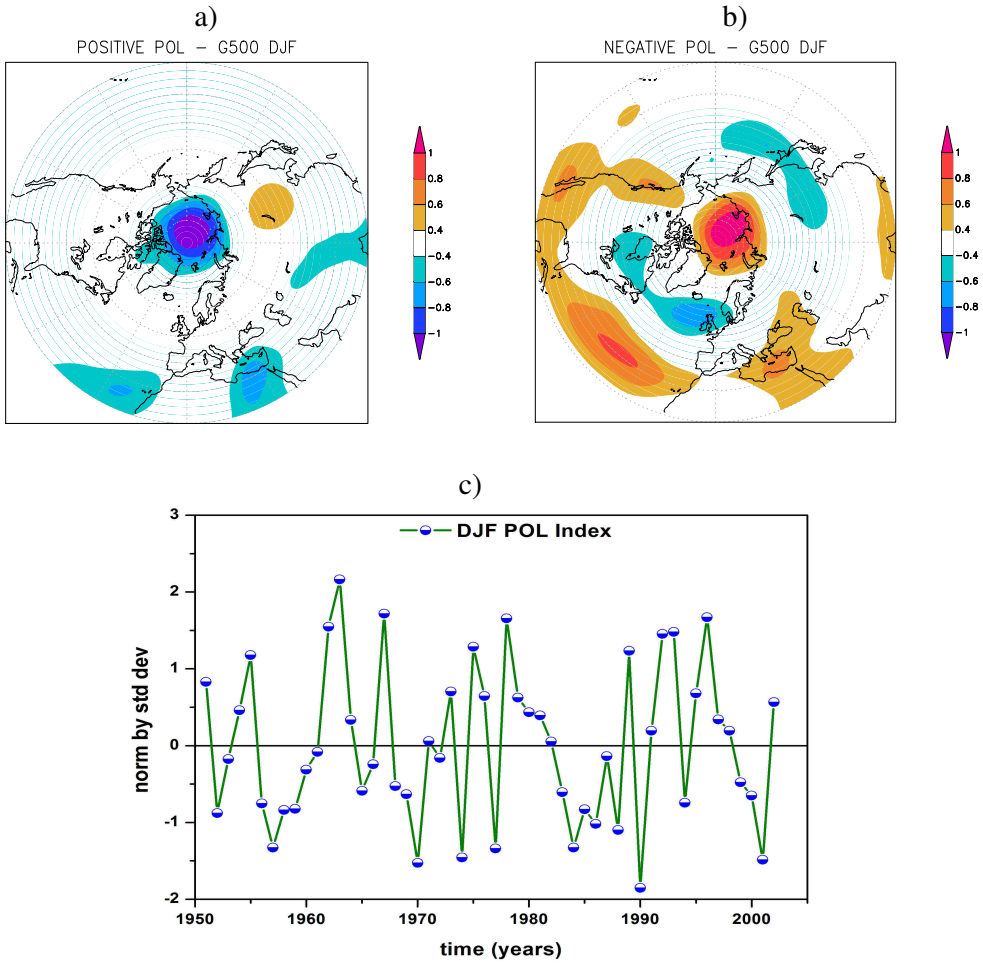

Figure 2.8 The composite map between the normalized POL index and the normalized geopotential height at 500 mb for DJF: a) the positive phase (POL Index > +0.75 standard deviation) and b) the negative phase (POL Index < -0.75 standard deviation); c) The time series of the normalized POL index for winter (DJF)

The Polar/Eurasian pattern is associated with above-average temperatures in eastern Siberia and below-average temperatures in eastern China and above-average precipitation in the polar region north of Scandinavia.

2.2.7 El Niño-Southern Oscillation

Of all the oceans, the tropical Pacific exhibits the biggest fluctuations in surface temperature, on timescales of several months to several years. This region of the ocean has a particularly strong influence on world climate, so variations in its temperature field can have a global impact.

The **El Niño Southern Oscillation** (**ENSO**) is an anomalous large scale ocean-atmosphere system associated with strong fluctuations in ocean currents and surface temperatures. It causes abnormal atmospheric and environmental conditions, primarily in equatorial regions within the Pacific Basin. **ENSO** is a major example of the interrelationship between ocean currents and atmospheric conditions and it consists of two components: **El Niño** and the **Southern Oscillation**. **ENSO** is associated with floods, droughts, and other disturbances in a range of locations around the world. These effects, and the irregularity of the **ENSO** phenomenon, make predicting it of high interest.

El Niño involves warming of the tropical Pacific surface waters, weakening the usually strong SST gradient across the Pacific, with associated changes in ocean circulation. It's linked atmospheric counterpart, the **Southern Oscillation** (**SO**), involves changes in trade winds, tropical circulation and precipitation. The term "**Southern Oscillation**" refers to the variability of the strength of the Walker Circulation system and is quantified through the Southern Oscillation Index. During **El Niño** events (Figure 2.9.a) there is a weakening of the Walker circulation, generally bringing drier conditions to the western Pacific region. During La Niña events (Figure 2.9.b) the Walker circulation is especially strong, and rainfall may be unusually high over Indonesia.

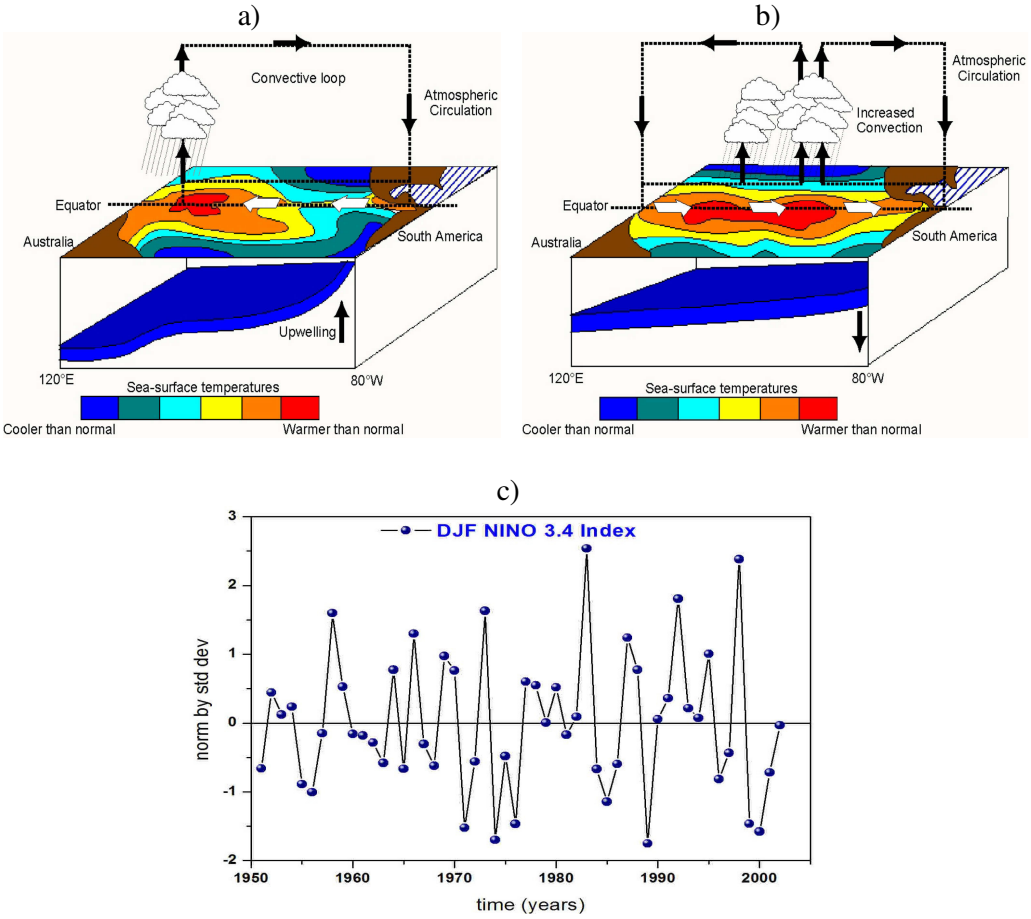

Figure 2.9 A schematic view of ENSO phenomenon:
a) El Niño conditions and b) La Niña conditions
c) The time series of the normalized NINO 3.4 index for winter (DJF)

2.2.8 Pacific Decadal Oscillation

The "**Pacific Decadal Oscillation**" (**PDO**) is a long-lived **El Niño**-like pattern of Pacific climate variability. While the two climate oscillations have similar spatial climate fingerprints, they have very different behaviour in time (Figure 2.10). Decadal to inter-decadal variability of the atmospheric circulation is most prominent in the North Pacific, where fluctuations in the strength of the winter Aleutian Low pressure system co-vary with North Pacific SST in the **PDO**.
Two main characteristics distinguish **PDO** from **ENSO**: first, the **PDO** "events" persist for 20-to-30 years, while typical ENSO events persist for 6 to 18 months; second, the climatic fingerprints of the **PDO** are most visible in the North Pacific/North American sector, while secondary signatures exist in the tropics - the opposite is true for **ENSO**. Several independent studies find evidence for just two full **PDO** cycles in the past century: "cool" **PDO** regimes prevailed from 1890-1924 and again from 1947-1976, while "warm" **PDO** regimes dominated from 1925-1946 and from 1977 through (at least) the mid-1990's.

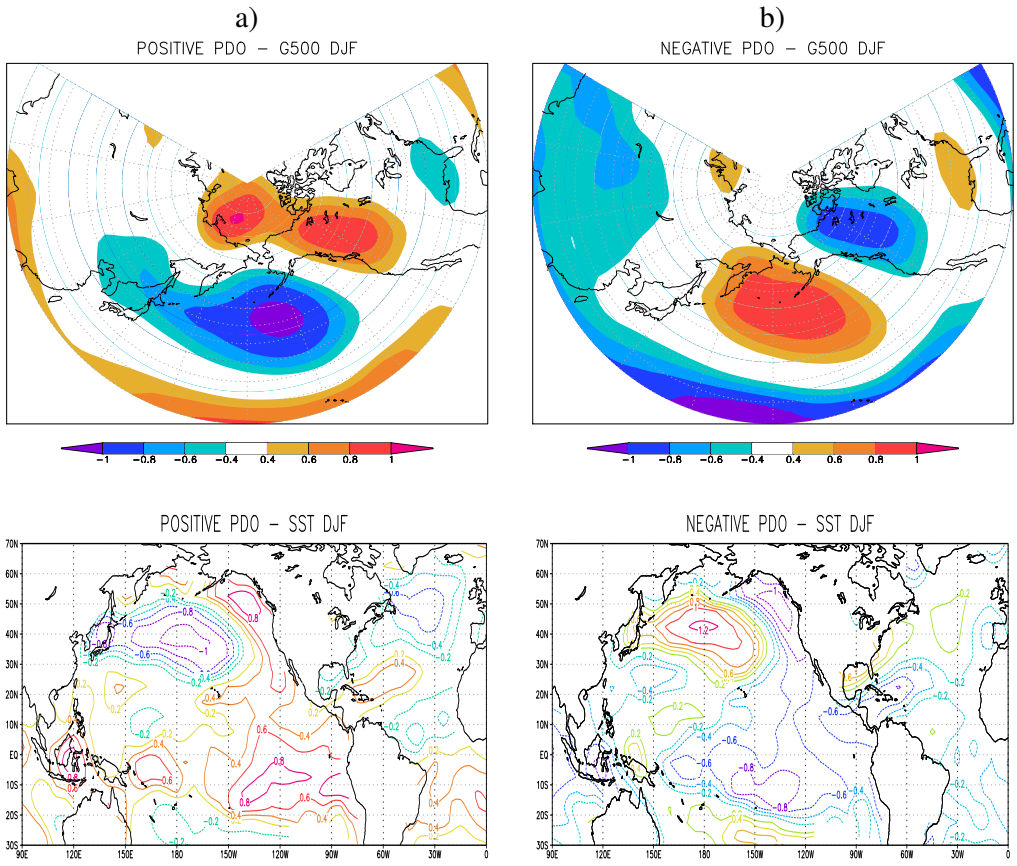

Figure 2.10 The composite map between the normalized PDO index and the normalized geopotential height at 500 mb and normalized SST for DJF: a) the positive phase (PDO Index > +0.75 standard deviation) and b) the negative phase (PDO Index < -0.75 standard deviation)

The measurement of the intensity of the **PDO** is made via different indices: the North Pacific index (NPI; Trenberth and Hurrell, 1994), **PDO** index (Figure 2.11) (Mantua et al., 1997) and the Inter-decadal Pacific Oscillation (IPO; Power et al., 1999). Modulation of **ENSO** by the **PDO** significantly modifies regional teleconnections around the Pacific basin (Salinger et al., 2001) and affects the evolution of the global mean climate.

The **PDO** is detected as warm or cool surface waters in the Pacific Ocean (Figure 2.10 – lower maps), north of 20° N. During a "warm", or "positive", phase, the west Pacific becomes cool and part of the eastern ocean warms; during a "cool" or "negative" phase, the opposite pattern occurs.

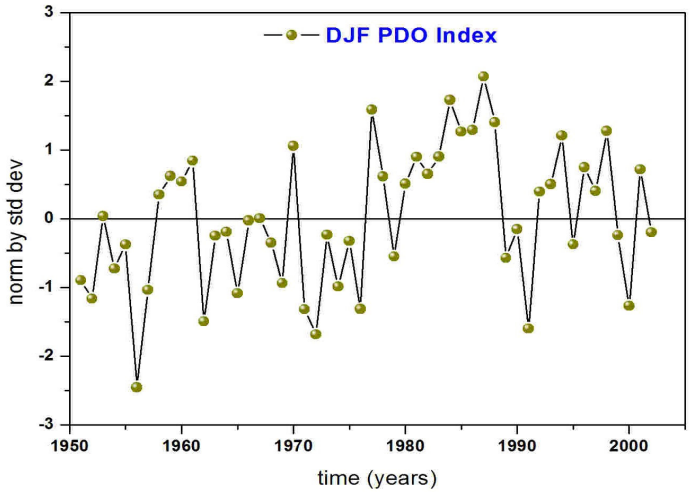

Figure 2.11 The time series of the normalized PDO index for winter (DJF)

Chapter 3

Extreme events in Elbe's river catchment area and their associated circulation patterns

"However big floods get, there will always be a bigger one; so says one theory of extremes and experience suggests it's true"
(President's Water Commission, 1950)

3.1 Introduction

Extreme events became an important research topic in the last years and the study of their variations has been intensified considerably (Easterling et al., 2000; Gong et al., 2004; Ekström et al., 2005; Palutikof et al., 1999). By definition, extreme events are rare, but they do occur and sometimes records are broken.
Special attention has also been paid to those extremes related to hydrological variables, like drought or floods, since they produce a huge amount of material losses and human casualties (Yiou et al., 2006; Mares et al., 2008). Between 1998 and 2002, Europe suffered over 100 major damaging floods, including the catastrophic floods along the Danube and Elbe rivers in 2002 (Ulbrich et al., 2003 a, b; Bronstert et al., 1998). Since 1998, floods have caused around 700 fatalities, the displacement of about half a million people and at least € 25 billion in insured economic losses (European Environment Agency, 2003). Severe floods in the Danube river in 2005 caused further damage, when water levels have reached historical values, especially in the north-western part of Romania (Stanciu et al., 2005).

Using the theory of extreme values, one can estimate mean changes and/or the distribution variance as well as the intensity and frequency of extreme events. Extreme value theory is concerned with probabilistic and statistical questions related to the lowest or highest values in a sequence of random variables (Coles, 2001).

In flood frequency analysis, methods such as Generalized Extreme Value (GEV) and Peak over Threshold (POT) have been used. However, hydrological time series do not necessarily fulfil the basic requirements of extreme value theory. They are a result of complex processes (snow melt, precipitation, soil humidity, etc) and a univariate distribution with two or three parameters is not necessarily a good approximation of their complex nature (Klemes, 2000). It is important to detect the extremes in the data, by applying GEV or POT, in such a way that these distributions would fit them. The POT approach is assumed to be more precise than GEV, which takes into account just one value per year (e.g. annual maxima), because the annual maxima are not always true extremes (Leonard et al., 2008).

If daily data is available, the POT method is proposed for applications since it makes use of more data sets and it adapts to heavy-tailed distributions better (Cloes, 2001). However, one of the main concerning of the POT method is the choice of the threshold and the possible non-independence of the extreme values considered in the analysis. GPD is used in studies related to the extreme values both in hydrology and climatology (Katz et al., 2002; Naveau et al., 2005), as well as to damage caused by these events (Smith, 2003).

Since floods are caused frequently by unusual weather situations, it is important to identify typical weather patterns associated with the occurrence of these extreme events. Although many studies have related the atmospheric circulation to different climatic variables, like precipitation and/or temperature (Fargoso and Gomes, 2008; Brunetti et al., 2002; Wibig, 1999; Kyselý and Beranová, 2008; Yiou and Nogaj, 2004), little has been done to associate the large-scale weather features to the occurrence of hydrological extremes. By using river discharge, an advantage may arise, due to the fact that this variable is less sensitive than precipitation, because it represents a spatial integral of the precipitation falling over large areas, especially when the catchment areas are large enough.

Extreme events need to be analyzed for relatively long periods (Knox, 2000) and on daily time scale, in order to capture the synoptic features which are responsible in triggering them. Since most of the atmospheric data sets, have a monthly to seasonal resolution, it is rather difficult to make detailed studies of synoptic features related to the occurrence of different extreme events (Jacobeit et al, 2003). In the context of the newly developed daily SLP data set, in the framework of EMULATE project (Ansell et al., 2006), the aim of this chapter is to study the occurrence of extreme discharge events in Elbe's catchment area in relation with different circulation patterns and to statistically model the behaviour of these extreme.

3.2. Data and methods

3.2.1 Data description

The daily time series of Elbe discharge were recorded at Neu Darchau (53° 14′ N, 10° 53′ E), which is situated in the lower part of Elbe catchement area (last gauging station) and they were provided by the German Federal Institute of Hydrology (BfG) in Koblenz, Germany.

From this data set the daily values for every season of the year, for the period 1875-2002, have been selected. Winter seasons is defined as JFM (January-February-March), spring as AMJ (April-May-June), summer as JAS (July-August-September) and autumn as OND (October-November-December). The daily time series for each season are represented in Figure 3.1.

An important role in flood frequency analysis is to quantify and mitigate the risks of flooding that arises from the variability of extreme rainfall and precipitation. Although seasonal fluctuations of these parameters are an important source of variability, it is sometimes overlooked when considering and evaluating flood risk. The term "1 in 100 years" flood, doesn't specify weather a given extreme value is more likely to come from one season over another (Leonard et al., 2008).

Although in flood analysis the most used variable is the annual maximum, we will focus on the daily seasonal time series in order to capture the extreme events at a seasonal time scale. We choose the seasonal time scales because the annual maxima are not always true seasonal extremes which could be masked by the annual maxima.

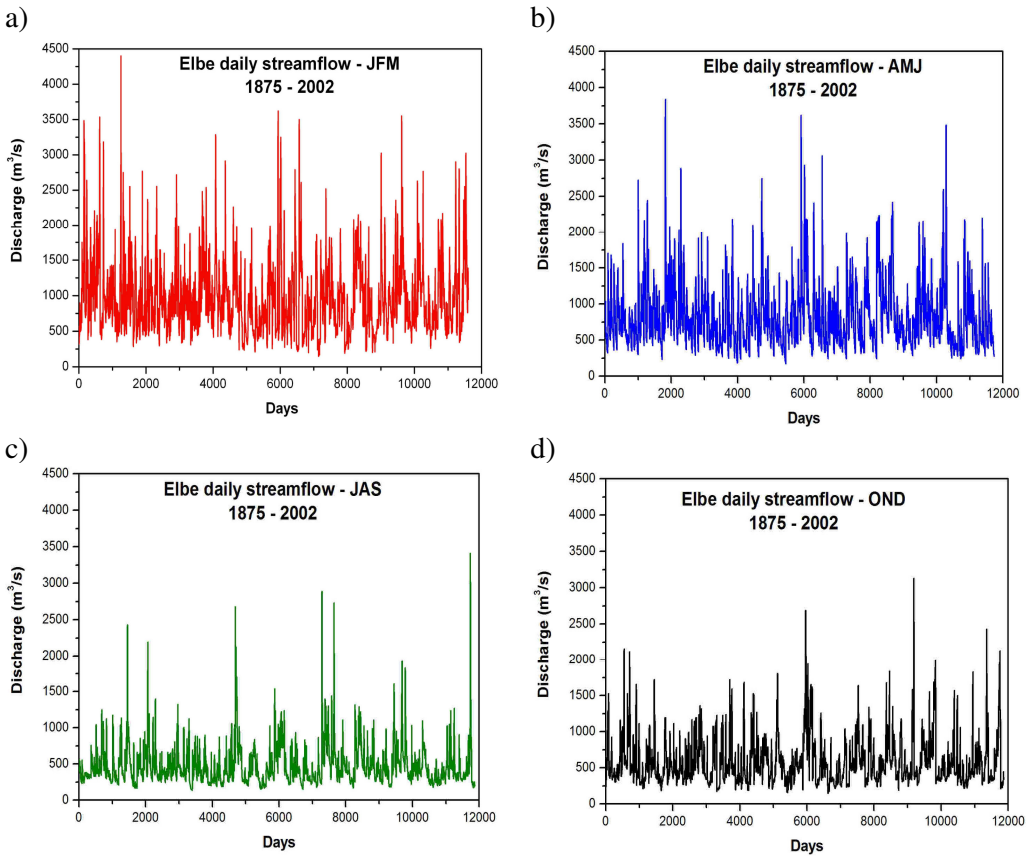

Figure 3.1 The time series of daily values for each season: a) JFM, b) AMJ, c) JAS and d) OND

The daily mean Sea Level Pressure (SLP) dataset used to compute the circulation patterns, related with streamflow extremes, was taken from the data reconstructed by Ansell et al. (2006) within the project European and North Atlantic daily to MULtidecadal climATE Variability (EMULATE, available online at http://www.cru.uea.ac.uk/cru/projects/emulate/). This data set was produced using 86 continental and island stations distributed over the region bounded between 70°W-50°E and 25°-70°N (Ansell et al., 2006). Although the coverage of these data sets is limited to the Atlantic-European sector, we choose to make use of it due to his long time series, which extends back to 1850.

3.2.2 Methodology

3.2.2.a Peak over Threshold

The analysis of the distribution of extremes is an important diagnostic tool for studying the occurrence of rare events (Coles, 2001; Naveau et al., 2005). The extreme value theory (EVT) aims at studying the statistics of extreme phenomena. To study the distribution of extreme values, two methods can be applied: Generalized Extreme Values (GEV) method and Peak over Threshold (POT) method.

The classical approach to perform an extreme value analysis is to fit the annual maxima values with the Generalized Extreme Value (GEV) cumulative distribution function:

$$F(x) = \exp\left\{-\left(1+\xi\frac{x-\mu}{\sigma}\right)^{-1/\xi}\right\} \qquad (1)$$

where μ is the location parameter, σ >0 is the so-called scale parameter and ξ is the shape parameter which determines the tail of the distribution. When $\xi \approx 0$ the GEV distribution corresponds to the Gumbel family, conversely for ξ >0 the Fréchet form is adopted and for ξ <0 the Weibull form is adopted. The annual maxima method developed by Gumbel (1960) considers only the largest value for each year.
To solve the problem of working only with one data per year the Generalized Pareto Distribution (GPD) was introduced (Pickands, 1975). The GPD method models all values larger than a given threshold *u*. Distribution of the values selected using POT should have an approximate Generalised Pareto Distribution (GPD), for a high sufficient threshold. The advantage of the GPD, when compared with GEV, is that the GPD estimates also take into account all observations that exceed the threshold. The difference between these values and the threshold *u* are called exceedances over the threshold and it is assumed to follow a GPD distribution whose cumulative distribution function is defined by:

$$F(y;\sigma,\xi) = \begin{cases} 1-(1+\xi y/\sigma)^{-1/\xi}; & \xi \neq 0,\ \sigma > 0 \\ 1-\exp(-y/\sigma); & \xi = 0,\ \sigma > 0 \end{cases} \qquad (2)$$

where σ >0 is the location parameter, $-\infty < \xi < \infty$ is the shape parameter and *y* are the exceedances over the threshold *u* ($y = x - u > 0$).
Depending on the value of ξ we can have three possible cases:

- ξ=0, a light-tailed (or exponential) distribution
- ξ>0, a heavy-tailed (or Pareto) distribution
- ξ<0, a bounded (or beta) distribution

The methods for choosing the threshold *u* are explained in section 3.3.

3.2.2.b Return levels

When considering extreme values of a random variable, one is interested in the return level of an extreme event, defined as the value, Z_p, such that there is a probability p that Z_p is exceeded in any given year. Alternatively, the level that is expected to be exceeded on average every once in a $1/p$ years ($1/p$ is often referred as the return period). For example, if the 100-year return level for discharge at a given station is found to be 20.5 m^3/s, then the probability of discharge exceeding 20.5 m^3/s in any given year is 1/100=0.01. The return level z_p is defined as:

$$Z_p = u + \frac{\sigma^*}{\xi}\left[\left(n_y p \zeta_u\right)^{\xi} - 1\right]$$

where n_y is the number of observations per year and ζ_u is the probability of an individual observation to exceed the threshold u.
The advantage of the return level is that for instance, one could obtain 200-year return levels of water stages with only 150 years of data.

3.2.2.c K-means cluster analysis

The method employed to detect the circulation patterns associated with the extreme events in the Elbe river streamflow is the *k-means* cluster analysis. We used the algorithm of Hartigan and Wong (1979). This method partitions the data set into a predefined set of clusters, in such a way to minimize the spread within them. The algorithm then searches for the best partition, given random centroids. By repeating this algorithm with random initialization and checking for the reproducibility of the centroids, this method can provide a heuristic criterion to asses the validity of the partitioning into distinct *k* clusters (Michelangeli et al, 1995).

After deciding which clustering method to employ, the decision of the number of clusters to retain is an important one. The atmospheric regimes over Europe, both in winter and in summer, are generally classified into four weather regimes (Corti et al., 1999; Yiou et al., 2008; Michelangeli et al., 1995; Cassou et al., 2004), regardless of the method used to determine the classification. The aim of our paper is not to try to identify the "best" number of clusters to be retained, and therefore we choose to retain 4 clusters for each season. A visual inspection of the clusters $k>4$, indicates that the patterns tend to repeat themselves.

The steps followed to identify the circulation patterns associated with the extreme events, in the Elbe cacthment area, are as follows:

1. We have selected for each season the days in the SLP data when the discharge of Elbe was above the threshold which defines the extreme events. This threshold varies with the season.
2. We have applied step 1 algorithm for 1, 2…up to 7 days lag (SLP lags the extreme event) in the SLP field.
3. A composite map was then created for the SLP field for these 7 days. The composite map was constructed based on "n" maps X 7 (number of days), where "n" is the number of times when the threshold was exceeded (e.g. in winter n=623, which means that for the whole period analysed Elbe's discharge exceeded this threshold 623 times).
4. This composite map, containing the "n" maps, was then subjected to *k-means* cluster analysis, in order to identify which are the dominant circulation patters which trigger extreme events in Elbe's catchment area.

Although cluster analysis is most of the times used together with PCA analysis or other statistical methods employed to filter out the data, we have applied k-means clustering method directly to the composite maps since we have already filter out the data by subtracting just the days above a certain threshold in the discharge time series.

3.3 Application of the General Pareto Distribution to seasonal Elbe river discharge

The GPD distribution uses more information than a model based only on block maxima (e.g. the highest or the lowest value in the year). For this reason we fitted the GPD distribution to our times series. This method contrasts with block maxima approach through the characterisation of an observation as an extreme if it exceeds a high threshold. A threshold which is too low is likely to violate the asymptotic basis of the model, leading to biases, while a threshold which is too high will generate just few excesses with which the model can be estimated, leading to a high variance (Coles, 2001). One of the most difficult parts of the POT approach is to identify a suitable threshold. We have focused on two methods to identify a suitable threshold (just the plots for AMJ are shown further):

1. An exploratory technique is carried out prior to the model estimation (mean residual plot). The idea of the method is to identify the threshold up to where the line is almost linear, taking into account the 95% confidence bounds (Figure 3.2.a).
2. The assessment of the stability of parameter estimates based on the fitting of the models across a range of different thresholds. The maximum likelihood estimates of the modified scale and shape parameters against u for the daily seasonal times series are shown in Figure 3.2.b.

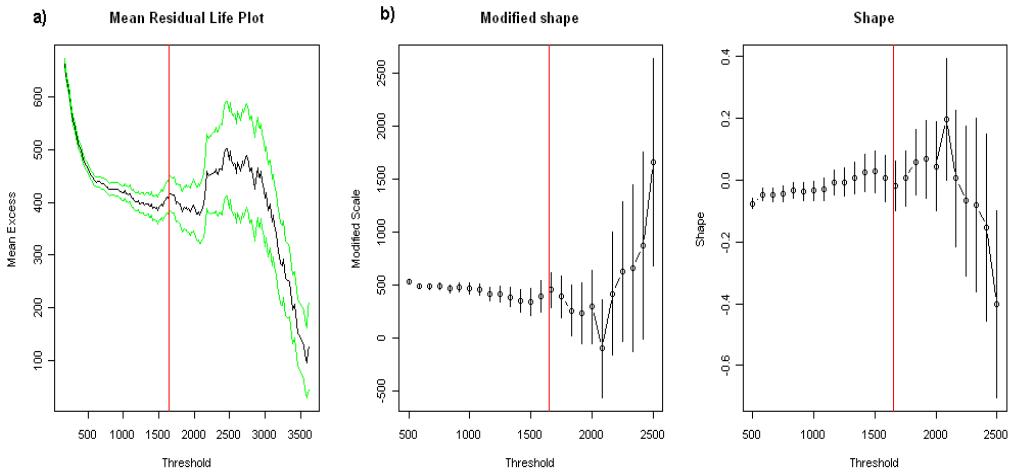

Figure 3.2 Mean residual plot of AMJ daily discharge thresholds: a) mean excess discharge and b) GPD fits for a range of 50 thresholds from 500 to 2500 m^3/sec
The red line represents the chosen threshold (1600 m^3/sec, in this case)

Using the methods described above and analysing the graphs in Figure 3.2, the thresholds identified for each season are shown in Table 3.1. To test the accuracy of the two methods in finding a proper threshold we have also computed the 90 and 95 % percentile. In the case of all season the threshold identified using the POT method is situated between the values of the 90% and 95% percentile (Table 3.1). We have applied the composite and cluster analysis using the values corresponding to the 90% and 95% and the results remain almost identical (not shown). Taking this

into account we will show further just the results with the thresholds identified throughout the POT method.

Table 3.1. The threshold values for the POT model, the 90th and 95th percentile, corresponding to each season

	Threshold		
Season	**90th percentile (m^3/s)**	**POT (m^3/s)**	**95th percentile (m^3/s)**
JFM	1620	**1900**	1920
AMJ	1430	**1650**	1680
JAS	795	**850**	990
OND	1000	**1000**	1225

The GPD distribution estimated parameters together with the standard errors are shown in Table 3.2. As it can be inferred from the values of the shape parameter (ξ) all the seasons, except summer, the distributions tend towards a normal distribution (ξ has values close to 0). For summer, ξ=0.171, which implies that the distribution has a heavy-tail and is more exposed to extreme events compared to the other seasons.

Table 3.2. The seasonal estimates of the GPD model and the corresponding standard errors

Season	σ (scale parameter)	ξ (shape parameter)
JFM	487.752 (32.118)	-0.048 (0.053)
AMJ	429.134 (23.821)	-0.027 (0.039)
JAS	266.263 (13.123)	**0.171 (0.038)**
OND	346.596 (14.260)	-0.027 (0.029)

To test if GPD fits well our data sets, the diagnostic plots for each season are represented in Figure 3.3. For all seasons, the probability and quantile-quantile (Q-Q) plots are approximately linear, indicating that the assumed form of distribution is reasonable.
The return level plots are shown in the left corner for each season along with the point wise 95% confidence bound, estimated by the delta methods. A consequence of the positive value for the shape parameter, during summer, is the fact that the return level curves are non-linear. For the other seasons, taking into account that $\xi \approx 0$, the return level curves are almost linear (Figure 3.3).

Once the best model for the time series has been determined, the interest is in deriving the return levels, corresponding to different return periods. The return level is the level exceeded on average every once in T years. Table 3.3 gives the estimates of the return level for the best fitting model for T= 2, 5, 10, 50 and 100 years. We also computed the associated 95% confidence intervals.

Discharge values between 3500 and 4000 m^3/s have return periods ranging from 5 to 100 years, for the winter, spring and autumn. Taking into account that for these months the shape parameter is light tailed, the error band is not too large for return periods above 50 years.

For summer, discharge values reaching even 5000 m^3/s have return periods between 50 to 100 years. These high values, compared to the other seasons, are determined by the value of the shape parameter. A positive shape parameter (heavy-tailed distribution) induces larger biases for the return periods, especially the ones above 10 years.

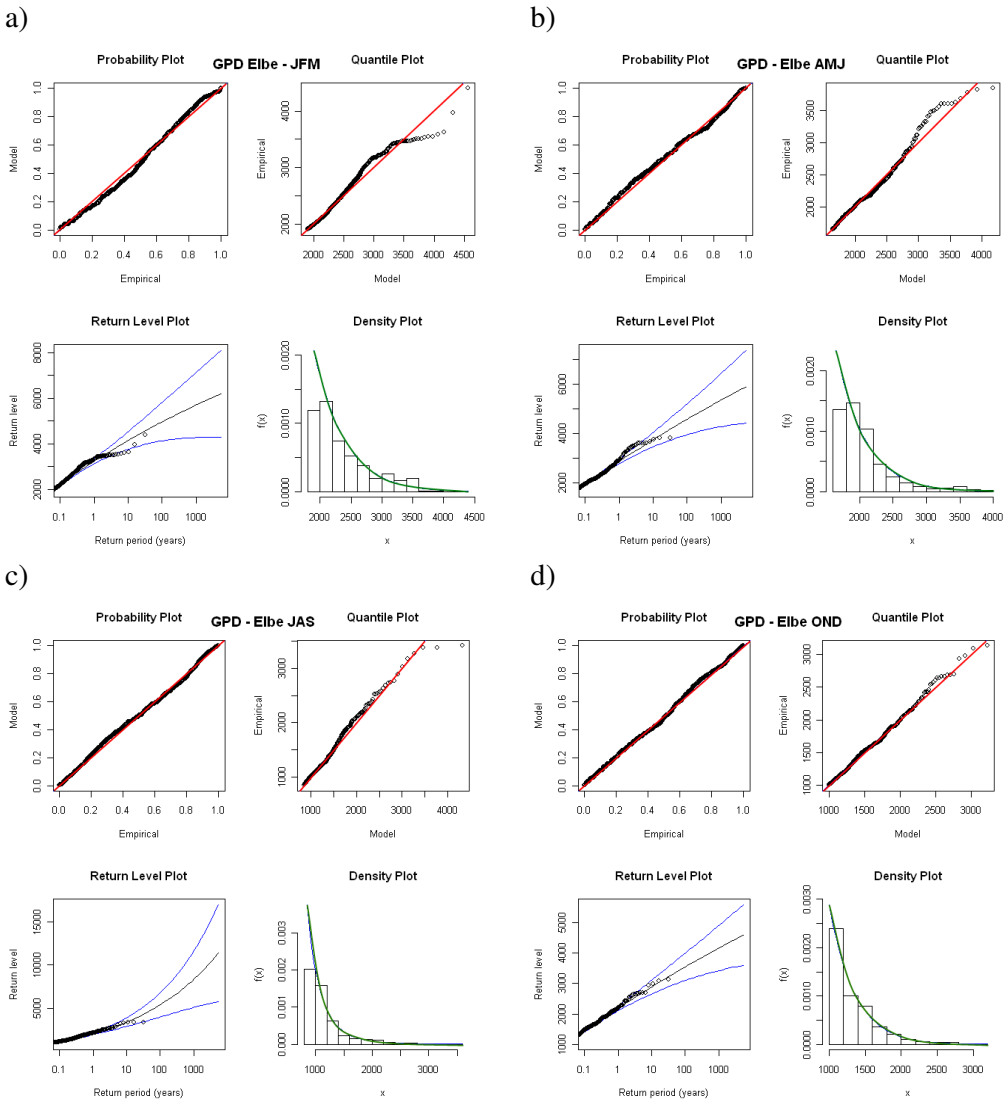

Figure 3.3 The diagnostic plots for the GPD fit to: a) JFM; b) AMJ; c) JAS and d) OND The red line represents the linear fit (line of equality represents perfect fit), blue lines represent the upper and lower bounds of the 95% confidence interval and the green line represents the fitted GPD density

Table 3.3. Estimates of the return level for different return periods. Between the brackets are the values for the 95% confidence level.

Years	JFM (m^3/s)	AMJ (m^3/s)	JAS (m^3/s)	OND (m^3/s)
100	**4956.19** (4366.87, 5563.51)	**4584.02** (4105.19, 5062.85)	**5398.39** (4739.34, 6057.44)	**3544.07** (3236.32, 3851.83)
50	**4728.37** (4186.71, 5280.47)	**4340.22** (3929.10, 4779.26)	**4716.85** (4155, 5277.15)	**3350.51** (3066.17, 3634.85)
20	**4402.93** (3995.89, 4891.50)	**4010.71** (3701.06, 4395.98)	**3931.17** (3484.72, 4377.63)	**3088.89** (2849.99, 3341.59)
10	**4147.01** (3831.88, 4585.62)	**3755.87** (3513.39, 4099.54)	**3413.34** (3041.91, 3784.76)	**2886.56** (253198, 2883.58)
5	**3882.39** (3648.44, 4228.78)	**3496.19** (3311.49, 3765.43)	**2953.27** (2654.52, 3258.03)	**2680.33** (2531.98, 2883.58)
2	**3518.74** (3371.63, 3728.99)	**3145.05** (3021.16, 3315.39)	**2422.92** (2245.04, 2650.83)	**2401.61** (2300.07, 2535.74)

3.4 Circulation patterns associated with extreme river discharge events

3.4.1 Winter circulation patterns

The four circulation patterns and the composite map for the winter season are shown in Figure 3.4. The composite map (Figure 3.4.a) for the 623 days with discharges above 1900 m^3/s, from which the Circulation Patterns (CPs) are derived, indicates that the extreme events in Elbe's catchment area are associated with a tripole-like pattern in the SLP field. It contains a prominent low extending from the Atlantic Ocean towards the western part of Europe and Scandinavia and two positive centres situated over Greenland and the southern part of Europe. Consequently, circulation in the days associated with extreme discharge events is characterized by a strong south-westerly flow, which brings moist air from the ocean over the continent. Obviously, the circulation patterns observed in each of the 623 days are not identical. Therefore, an attempt was made to classify the circulation types causing extreme discharges in Elbe's catchment area.

CP1 (Figure 3.4.b), corresponding to 150 days, is associated with a strong negative anomaly centred over Greenland and extending to central Atlantic and a positive anomaly centre over Scandinavia. Southerly flows, associated with this type of circulation, bring cold air from the continent which meets warmer and humid air masses from the ocean causing abundant precipitation or snowfalls.

CP2 (Figure 3.4.c) is similar to CP4, except the fact that the negative anomaly is stronger over the Atlantic and weaker over the continent and favours strong easterly or north-easterly flows.

For the winter season, CP3 (Figure 3.4.d) and CP4 (Figure 3.4.e) are the most frequent patterns in triggering extreme discharge events. CP3, representing 170 days, is characterized by a dipole-like pattern, with a negative anomaly centre situated over

the Scandinavia and western part of Europe and a positive anomaly centre over the southern part of Europe. This kind of pattern favours the advection of maritime air masses from the ocean during winter, which is associated with intense precipitation over the western part of Europe and hence with high discharges over Elbe's catchment area. A similar pattern has been identified by Kingston el al. (2006) which showed that high flow in the northern European rivers is associated with a stronger and more north-easterly Icelandic Low and/or Azores High.

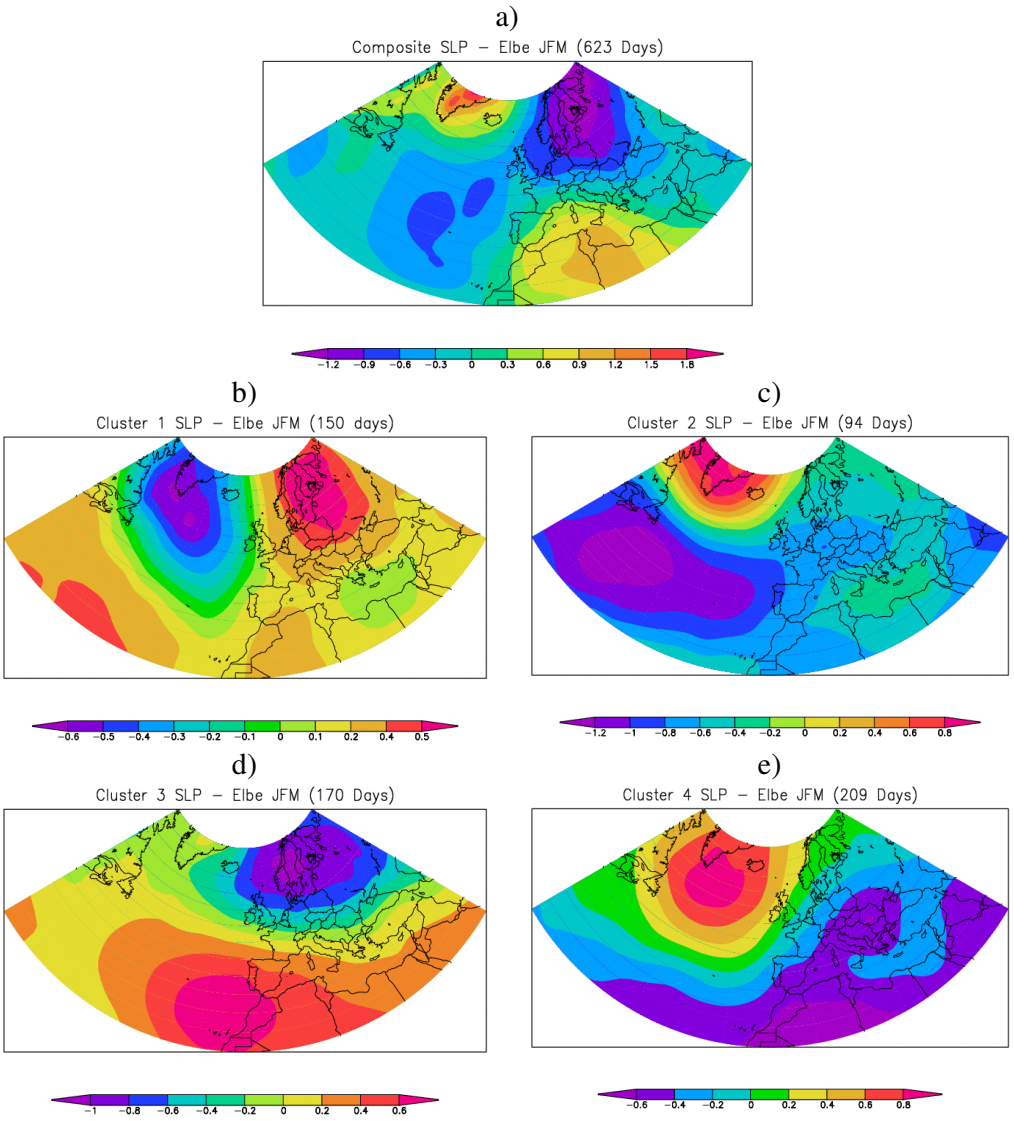

Figure 3.4 The composite map (a) and the four circulation types (b-e) associated with extreme discharge events for JFM (the values are plotted in standardized anomalies) JFM discharge threshold > 1900 m^3/s

CP4, which shows up in 209 days, is characterized by a vast negative anomaly located over the southern Europe which extends over the north-east Atlantic towards the Azores and a positive anomaly centre situated over the northern part of Atlantic

and Greenland. This type of pattern, with a strong gradient located close to Elbe catchment area, causes strong north-easterly flows which bring cold air and intense precipitation which can be either snowfall or rain. A pattern similar to CP4 was identified by Bednorz (2007), which found that heavy snowfall events over the northern part of Germany and north-western part of Poland are caused by a circulation pattern similar to CP4.

3.4.2 Spring circulation patterns

During spring the frequency of the four circulation patterns is almost the same. The composite map (Figure 3.5.a) for the 634 days with discharges above 1650 m^3/s, is associated with a strong negative anomaly over Europe which extends also in the eastern part of the Atlantic Ocean and a positive anomaly centred over Greenland. This type of pressure system causes strong north-easterly winds which can cause intense precipitation over Elbe's catchment area.

CP1 (Figure 3.5.b), which is associated with 158 days of extreme discharge events, has a dipole-like structure with negative anomalies over Greenland and Atlantic Ocean and positive anomalies over southern part of Europe. This type of circulation is associated with south-westerly winds, which carry warm and humid air towards the continent, causing rainfall and high discharges.

CP2 (corresponding to 139 days) resembles the pattern of the composite map, the main difference being the location of the centre of negative anomalies, CP2 (Figure 3.5.c) having a strong negative anomaly centred over Scandinavia.

The third type of circulation (Figure 3.5.d), associated with 158 days, has a strong negative anomaly over the Mediterranean region and southern Europe and a strong positive centre over Scandinavia. The negative anomaly over Mediterranean region is associated with easterly winds which can carry humid air from the Mediterranean Sea and Black Sea towards central Europe.

In case of CP4 (Figure 3.5.e) high discharge events are associated with strong negative anomalies which extend from the central Atlantic towards central Europe and a positive anomaly over Greenland. The easterly or south-easterly flow associated with this kind of circulation brings warm air from southern part of the continent and cold air form the north, which can cause episodes of heavy precipitation, especially over the gradient area where Elbe's catchment is also located.

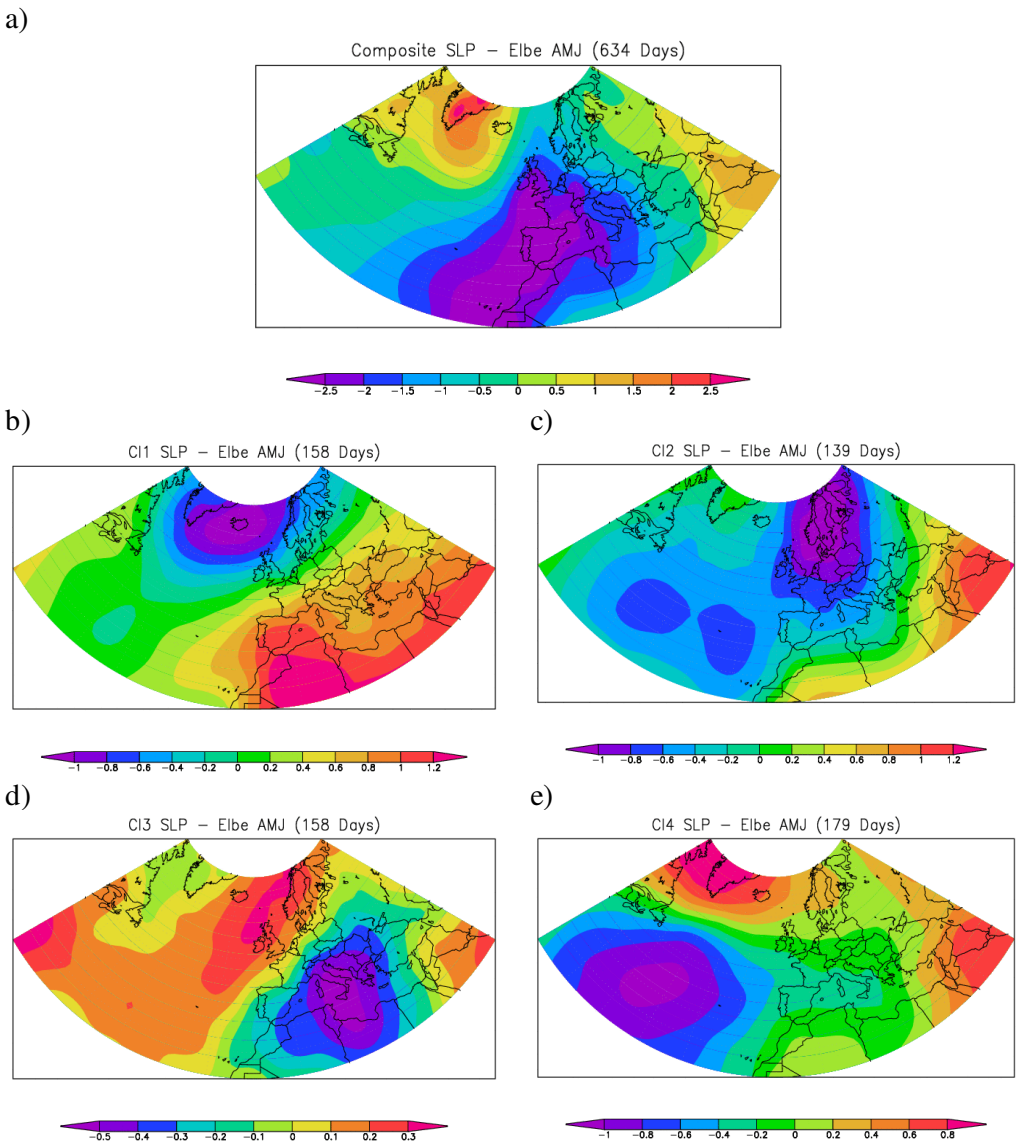

Figure 3.5 As in Figure 3.4, but for AMJ.
AMJ discharge threshold > 1650 m^3/s

3.4.3 Summer circulation patterns

The circulation patterns that control the extreme discharge events in summer are shown in Figure 3.6. The composite map (Figure 3.6.a) associated with the 974 days with discharges above 850 m^3/s, is associated with a centre of negative pressure anomalies over the Mediterranean regions and the southern part of Europe and positive pressure anomalies over the Scandinavian region. This kind of pattern favours north-easterly winds, which carry cold air form the northern part of Europe

which in connection with the warm and moist air carried form the Mediterranean region leads to intense convective precipitation events, especially in summer. The circulation patterns with the highest frequency for summer extreme discharge events are patterns two and three, respectively.

CP1 (Figure 3.6.b), associated with 144 days, has a strong and intense positive anomaly in the SLP field situated over central Europe and a strong negative centre situated in the central Atlantic Ocean. There is an inflection point just north-east of Germany, which can imply fronts towards Germany. Although this king of pattern is normally associated with dry and hot temperatures and also with droughts over central and southern part of Europe, it can induce also heavy precipitation and flash floods, mostly from convective precipitation.

CP2 (Figure 3.6.c) resembles the negative phase of summer North Atlantic Oscillation (NAO). This pattern implies strong negative anomalies over Europe with extension over the central Atlantic Ocean and positive anomalies centred over Greenland. A similar pattern was found by Cassou et al. (2005), which found that this pattern inhibits the occurrence of extreme hot days over Europe.

CP3 (Figure 3.6.d) resembles the summer blocking pattern (Cassou et al. 2005; Yiou et al., 2008), but in our case the positive centre anomaly is shifted towards south-west over the Atlantic region and British Isles. This pattern shows a strong positive anomaly from the Atlantic Ocean extending towards Scandinavia and strong negative anomaly over south-eastern part of Europe. This blocking pattern yields an anticyclonic circulation over the British Isles and the north-western part of Europe. Although this kind of pattern is usually associated with European droughts and heatwaves (Cassou et al., 2005; Fisher et al., 2007), yet it can produces also floods, throughout episodes of convective precipitation (Yiou et al., 2008).

CP4 (Figure 3.6.e), which has the lowest frequency of occurrence (115 days), yields strong negative anomalies over Scandinavia and the northern part of Europe and positive anomalies over the southern part of Europe. Usually this king of pattern is associated with easterly winds and intense precipitation.

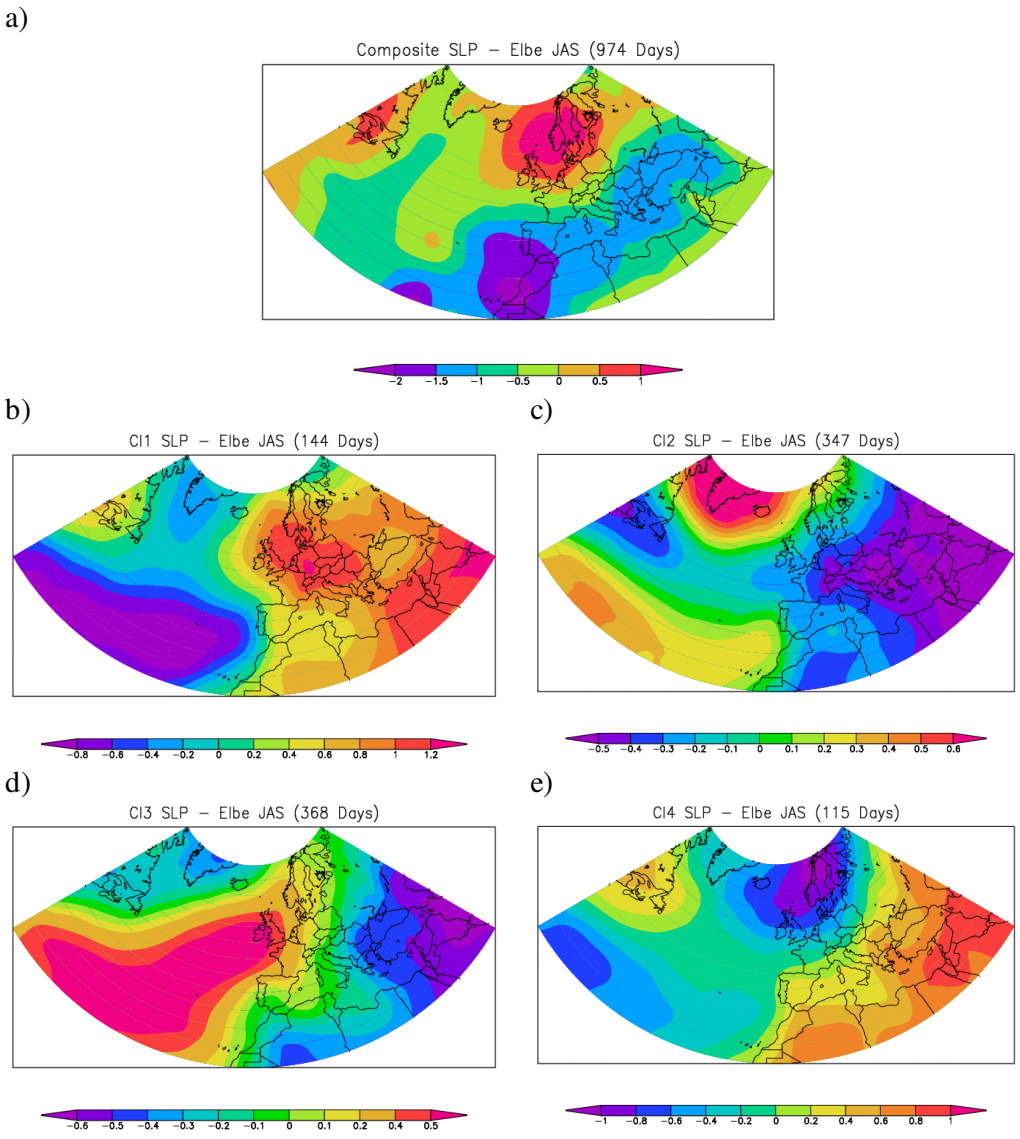

Figure 3.6 As in Figure 3.4, but for JAS.
JAS discharge threshold > 850 m^3/s

3.4.4 Autumn circulation patterns

For autumn the frequency of the four circulation patterns is almost the same. The composite map (Figure 3.7.a) for the 1195 days with discharges above 1000 m^3/s, resembles the positive phase of the Scandinavian pattern (Barnston and Livezey, 1987), which consists of a very strong positive anomaly situated over Scandinavia and weaker centres of opposite sign over western Europe and eastern Russia/western Mongolia. The positive phase of the Scandinavia pattern is associated with above-average precipitation across central and southern Europe and below-average precipitation across Scandinavia.

The first CP (Figure 3.7.b) for autumn (284 days) favours a cyclonic circulation over the north-western part of Europe and induces south-westerly winds. CP2 (Figure 3.7.c) resembles the composite map, yielding north-easterly winds associated with the transport of cold air from the north. This pattern can be associated with a stationary front, which in turn can cause intense precipitation, especially over the catchment area which is situated over the region with a strong gradient.

CP3 (Figure 3.7.d) and CP4 (Figure 3.7.e) are associated with strong negative anomalies over the Scandinavian region and positive anomalies over southern part of Europe. In the case of CP4 there is another positive centre located over Greenland. Both CPs lead to north-westerly flows and the advection of humid air from the ocean.

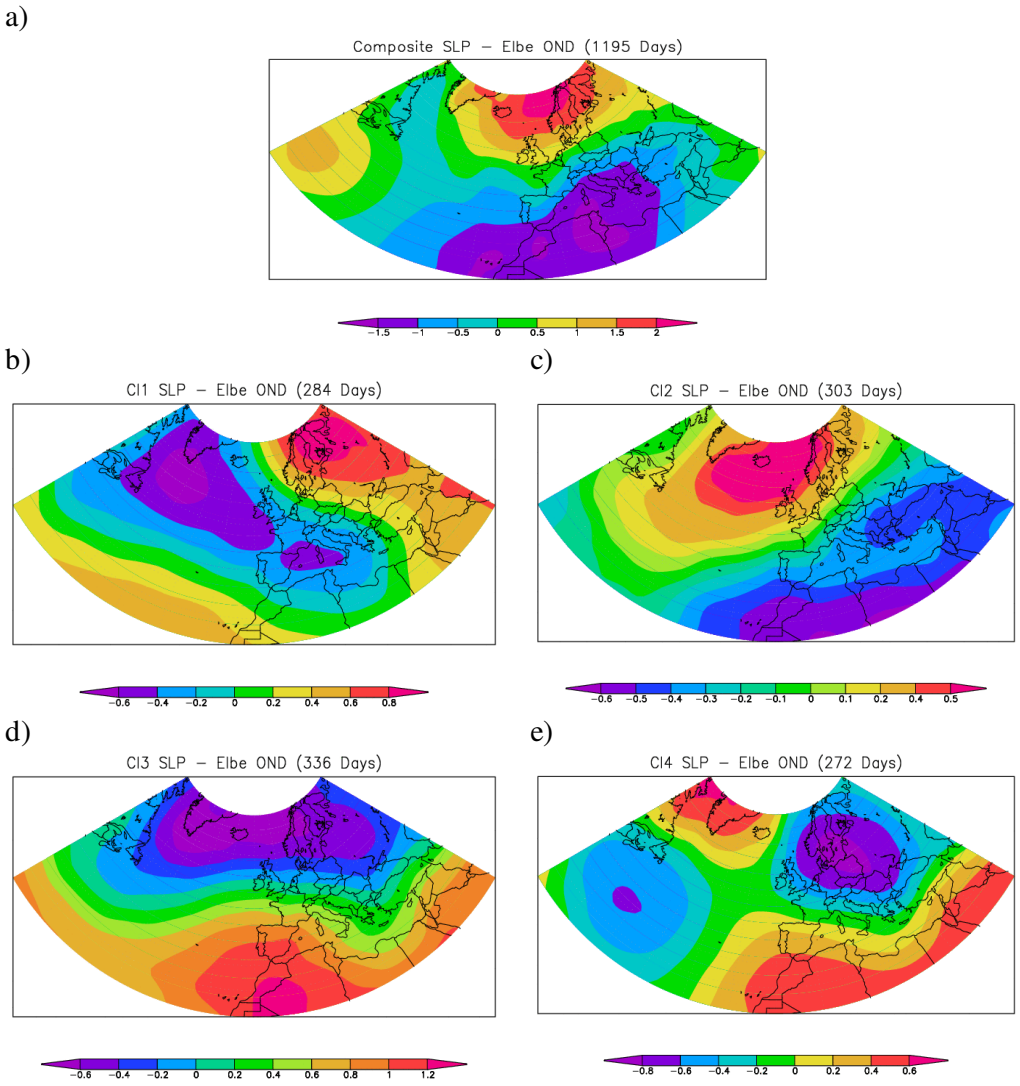

Figure 3.7 As in Figure 3.4, but for OND.
OND discharge threshold > 1000 m^3/s

3.5 Discussions

As explained in section 3.2, the classification of the main large-scale atmospheric patterns, associated with extreme events, yields four different clusters for each season. Our intention is not to relate the extreme events with some particular large-scale atmospheric phenomena, like NAO or the El-Nino Southern Oscillation (ENSO), but to try to show which are the main large-scale atmospheric conditions associated with extreme events in Elbe's streamflow.

The main circulation patterns, which are responsible for triggering extreme discharge events in the Elbe's catchment area, were identified by making use of the k-means cluster analysis method applied to the SLP field over the North Atlantic – European domain. Each pattern is defined by the normalized anomalies of the atmospheric conditions that prevailed 1 up to 7 days prior to an extreme event.

The results from this study indicates that for winter the most prominent circulation patterns which causes extreme discharge events are the ones associated with a strong negative centre above northern Europe and Scandinavia associated with north-westerly winds. Jacobeit el al. (2006) found a similar pattern associated with prominent discharge events in central Europe. High extreme events are also generated by a circulation pattern which has a strong positive anomaly situated over the eastern part of Greenland and a strong negative anomaly centred over the southern part of Europe, which triggers strong north-easterly winds which carries cold air. For both cases the catchment of Elbe's river is situated on the pressure gradient between the positive and negative centres.

For spring all patterns have a similar occurrence rate. There is no clear distinction between the frequencies of the circulation patterns, each of them having more or less the same influence on the extreme events. The composite map and CP emphasize a strong negative anomaly over Europe, associated with cyclonic circulation. CP3 and CP4 are associated with easterly flows.

Extreme discharge events, during summer, are associated mainly with two circulation patterns. The first pattern resembles the negative phase of summer NAO (Yiou et al., 2008; Cassou et al., 2005) and the second pattern is similar to the blocking pattern identified by Cassou et al. (2005). The first pattern is associated with a cyclonic circulation which covers most part of Europe. The blocking pattern identified in Elbe's case is shifted towards south-west over the Atlantic. This pattern render an anticyconic circulation over the British Isles and north-western part of Europe, but it can also produce intense convective precipitation episodes and flash floods, especially when this episodes take place at the end of a heat wave (Yiou et al., 2008).

The composite map of autumn and the second CP which trigger extreme discharge events resembles the positive phase of the Scandinavian pattern, yielding a strong positive SLP anomaly over Scandinavia which extends towards Greenland and a strong negative centre over the Mediterranean region, which favours easterly winds and high discharges over the northern part of Europe. CP3 and CP4 are favourable to cyclonic circulation and north-westerly winds and to the advection of humid air from the ocean.

3.6 Conclusions

In this study we have investigated the behaviour of extreme events occurring in the daily values of the Elbe river streamflow and the circulation patterns associated with these extremes. We have applied the POT approach to the seasonal daily times series of Elbe's discharge. The aim was to identify the threshold at which an event can be considered as an "extreme" and to analyze the shape of the distribution. Testing the mean residual plot and the assessment of the stability of parameter estimates, different thresholds are identified for each season, which are situated between the 90% and 95% percentile of the time series.

The results indicate that for winter, spring and fall the times series have normal tail behaviour, meanwhile for summer the distribution has heavy-tail behaviour, summer being more exposed to the occurrence of extreme events compared to the other seasons. These findings were confirmed by analyzing the Q-Q and P-P plots, which were almost linear for all seasons, indicating that the chosen model (GPD) fits well our data sets.

The return periods, derived based on the return level plots, might be used as a measure of safety when taking into account the construction and design of river dams (Leonard et al., 2008). Since the tail of the distribution is normal for winter, spring and fall, the band of errors is not too large for return periods above 10 years. For summer, the corresponding heavy-tail distribution induces large biases for return periods above 10 years. Although summer is usually characterized by low flows in the case of Elbe river, the highest values for the 100 years return period was identified for this specific season. One explanation for these results might be that extreme events in summer are mostly associated with heavy rain episodes and the values of the discharge are growing rapidly, reaching very high values. We have also to take into account that the tail of the distribution, for summer, has a heavy-tail behaviour and that induces high errors for the return periods above 10 years.

From our analysis we can conclude that the behaviour of Elbe daily streamflow is well statistically modelled by the General Pareto Distribution and that distinct circulation patterns are responsible for triggering extreme discharge events for different seasons. We expect that a seasonal analysis of extreme events will yield a deeper understanding of catastrophic floods along the Elbe river. Historical data may also help to estimate trends in the occurrence of extremes (Muddelsee et al., 2003).

Chapter 4

Prediction of spring Elbe discharge based on stable teleconnections with winter global temperature and precipitation

4.1 Introduction

One of the most difficult issues of hydrology is how to appreciate the seasonal variability of rivers discharge. Water is a vital resource for human as well as natural ecosystems. It has been established that changes in the cycling of water between land, sea and air can have significant impacts on the environment, economy and society through their effects on the water resources and their management (Arnell, 1995, 1999; Arnell and Reynard, 1996). The availability of water is greatly influenced by climate conditions that vary on seasonal, interannual, and decadal time scales. Characterisation of hydrological variability on climatic timescales and identification of connections to climate forcings provide potential improvement for hydrological forecasts when these forcings are predictable or slowly evolving (Souza and Lall, 2003; Croley, 2003).

Over the last years, interest in seasonal predictability of river discharge variability over Europe has increased markedly (Trigo et al., 2004; Rimbu et al., 2004; Rimbu et al., 2005). On seasonal timescales, anomalous atmospheric conditions are often linked with seasonal variations in the rivers streamflow, via variations in precipitation and temperature (Dettinger and Diaz, 2000; Cullen et al., 2002). For example, spring and summer rainfall and temperature anomalies across Europe may be forecasted from prior knowledge of varying boundary conditions such as anomalous sea surface temperature in the North Atlantic (Colman, 1997; Colman and Davey, 1999; Wilby, 2001) and/or the tropical Pacific (Kiladis and Diaz, 1989; Lloyd-Hughes and Saunders, 2002; van Oldenborgh et al., 2000). Spring precipitation over central Europe is higher than normal average following warm El Niño events combined with lower SSTs west of Ireland (Lloyd-Hughes and Saunders, 2002). Predictability is found to be higher in El Niño-Southern Oscillation (ENSO) extreme years (Branković and Palmer, 2000), implying that at least part of the available skill can be attributed to the forcing from the tropical Pacific Ocean.

Two of the most important phenomena that influence streamflow variability are the North Atlantic Oscillation (NAO) and ENSO (Dettinger and Diaz, 2000; Cullen et al., 2002). The indices of these large-scale climatic patterns are used as predictors for seasonal streamflow anomalies over Europe (Rimbu et al., 2005, Cullen et al., 2002, Trigo et al., 2004). Significant lag-correlations were identified between NAO index and several river streamflow anomalies from the Iberian Peninsula (Trigo et al., 2004) and Tigris-Euphrates streamflow anomalies (Cullen et al., 2002). Rimbu et al. (2004) found significant lag-correlation between NAO and ENSO indices and Danube streamflow. However, the association between NAO and ENSO and streamflow from the Iberian Peninsula (Trigo et al., 2004) and from south-east Europe (Rimbu et al., 2004; Cullen et al., 2000) is non-stationary, i.e. the strength of the correlation between these two phenomena and streamflow anomalies

has changed over time. These teleconnection patterns, though dominant on a large scale, often fail to provide forecast skill in individual basins (McCabe and Dettinger, 2002; Grantz et al., 2005). The predictability of precipitation and streamflow from Europe using NAO and ENSO as predictors is limited due to non-stationarity. One way to improve the seasonal forecast for streamflow would be to identify stable predictors.

This chapter describes a forecasting scheme for spring Elbe streamflow based on **stable** lag-correlation with temperature and precipitation indices. It is shown that when climate indices from key regions are used together as predictors, the forecast improves compared to the case when they are used separately.

4.2 Data and methodology

4.2.1 Data sets description

The monthly time series of Elbe discharge, used in this chapter, were computed from the daily values of the river streamflow (see Chapter 3.2) The hydrological discharge regime is characterized by a pronounced seasonal cycle the rising limb of which is situated between January and April and the falling one between June and September, the highest values being recorded in April. These high discharge values recorded in the spring months may be related with the melting of the snow in the catchment area and the soil humidity.

Taking into account that the highest discharge values are recorded in the spring season (Figure 4.1 - upper right), we focused our analysis on this specific season (March/April/May). The spring Elbe streamflow for the period 1902-2001 is presented in Figure 4.1. It shows strong interannual and decadal variations. The strongest positive discharge anomaly during the analyzed period occurred in the 1940-1942, a period dominated by strong climate anomalies (Brönnimann et al., 2004; Brönnimann, 2007).

From the monthly time series we computed the seasonal spring mean, by averaging the months March/April/May (MAM). From the seasonal means we calculate the seasonal anomalies against the mean over the period 1902-2001. The time series was detrended and normalized by the corresponding standard deviation to obtain normalized anomalies of Elbe streamflow for MAM.

As large scale predictors we used the following data sets:

a) The SST was taken from the Kaplan data set (Kaplan et al., 1998). This data set has a resolution of 5ºlat x 5ºlon and covers the period 1901-2001. We used the winter SST field - December/January/February (DJF). The time series were detrended and normalized by the corresponding standard deviation to obtain normalized anomalies of SST for DJF.

b) The temperature (TT) and precipitation (PP) was taken from CRU (Climatic Research Unit) TS2.1 data set (Mitchell et al., 2003). The data sets have a 0.5º x 0.5º horizontal resolution and cover the period 1902-2001. The same data processing was used as for SST.

c) We also used the time series of the monthly teleconnection indices described in Table 4.1. The seasonal values of these indices were calculated using the same methodology as for the Elbe streamflow data, but for the winter season (DJF).

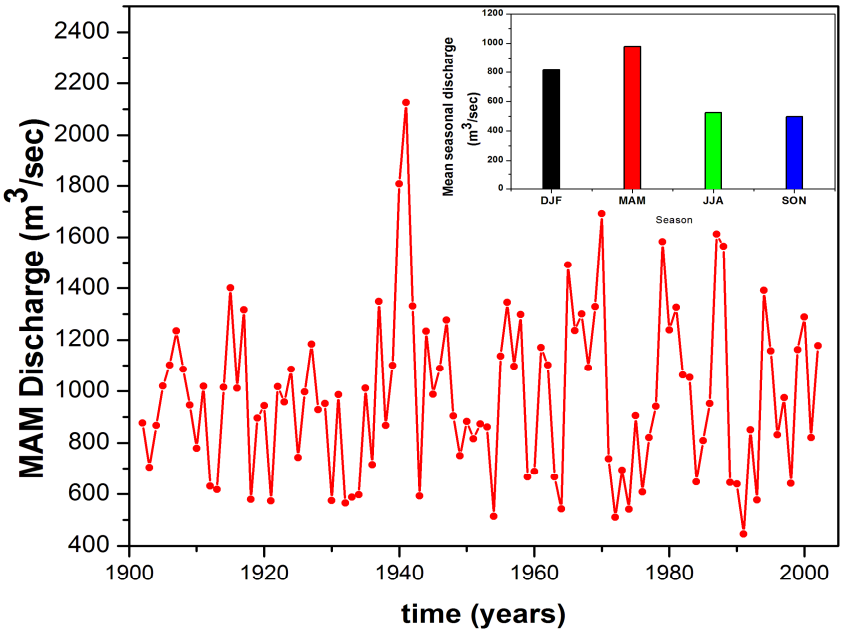

Figure 4.1 The time series of MAM Elbe discharge recorded at Neu Darchau (53° 14′ N, 10° 53′ E) for the period 1902-2001 and the seasonal mean discharge of Elbe (upper-right). Units are $m^3 s^{-1.}$

Large-scale sea level pressure (SLP) patterns associated to the river streamflow variability are based on the updated version of the SLP data set constructed by Trenberth and Paolino (1980). This data set has a 5ºlat x 5ºlon resolution.

Table 4.1. Teleconnection indices used in this study, time period and their source

Name	**Explanation**	**Period**	**Data source**
EA	East Atlantic	1950-2001	http://www.cpc.noaa.gov/data/teledoc/ea.shtml
EA/WR	East Atlantic/Western Russia	1950-2001	http://www.cpc.noaa.gov/data/teledoc/eawruss.shtml
NAO	North Atlantic Oscillation	1902-2001	http://www.cru.uea.ac.uk/cru/data/nao.htm
NINO 3.4		1902-2001	http://ingrid.ldgo.columbia.edu/SOURCES/.Indices/.nino/.KAPLAN/
POL	Polar/Eurasia	1950-2001	http://www.cpc.noaa.gov/data/teledoc/poleur.shtml
SCA	Scandinavia	1950-2001	http://www.cpc.noaa.gov/data/teledoc/scand.shtml

4.2.2. Stability criteria and stability maps

For the forecast scheme all the data sets were separated into two parts: a) the calibration period (1902-1971) and b) the validation period (1972-2001).
The forecast scheme for seasonal prediction of spring Elbe streamflow anomalies using SST, TT and PP from previous winter is based on a methodology similar to that used for seasonal prediction of Danube streamflow (Rimbu et al., 2005). The basic idea of this scheme is to use SST, TT and PP anomalies from regions with stable teleconnections as predictors (Lohmann et al., 2005). However, in our study we have used a different criterion to define the stability of the correlation (Lohmann et al., 2005) and we added new predictors, i.e. the anomalies of TT and PP over land, comparative with previous studies (Rimbu et al., 2005). We correlate the spring streamflow anomalies with global SST, TT and PP anomalies from previous winter in a moving window of 31 years. The correlation is considered to be stable for those grid-points where spring streamflow and winter SST, TT or PP anomalies are significantly correlated at 90% level (r=0.24) or 80% level (r=0.17) for more than 80% of the 31-year windows covering the period 1902-2002. The regions where correlation is positive and stable at 90% (80%) level will be represented as red (orange) on a global map. The regions where correlation is negative and stable at 90% (80%) level will be represented as blue (violet). Such maps will be referred to in our study as stability correlation maps. The stability correlation maps derived in our study remain qualitatively the same if the significance levels that define the stability of the correlation vary within reasonable limits.

To better understand how the correlation stability maps are constructed we present as an example the decadal variation of the correlation between spring Elbe streamflow and SST anomalies from several grid points (Figure 4.2). The spring streamflow and winter SST from (140.5°W, 10.5°N) grid point are positively correlated for all 31-year windows covering the period 1901-2002 and above the 90% significant level for more than 80% windows. The streamflow and SST from the grid point (70.5°E, 5.5°N) is positive and above 80% significance level for more than 80% windows (Figure 4.2). Therefore, these grid points are stable correlated with streamflow and are represented on the stability map of correlation as red and orange, respectively (Figure 4.3.a).

The spring streamflow and SST from the grid points (70.5°W, 30.5°N) and (170.5°E, 40.5°N) are negative and above 90% and 80% significance level, respectively, for more than 80% windows. Also these grid points are stable correlated with streamflow and are represented on the stability correlation map as blue and violet, respectively (Figure 4.3). On the contrary, the streamflow and SST from the grid point (55.5°W, 10.5°N) are significantly correlated for less than 80% windows, and therefore the correlation is unstable according to our criteria. Such a grid point appears in white colour on the stability map of correlation (Figure 4.3).

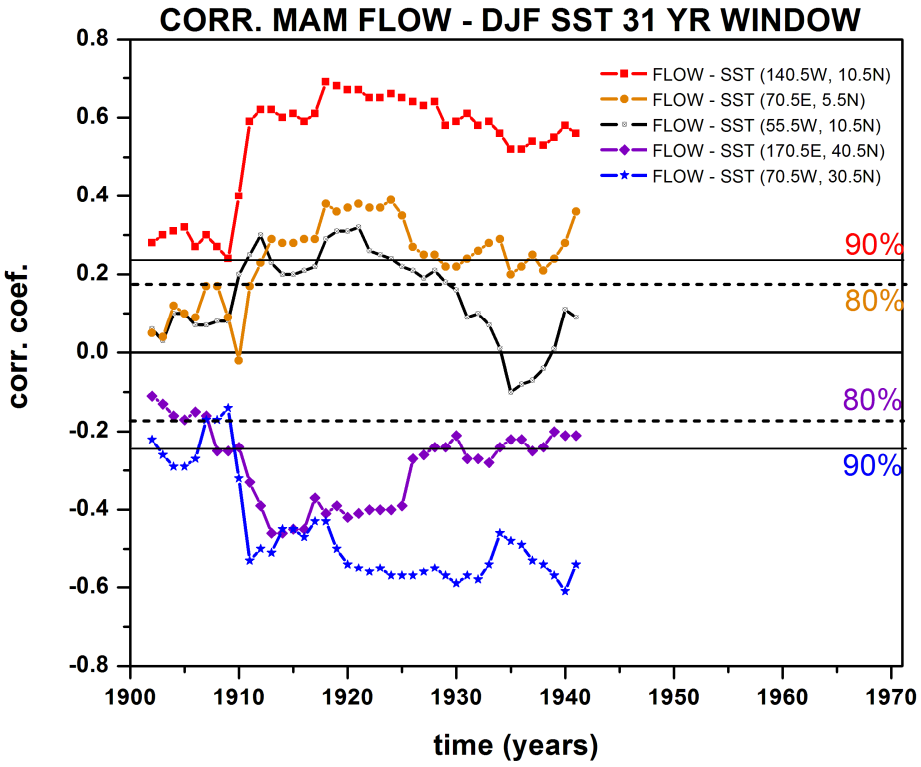

Figure 4.2 Running correlation (31 year window) between spring flow and winter SST anomalies from the grid points indicated in the upper-right corner of the figure. The correlation is plotted at the beginning of each 31-year window. The first points represent the correlation between spring flow from 1902-1933 and SST from 1901/1902-1932/1933.

4.2.3 Model evaluation

Several methods are common to assess the skill of forecast models (i.e. Wilks, 1995; von Storch and Zwiers, 1999). We employ the percentage improvement in the root-mean-square error over a climatological forecast ($RMSE_{cl}$) and over persistence ($RMSE_{per}$). The RMSE skill measure is one of the most robust. Climatology is taken as the standardized long-term average prior to each year being forecasted, while persistence is taken as winter (DJF) Elbe streamflow standardized anomalies. We computed the skill score S (Wilks, 1999), defined as:

$S = 1 - \frac{RMSE(forecast)}{RMSE(reference\ forecast)}$, where the reference forecast is either climatology or persistence.

The skill score is one for perfect forecasts, zero for forecasts no better than the reference forecast and is unbounded below zero for forecasts that are worse than the reference forecast.

4.3 Stable teleconnections of the Elbe streamflow

4.3.1 Sea surface temperature

The stability correlation map between spring streamflow and winter SST (Figure 4.3) emphasizes several stable regions during the period 1902-1971. The spring streamflow is stable correlated with winter SST anomalies from parts of the central and eastern Pacific, several regions of the North Atlantic, the west coast of Europe, the eastern Mediterranean and the Red Sea. Consistent with this result, significant positive correlations between ENSO indices and river flow from Europe (Dettinger and Diaz, 2000; Rimbu et al., 2004) as well as precipitation over Europe (Mariotti et al., 2002) were identified.

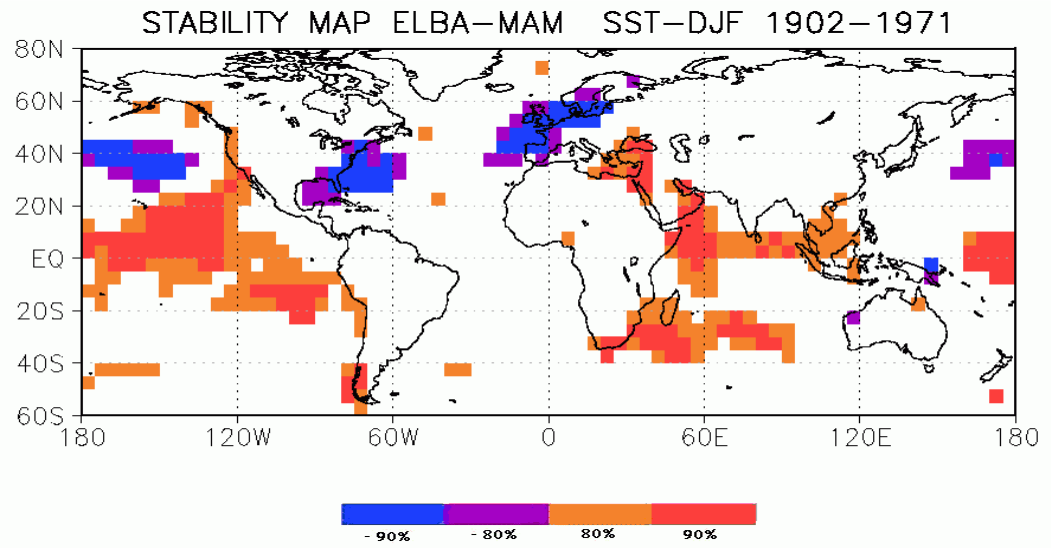

Figure 4.3 The stability map of the correlation between spring flow and winter SST anomalies. Regions where the correlation is stable, positive and significant at 90% (80%) level for at least 80% windows are shaded with red (orange). The corresponding regions where the correlation is stable but negative are shaded with blue (violet).

Table 4.2. The coordinates (latitude, longitude) of the winter SST, TT and PP indices used in this study

SST	TT	PP
170.5ºW-125ºW; 5.5ºS-25.5ºN	65.5ºW-45.5ºW; 15.5ºS-5.5ºN	0.5ºE-45.5ºE; 40.5ºN-50.5ºN
170.5ºW-140ºW; 30.5ºN-45.5ºN	165.5ºW-130.5ºW; 60.5ºN-70.5ºN	
85.5ºW-55ºW; 25.5ºN-45.5ºN	90.5ºW-65ºW; 50.5ºN-80.5ºN	
20.5ºW-5ºE; 40.5ºN-50.5ºN	5.5ºW-45.5ºE; 50.5ºN-70.5ºN	
15.5ºW-20ºE; 50.5ºN-60.5ºN	20.5ºE-70.5ºE; 15.5ºN-40.5ºN	
50.5ºE-65ºE; 0.5ºN-20.5ºN	115.5ºE-130.5ºE; 55.5ºN-70.5ºN	
45.5ºE-60ºE; 40.5ºS-20.5ºS		
105.5ºW-85ºW; 25.5ºS-10.5ºS		
25.5ºE-40.5ºE; 30.5ºN-45.5ºN		

We consider that the SST anomalies from these regions represent stable predictors for Elbe spring streamflow anomalies. Based on the stability map we defined 9 SST indices by averaging the normalized SST anomalies for the regions described in Table 4.2 (first column).

The first EOF (see Appendix A for definition) of these indices (Figure 4.4.a) which explains 33.39% of the total variance has a spatial structure consistent with the SST pattern identified in the stability map.

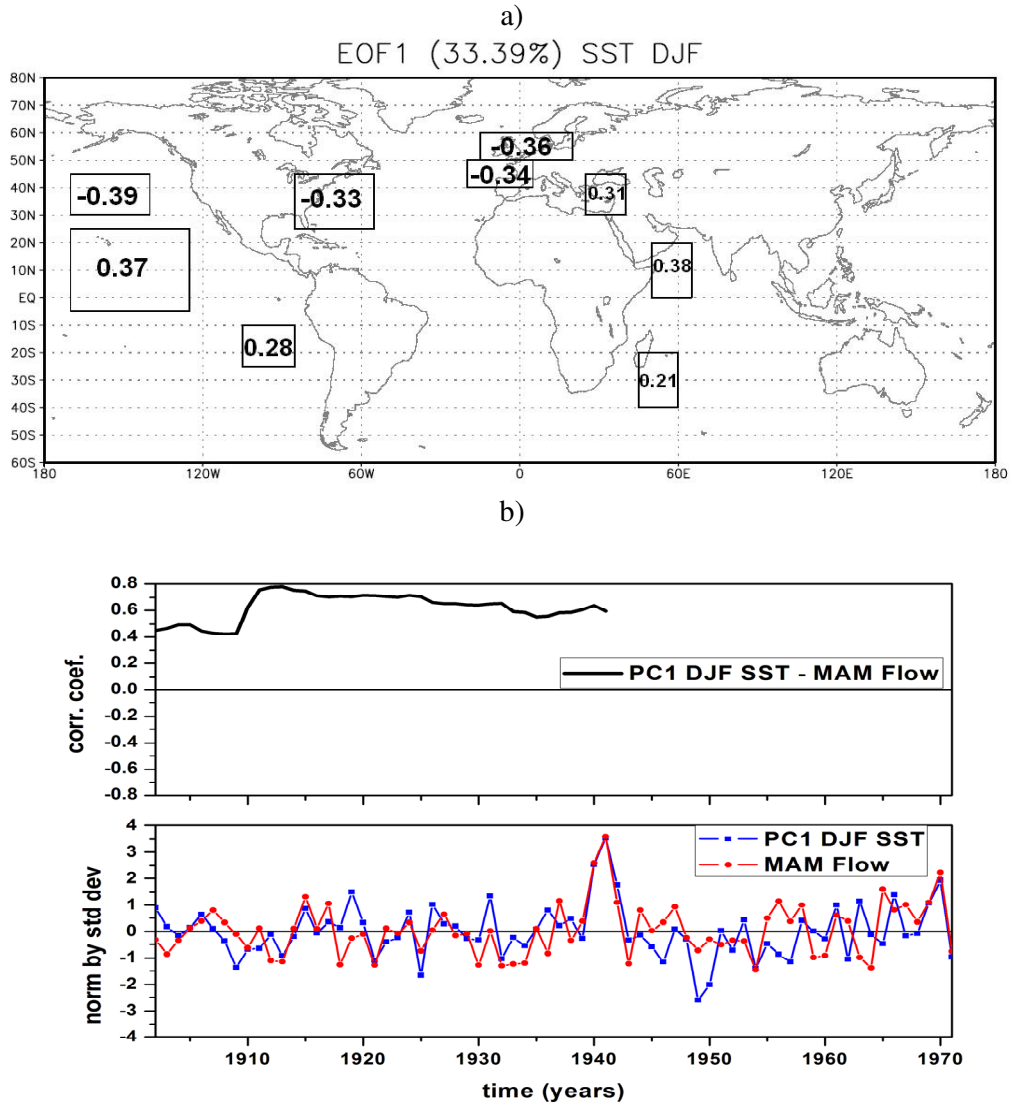

Figure 4.4 a) First EOF of the SST indices (see Table 4.2 for definition) and b) Running correlation (31 year window) between spring flow and PC1 of SST indices (upper panel) and spring flow anomalies (red line) and PC1 (blue line) of winter SST from stable regions.

The correlation between the first time coefficient (PC1) associated to EOF1 and spring streamflow anomalies for a 31-year moving window (Figure 4.4.b - upper part), for the period 1902-1971, is significant at 95% level (following the t-test). The time series of PC1 shows variations similar with Elbe spring streamflow for the same period (Figure 4.4.b - lower part). The correlation between the two time series, over the entire period (1902-1971) is r= +0.56 and is significant at 95% level.

The highest values of spring Elbe discharge during the period 1901 to 2002 are recorded in 1941 (Figure 4.1) which is well predicted by PC1 of winter SST indices as defined above (Figure 4.4.b). This strong positive discharge anomaly can be related to the very strong El Niño event, developing in that period (Brönnimann et al., 2004). Indeed, the SST anomaly map for the 1940/41 winter (Figure 4.5.a) shows strong anomalies in the regions stably correlated with spring streamflow (Figure 4.3). Besides a strong Pacific-North American pattern that accompanies this El Niño event, significant positive sea level pressure anomalies are recorded in the Iceland region as well as negative sea level pressure anomalies over central and eastern Europe including the Elbe region (Figure 4.5.b).

Such a circulation pattern is consistent with high winter precipitation anomalies over the Elbe catchment area during winter. These winter precipitation anomalies, which partly can be snow or ice, are likely to be responsible for the positive streamflow anomalies recorded in spring 1941.

a)

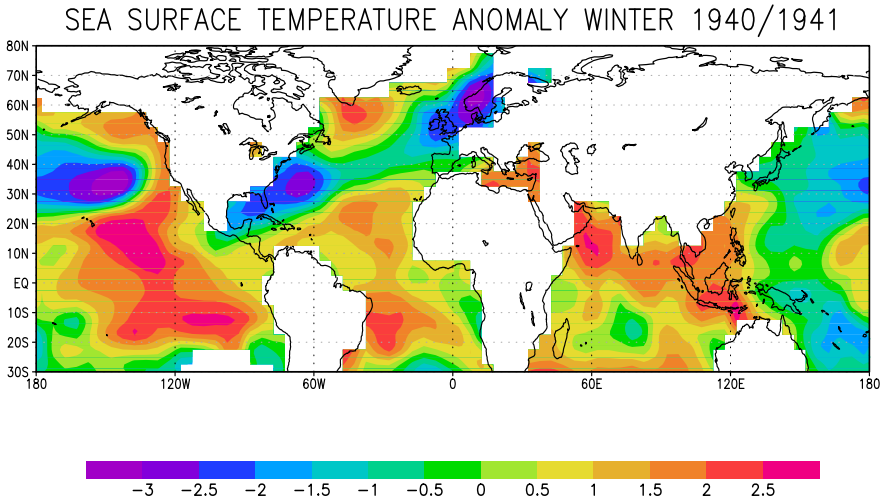

b)

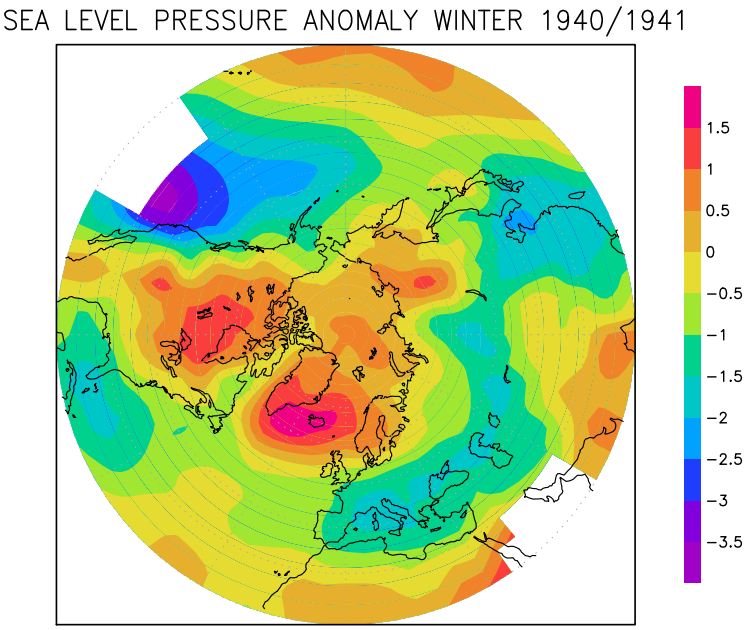

Figure 4.5 a) Sea surface temperature anomalies and b) sea level pressure anomalies for the winter 1940/41. Units ºC and hPa.

4.3.2 Surface temperature over land

The stability correlation map between spring streamflow and winter TT (Figure 4.6) shows stable regions in the Amazonian domain, the northern part of Canada, the central and northern part of Europe, the Middle East and a small part of Siberia. The TT correlation pattern associated with spring streamflow in the Northern Hemisphere projects well on the corresponding pattern associated with NAO, consistent with a strong influence of winter NAO on spring streamflow anomalies in the Europe (Dettinger and Diaz, 2000; Trigo et al., 2004). However, from Figure 4.6

we can see that spring Elbe streamflow is stable correlated not only with NAO-related TT anomalies but also with TT anomalies from other regions. This suggests that other winter phenomena, not necessarily related with NAO, influence the spring streamflow anomalies also. For example, the stable correlation pattern from the northeastern part of South America could be related to ENSO (Marengo, 1992; Ronchail et al., 2002), while those from northern North America could be connected with winter snow cover anomalies (Sobolowski et al., 2007).

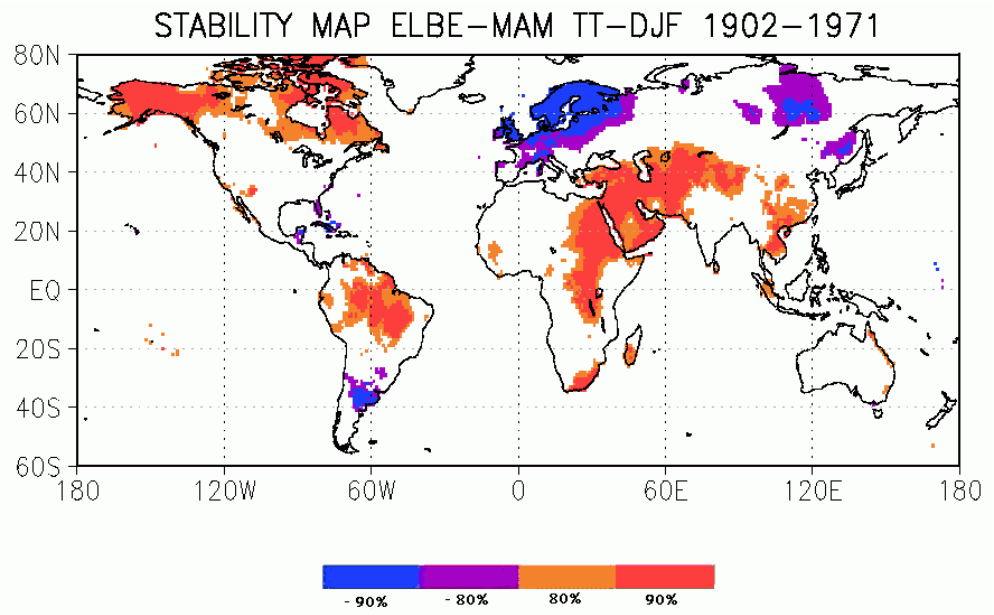

Figure 4.6 As in Figure 4.3, but for TT

Based on the stability map, we defined 6 TT indices by averaging the normalized TT anomalies for the regions described in Table 4.2 (second column). The first EOF computed on the basis of the indices defined above (Figure 4.7.a), which explains 40.20% of the total variance, has a structure coherent with the stability map.

a)

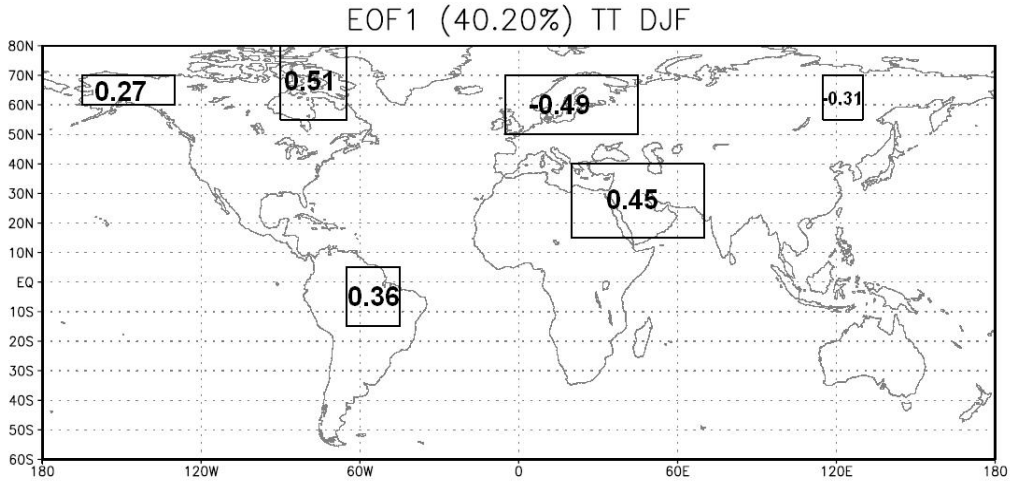

b)

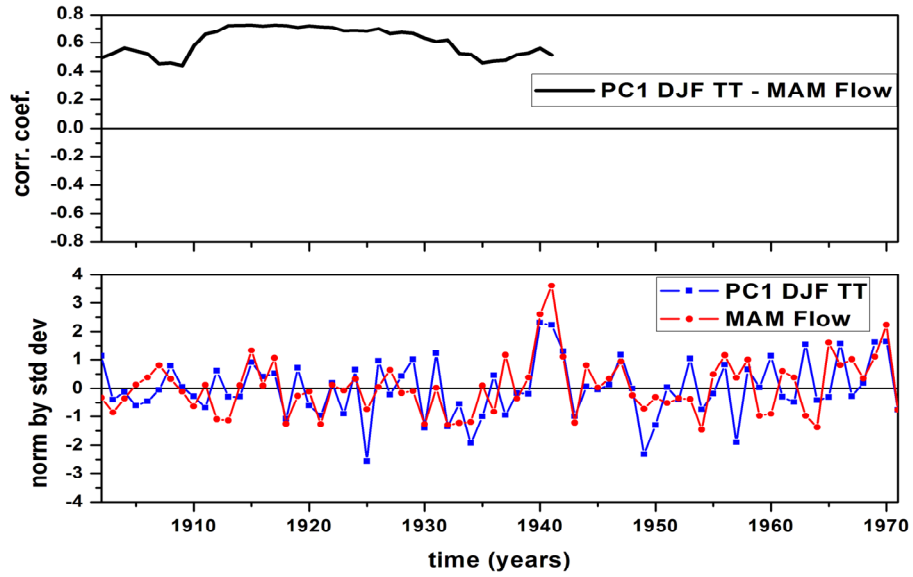

Figure 4.7 As in figure 4.4, but for TT

The correlation between the first time coefficient (PC1) associated to EOF1 and spring streamflow anomalies for a 31-year moving window (Figure 4.7.b - upper part), for the period 1902-1971, is also significant at 95% level. The time series of PC1 and Elbe spring streamflow is shown in Figure 4.7.b - lower part. The correlation between the two time series, over the entire period, is r= +0.54 (significant at 95% level).

4.3.3 Precipitation

For precipitation we identified just one significant stable region (Figure 4.8), which covers most of the central and south Europe. The stable correlation between winter PP anomalies from this region and spring streamflow anomalies of Elbe river is consistent with the strong relationship between PP anomalies and river discharge over Europe (Dettinger and Diaz, 2000). However the region of stable correlation is extended over a broad region of central and Eastern Europe.

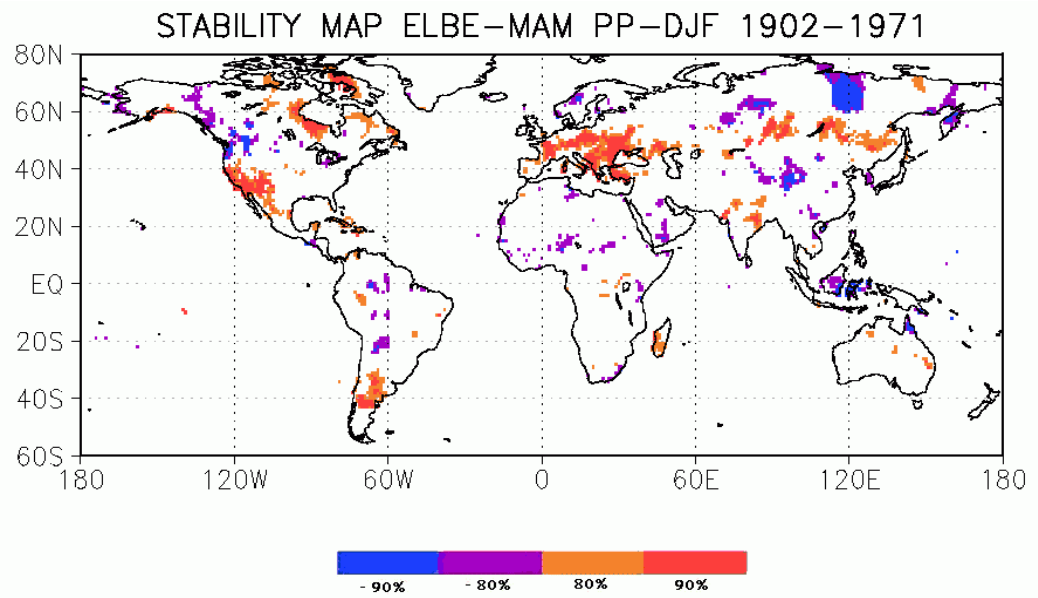

Figure 4.8 The stability map of the correlation between spring flow and winter PP anomalies. Regions with stable correlations are shaded.

The PP anomalies outside the catchment area are not necessarily directly related to spring streamflow anomalies. They can be related to SST or TT anomalies from the regions stably related with spring streamflow anomalies (Figures 4.3 and 4.6). There are also some stable grid points over the west coast of the U.S., but we will focus just on the European region.
The correlation coefficient for a 31-year moving window between MAM streamflow and a precipitation index, defined on the region (0.5ºE-45.5ºE; 40.5ºN-50.5ºN), is shown in Figure 4.9. The correlation coefficient between MAM streamflow and PP index is r= +0.50 during the period 1902-1971.

4.3.4 Combination of indices

To identify the most skilful predictors when considering the forecast scheme, we computed the EOF, taking into account all the indices defined above (SST+TT+PP). Beside the EOF analysis we also tried to develop a forecast model based on linear regression (not shown). We used a step-wise regression model in order to identify the optimal number of indices to be used for the flow prediction. Taking into account that the results using the EOF analysis and the ones obtained using regression were almost similar, we have decided to present just the results for the EOF analysis.

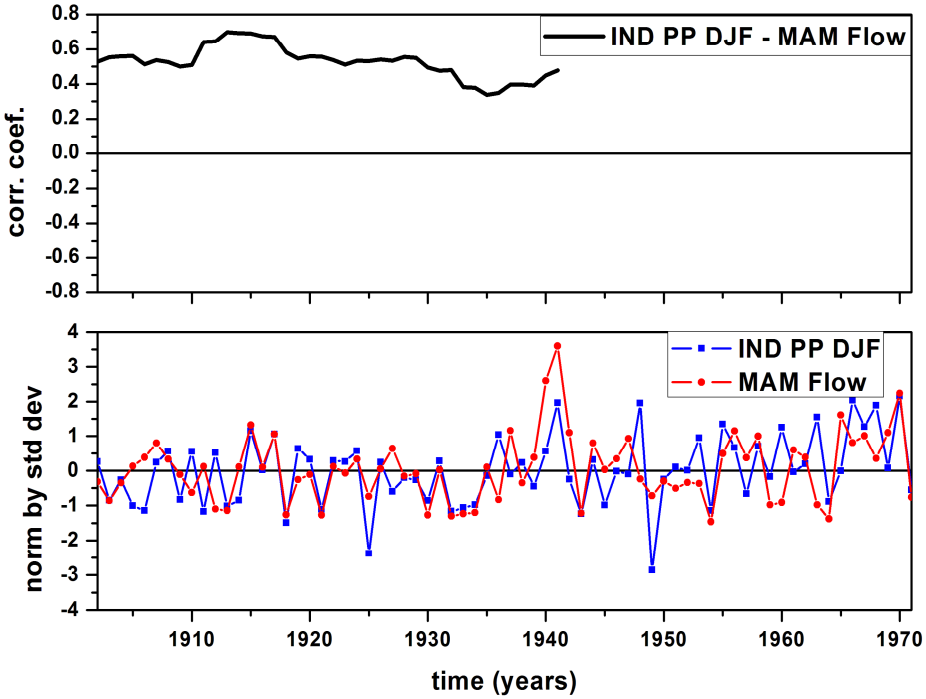

Figure 4.9 Running correlation (31 year window) between spring flow and PP index (see Table II for definition) (upper panel) and spring flow anomalies (grey line) and winter PP index (dark line) from the stable region.

The first EOF (Figure 4.10) explains 35.05% of the total variance. The correlation coefficient for the 31-year moving window between the first time coefficient (PC1) corresponding to EOF1 and MAM streamflow is higher than when considering each index separately (Figure 4.11).

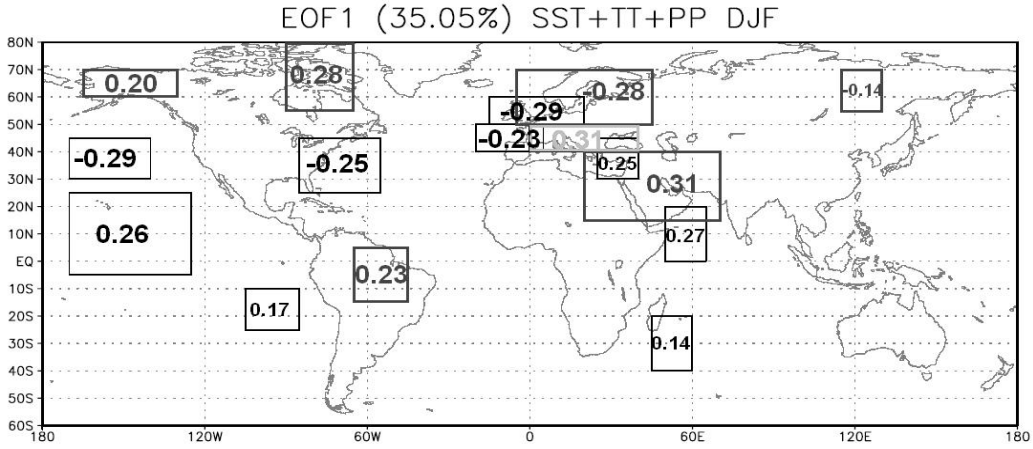

Figure 4.10 First EOF of the (SST+TT+PP) indices identified in Figures 4.3, 4.6 and 4.8 (see Table 4.2 for definition)

The correlation coefficient for the 31 years running window is significant at 95% level, in contrast with the correlation between spring streamflow and winter NAO and NINO indices. The correlation coefficient between spring streamflow and PC1 is 0.59 (Figure 4.11 - lower panel), which is higher than when we considered each predictor separately. The correlation coefficient between spring streamflow and winter NAO (NINO3) index, over the same period, is -0.27 (0.26). Furthermore, the PC1 is also a better predictor than previous winter Elbe discharge (Figure 4.11 - upper panel). We can conclude that PC1 is a better predictor for spring streamflow than winter NAO and Niño3 indices as well as previous winter Elbe discharge, especially when considering SST+TT+PP indices together.

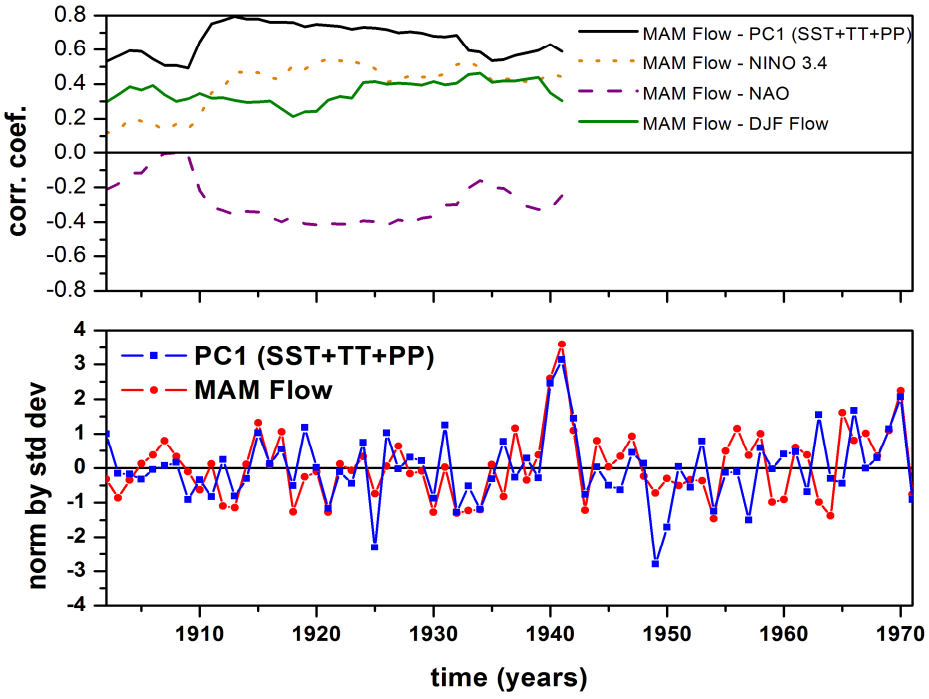

Figure 4.11 Running correlation (31 year window) between spring flow and PC1 of (SST+TT+PP) indices (black line), NAO index (magneta), Niño3 index (orange dotted line) and winter flow anomalies (green line)[upper graph] and the time series of PC1 (blue line) of winter (SST+TT+PP) from the stable regions and spring flow anomalies (red line)[lower graph]

Taking into account that other teleconnection patterns have also been found to have an important impact on the precipitation variability in the European region, we computed the correlation, in a 31-year window (Figure 4.12), between Elbe spring anomalies and other teleconnection indices from the North Atlantic region, such as East Atlantic, East Atlantic/Western Russia, Scandinavian and Polar/Eurasian patterns (Barnston and Livezey, 1987). The influence of these teleconnection patterns on the variability of precipitation and temperature in different regions in Europe was emphasized in different studies (Slonosky et al.,

2001, Goodes and Jones, 2002; Martin et al., 2004; Rodriguez-Puebla et al., 2001; Trigo et al., 2006).

The correlation coefficients between Elbe streamflow and the winter time series of these teleconnection indices are shown in Figure 4.12. For this analysis we used just the period 1950-2001, due to the lack of data before 1950. Like in the case of NAO and NINO3, the correlation is much smaller when compared to PC1. One reason that could explain this is that these teleconnection patterns have weak projection on the precipitation field over the Elbe catchment area.

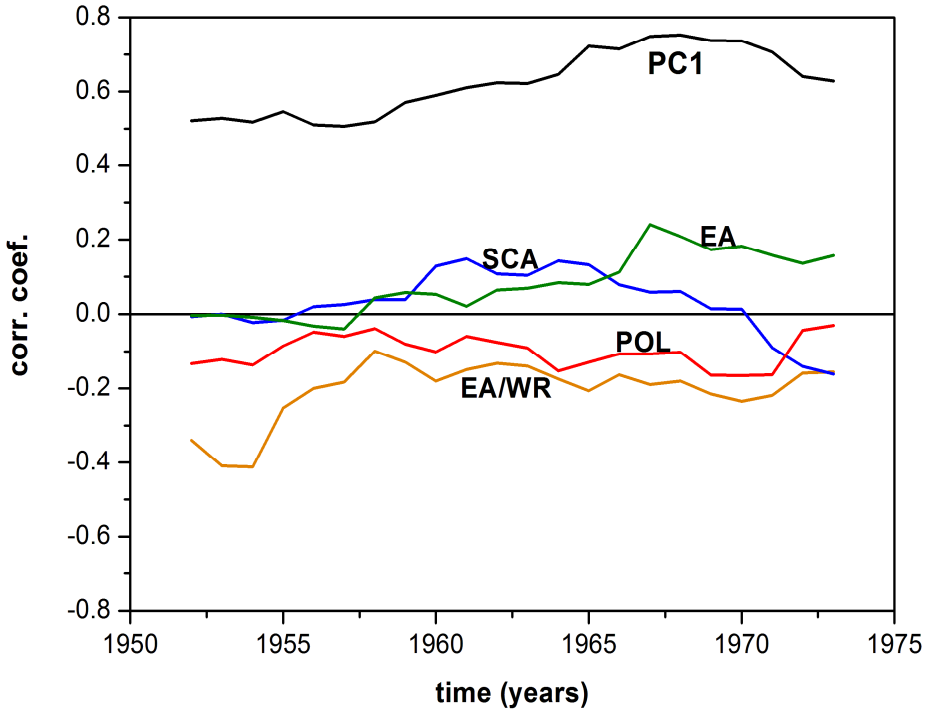

Figure 4.12 Running correlation (31 year window) between spring flow and teleconnection indices from the North Atlantic region.

4.4 Potential predictability

Rimbu et al. (2005) showed that prediction based on SST identified in stable key regions improves compared to prediction based on NAO and ENSO indices.
Assuming that the regions of stable teleconnections established for the period 1902-1971 do not change significantly for the period 1972-2001, we calculate the SST, TT and PP indices for the region defined above and the corresponding PC1 successively, using the data from 1902-1972, 1902-1973….to 1902-2001. The last values of PC1 based on these updated winter SST, TT and PP indices, represent the streamflow anomaly forecast for the next spring. The result of the forecast is represented in Figure 4.13. The predicted and observed spring streamflow anomalies are

significantly correlated (**r = 0.63**). The correlation between predicted spring streamflow anomalies based on winter NAO and Niño3 indices is **-0.16** and **0.17**, respectively. Therefore, the prediction based on our statistical scheme is a marked improvement compared to prediction based only on NAO and Niño3 indices.

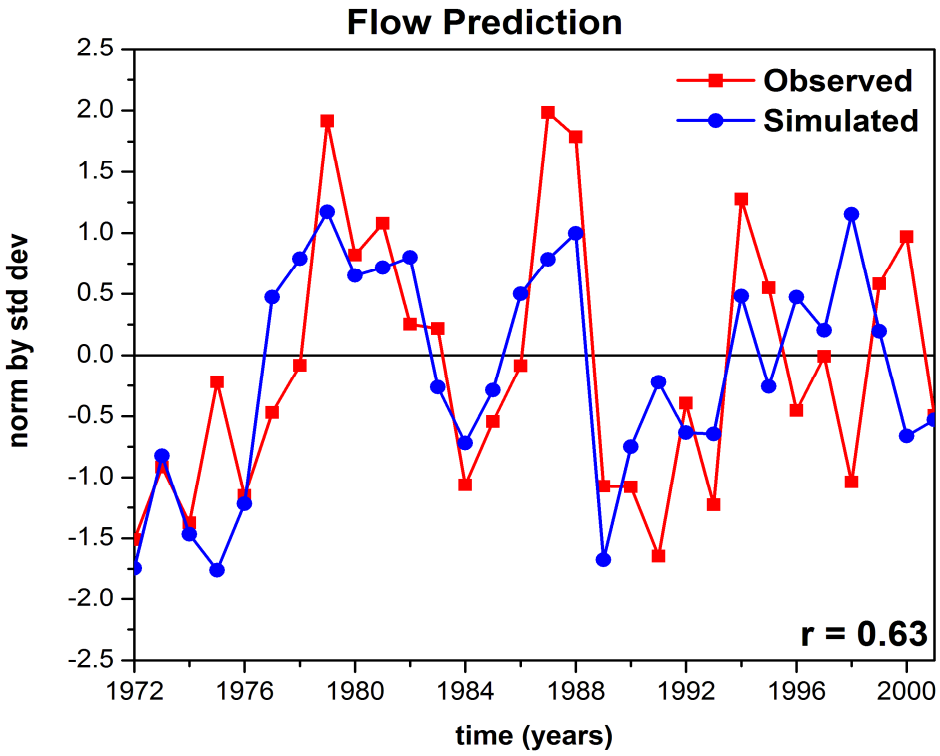

Figure 4.13 Observed (red line) and predicted (blue line) spring flow anomalies for the period 1972-2001 based on winter (SST+TT+PP) anomalies from the stable regions.

To better asses the skill of the forecast, we made use of the RMSE and the skill score (Wilks, 1995). The results of this analysis are shown in Table 4.3. From Table 4.3, it can be seen that although our forecast model is not very accurate, it does exhibit a useful skill that is approximately 20% better than both climatology and persistence. In the case of NAO and Niño3, the skill score shows negative values, which implies that the forecast based on them has less accuracy than climatology or persistence.

Table 4.3. Seasonal forecast skill score measured against climatology (second column) and against persistence (third column)

Predictand	S_{clim}	S_{pers}
PC1 (SST+TT+PP)	0.20	0.21
NAO	-0.51	-0.49
NINO	-0.28	-0.27

4.5 Discussions and conclusions

We have investigated the predictability of spring Elbe streamflow anomalies, using SST, TT and PP anomalies from previous winters as predictors. It appears that the teleconnections with SST, TT and PP are stable over various regions of the globe. Large areas in the central Pacific, North Atlantic, extending to the Red Sea, of winter SST anomalies area are stable correlated with Elbe spring streamflow, which is consistent with previous studies related to the impact of SST anomalies on European climate (Dettinger and Diaz, 2000; Marrioti et al., 2002; Rimbu et al., 2004; Rimbu et al., 2005). Several key regions where MAM streamflow is stably correlated were also identified in the global TT field. Key regions from the northern part of Canada, the Amazonian region, Europe, the Middle East and a small part of Siberia are stably correlated with MAM streamflow. For precipitation the most stable region is the central and northern part of Europe. Therefore, the spring Elbe streamflow anomalies are related not only with regional winter climatic anomalies but also with climate anomalies from several key regions located far from Elbe region. We have shown that the forecast skill improves when these remote predictors are considered in the forecast scheme.

The signal to noise ratio was increased by deriving the first EOF of the SST, TT and PP indices calculated over the stable regions. The corresponding time series (PC1) is then used as a predictor for the streamflow anomalies. We also found that the correlation coefficient increases when we calculate the EOF using all the indices (SST+TT+PP), comparing to the case when we make the analysis separately on each of them. It has been also found that the prediction of spring streamflow anomalies based on the method described above is better than the prediction based on NAO and ENSO.

Winter precipitation in central Europe is mainly influenced by cyclonic activity, carried by the dominant westerlies. During winter season the dominant patterns of climate variability over Europe which produces significant precipitation anomalies are NAO and ENSO (Mariotti et al., 2002; Cullen et al., 2002). However, the impact of ENSO on European climate could be dependent on the strength of the ENSO anomalies (van Loon and Madden, 1981) or on the phases of ENSO. Pozo-Vazquez et al. (2005) showed that the impact of La Niña events on European climate is stronger than the impact of El Niño events. Strong La Niña events during autumn give a detectable signal in winter precipitation over Europe. Such winter precipitation anomalies are likely recorded as Elbe streamflow anomalies in the next spring, consistent with the stable correlation between spring streamflow anomalies and winter precipitation.

The enhanced predictability of spring streamflow can be also related to the relatively high predictability of spring precipitation from winter SST as discussed in recent studies (Oldenborgh et al., 2000; Knipertz et al., 2003). Predictability is found to be higher in El Niño-Southern Oscillation extreme years (Branković and Palmer, 2000), implying that at least part of the available skill can be attributed to the forcing from the tropical Pacific Ocean. Merkel and Latif (2002) suggested that an El Niño-related weakening of the North Atlantic mean meridional pressure gradient and a southward shift of the North Atlantic stormtrack induce wetter conditions over central Europe and the western Mediterranean and colder temperatures over Scandinavia.

Our analysis shows that winter SST, TT and PP anomalies from several key regions provide a significant source of predictability for Elbe spring streamflow. Also a small, but significant potential predictability was detected for summer streamflow anomalies using previous spring SST, TT and PP anomalies from several key regions.

The forecast scheme shows an improvement of about 20% when compared with climatology and persistence and major advantages than the forecast based on different teleconnection patterns. We argue that a skilful prediction, based on stable teleconnections can provide guidance for water management in the Elbe river catchment area, with consequences for economy, agriculture and hydroelectricity.

Chapter 5

Decadal variability of the Elbe river streamflow

5.1 Introduction

Water is a vital resource for human as well as the natural ecosystems. The availability of water is greatly influenced by climate conditions that vary on seasonal, interannual and decadal time scales. Characterisation of hydrological variability on climate timescales and identification of connections to climate forcings provide potential improvement for hydrological forecasts when the climate forcings are predictable or slowly evolving (Souza and Lall, 2003; Croley, 2003). Evidence from long hydrological records shows that periods with anomalous hydrological behaviour (Arnell et al., 1993) are associated with persistent climate anomalies.

The possibility of predicting river flows months and even years in advance is of great interest to regional economies that depend heavily on hydroelectricity and irrigation. This has motivated development of methods for streamflow prediction that use climatic information, such as the El Niño-Southern Oscillation (ENSO) (e.g. Dettinger et al., 2000) and NAO (Rimbu et al., 2005).

Two of the most important phenomena that influence streamflow variability are the NAO and ENSO (Dettinger and Diaz, 2000; Cullen et al., 2002). The indices of these large-scale climatic patterns are used as predictors for seasonal streamflow anomalies over Europe (Rimbu et al., 2005; Trigo et al., 2004). Correlations with hydrological data have shown that, when NAO index is high, river flow is above average in northern Europe and below average in southern Europe (Shorthouse and Arnell, 1997; Dettinger and Diaz, 2000). Because river flows depend mainly on precipitation, it is evident that there is a strong connection between precipitation anomalies associated with extreme phase of NAO and river flow regimes in Europe.
On decadal timescales there are strong parallels between North Pacific temperatures and NAO that reflect much coherence of the Northern Hemisphere climate (e.g., Livezey and Smith 1999). Rimbu et al. (2002) found a strong influence of the global SST on the Danube river flow, at decadal scale.
In the tropical Atlantic a cross-equatorial dipolar SST anomaly pattern with a period of 12-13 yr has been identified, together with a 9-10 yr period over the tropical North Atlantic (Allen and Smith, 1996; Mehta, 1998). River flow anomalies may be related to some of the same climatic oscillations that underlie those in SST.

The goal of this chapter is to investigate the connection between Elbe river flow and large scale atmospheric circulation and SST at global scale, at decadal time scales and to identify the quasi-periodic patterns of Elbe flow variability. It is important to study the connection between the climate variability and hydrological regime, in order to understand the physical mechanisms that drive hydrological variability. Long-term variability may be of significant importance for the managers of water resources systems for whom the ability to forecast reservoirs inflows is highly desirable.

5.2 Data sets description

A detailed description of the data sets used in this chapter has already been made in the previous chapters, so they will be shortly mentioned here. In this part of the thesis we employ the following data sets:

- The annual means of Elbe discharge, computed from the daily data set defined in section ***3.2***.
- Temperature (TT) and precipitation (PP) data sets from CRU (***see 4.2***).
- SST from Kaplan data set (1998) (***see 4.2***).
- SLP data of Trenberth and Paolino (1980) (***see 4.2***)
- The time series of monthly AO index (Thompson and Wallace, 2000).

5.3 Methodology

Elbe river flow and PP data sets were processed in the same way. First, annual means were calculated from monthly means. Then, annual anomalies with respect to the mean and normalized by standard deviation, estimated for the period 1902-2002, were produced. The annual standardized anomalies were smoothed with a 7 year running mean filter to obtain the decadal component of the series.

For TT, SST and SLP the winter (DJF) means were calculated from monthly means. Then, we calculate the DJF anomalies with respect to the mean and normalized by standard deviation for the period 1902-2002. The DJF standardized anomalies were smoothed with a 7 year running mean filter to obtain the decadal component of the series.

To explain the decadal variability of the river streamflow in relation with large scale atmospheric circulation we have computed the composite maps between the time series of decadal anomalies of flow and TT, SST and SLP for the years of high (> 0.75), respectively low (<-0.75) values of Elbe time series. This threshold was chosen as a compromise between the strength of the climate anomalies associated to flow anomalies and the number of maps which satisfy this criteria. Further analysis has shown that the results are not sensitive to the exact threshold value used for our composite analysis.

5.3.1 Singular Spectrum Analysis

In order to identify the dominant decadal components in the flow time series we used Singular Spectrum Analysis. SSA is a novel and powerful tool for time series analysis that can identify intermittent oscillation spells in short, noise time series (Vautard et al., 1992). The basic oscillations into which a time series decomposes are not functions of a prescribed, harmonic form. Instead, their shapes are determined from the time series itself. SSA has been successfully applied to many geophysical and climatologically time series to study and predict periodic activities (Ghil and Mo, 1991; Ghil and Vautard, 1991, Plaut and Vautard, 1994).

Singular systems (or singular spectrum) analysis (SSA) was originally proposed for noise reduction in the analysis of experimental data and is now being

used to identify intermittent or modulated oscillations in geophysical and climatic time series. A time series provides useful information about the physical, biological or socioeconomic system that produced it. The purpose of time series analysis is to determine some of the system's key properties by quantifying certain features of the time series. These properties can then help understand and predict the system's future behaviour.

Predictability may be very limited in any non-linear system, whether it is stochastically forced or purely deterministic; any trend may vary over time, as may be the phase and amplitude of physical oscillations.

The Singular Spectrum Analysis (SSA) technique s a novel and powerful technique of time series analysis, incorporating the elements of classical time series analysis, multivariate statistics, multivariate geometry, dynamical systems and signal processing. SSA is based on the idea of sliding a window down a time series and looking for patterns that account for a high proportion of the variance in the views of the time series thus obtained. SSA is closely related to the Empirical Orthogonal Function Analysis (presented in Appendix A) and is used as a method of visualizing qualitative dynamics from noisy experimental data. Discriminating between "signal" and "noise" is a crucial aspect of applied time series analysis.

Like many techniques based on singular value decomposition, SSA implies constructing a complete orthonormal set of M vectors, or EOFs, onto which we project a data set. These EOFs define a coordinate system in an M-dimensional state space, and the projections of consecutive segments of the data onto EOFs represent a distribution of points expressed in these coordinates. If the data are noisy, all M dimensions will be required to describe this distribution completely, regardless of the coordinate system.

For signal detection and reconstruction we wish to identify those EOFs (state-space directions) dominated by signal and eliminate those dominated by noise.

The SSA method employed in this chapter is the one developed by Vautard and Ghil (1989). According to Vautard and Ghil (VG hereafter) there are three basic steps in SSA:

1. Embedding the sample time series in a vector space of dimension M.
2. Computing the M x M lag-covariance matrix C_D of the data.
3. Diagonalzing C_D.

Step 1. The time series $\{x(t) : t = 1,.....,N\}$ is embedded into a vector space of dimension M, by considering M lagged copies $\{x(t-j) : j = 1,.....,N\}$ thereof. The choice of the dimension of M is not obvious. Vautard et al (1992) suggests analyzing periods in the range (M/5, M)

Step 2. The lag-covariance matrix estimator C_D is then defined. C_D is estimated directly form the data, as a Toeplitz matrix [(1)] with constant diagonals.

Step 3. The covariance matrix calculated from the N sample points, is then diagonalized and the eigenvalues $\{\lambda_k : 1 \le k \le M\}$ are ranked in decreasing order (λ_k - gives the variance of the time series in the direction specified by the corresponding eigenvector E_k). The square roots of the eigenvalues are called *singular values* and the set $\{\lambda_k^{1/2} : 1 \le k \le M\}$ is called the *singular spectrum.*

Once these three steps have been completed, a number of other interesting results can be obtained. For each EOF E_k with components $\{E_{k,j} : j = 1,.....,M\}$, we can construct the time series of length N' given by:

$A_k(t) = \frac{1}{M_t} \sum_{k \in K} \sum_{j=1}^{M} x(t+j) E_{k,j}$, $t = 0,.....,N-M$ (5.1), called the *k*-th principal component (PC). It represents the projection of the original time series onto the *k*-th EOF. The sum of the power spectra of the PCs is identical to the power spectrum of the time series *x(t)* (Vautard et al., 1992). In this way the spectral contribution of various components can be studied.

In order to extract time series of length *N*, corresponding to a chosen subset of *k** eigenelements, the associated PCs are combined to form the partial reconstruction $R_k(t)$ of the original time series *x(t)*. Over the central part of the time series:

$$R_k(t) = \frac{1}{M_t} \sum_{k \in K} \sum_{j=1}^{M} A_k(t-j) E_{k,j} \qquad (5.2),$$

where $M \le t \le N'$ and $M_t = M$ near endpoint ($1 \le t \le M$ or $N'+1 \le t \le N$) the summation in j extends form 1 to t or from $(t-N+M)$ to M and $M_t = \mathbf{min}\{t, N-t+1\}$.

These series of length *N* are called reconstructed components (RCs). They have the property that they preserve the phase of the time series therefore *x(t)* and $R_k(t)$ can be superimposed.

When *k* contains the components of a single eigenvector E_k, $R_k(t)$ is called the *k*-th RC. The correct partial reconstruction of the signal, i.e., the reconstruction over the correct set $k^* = \{1,2,.....,S\}$ of EOFs, yields the optimal signal-to-noise (S/N) enhancement with respect to the noise.

5.4 Relation with precipitation and temperature over land

In this section we analyze the relation between decadal variations of the Elbe river flow and decadal variations of precipitation in the river catchment area and temperature over land. The time series of annual means of Elbe river discharge used in this study is presented in Figure 5.1 (blue line). The red line represents the decadal component obtained by smoothing the original time series with a 7 year running mean filter.

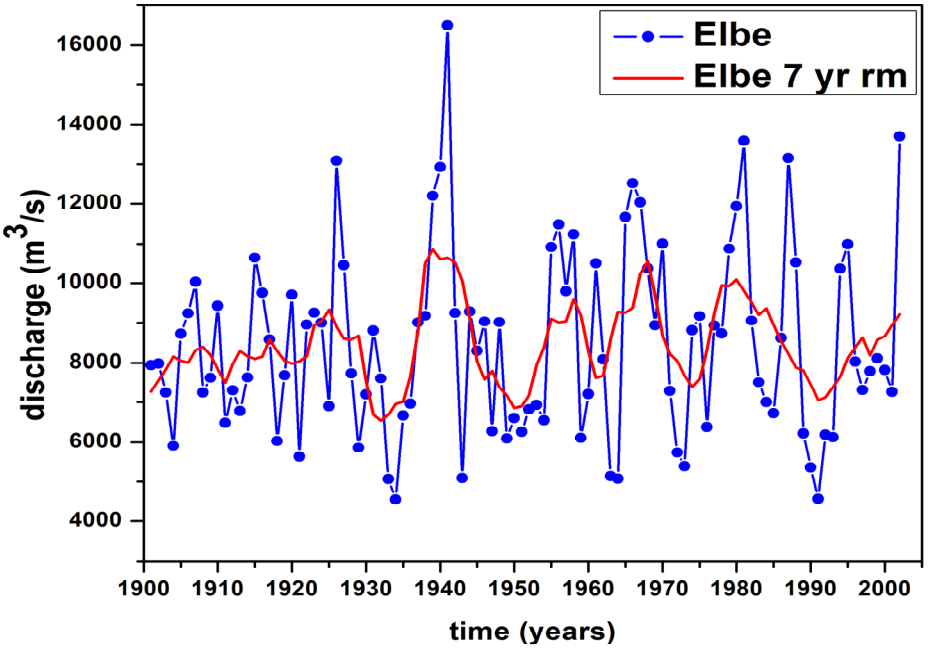

Figure 5.1 The time series of annual Elbe discharge (blue line) recorded at Neu Darchau (53° 14′ N, 10° 53′ E) for the period 1902-2002. Units are m^3s^{-1}. The red line represents the decadal component obtained by smoothing the series with a 7 year running mean

The correlation map between flow and PP has been constructed in order to see which are the PP patterns associated with the flow decadal variability (Figure 5.2). The map shows that the highest correlations are over Elbe's catchment area, especially in the upper basin.

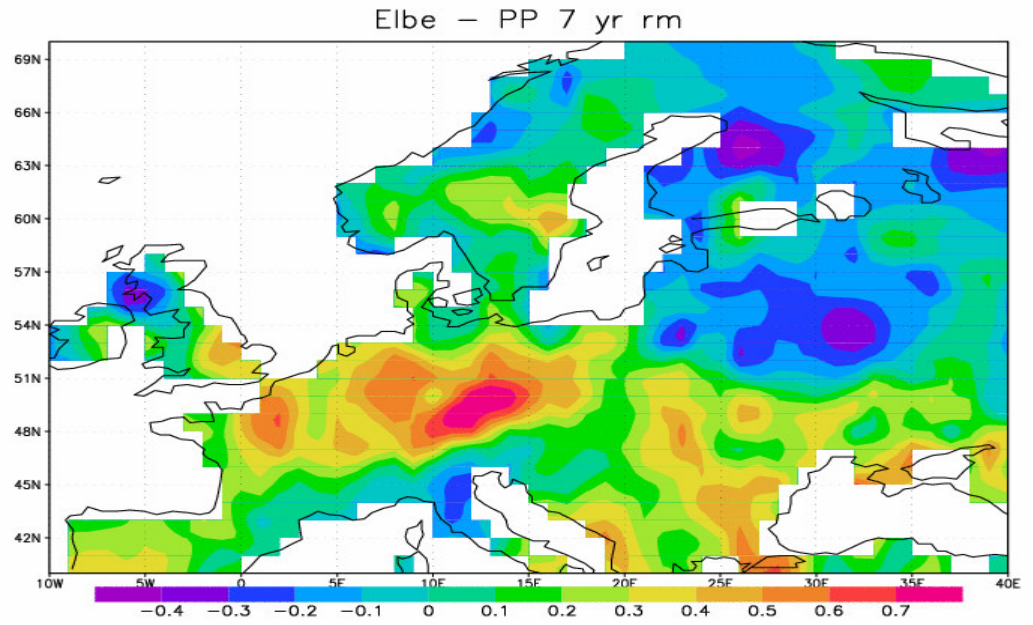

Figure 5.2 The correlation map between the decadal component of the annual Elbe flow and annual PP

Based on the correlation map with PP, we defined a PP index averaged over the catchment area (6-19ºE, 48-55ºN). The correlation coefficient between the time series of the normalized river flow anomalies and the time series of the PP index is 0.65 (Figure 5.3).

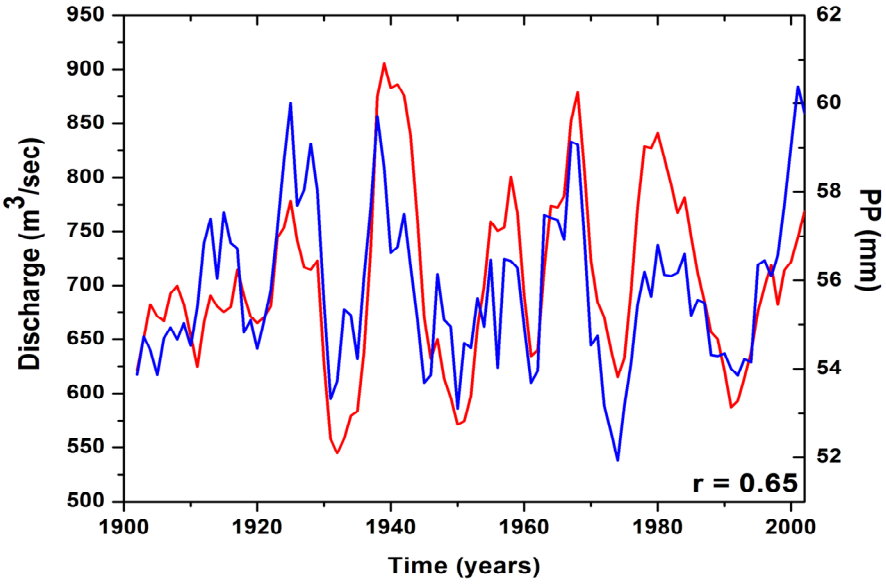

Figure 5.3 The time series of annual Elbe river flow (red line) and PP index (blue line). Both time series were smoothed with a 7 year running mean

The composite map between flow anomalies and DJF TT over land is presented in Figure 5.4. A strong out-of-phase relationship is found between flow anomalies and winter TT over the Scandinavian region. Positive anomalies are also found with the TT over the northern part of Canada. This pattern in the TT field is similar to the spatial impact associated to the negative phase of the Arctic Oscillation (Thompson and Wallace, 1998). A strong negative anomaly of TT in winter, centred over the Scandinavian region, can trigger enhanced discharge in spring. This can be due to snow melting and by retaining the water in the soil during winter. Taking into account that the highest discharge values for Elbe River are found in spring (see Figure 4.1), high discharges in spring will be highly reflected in the annual means.

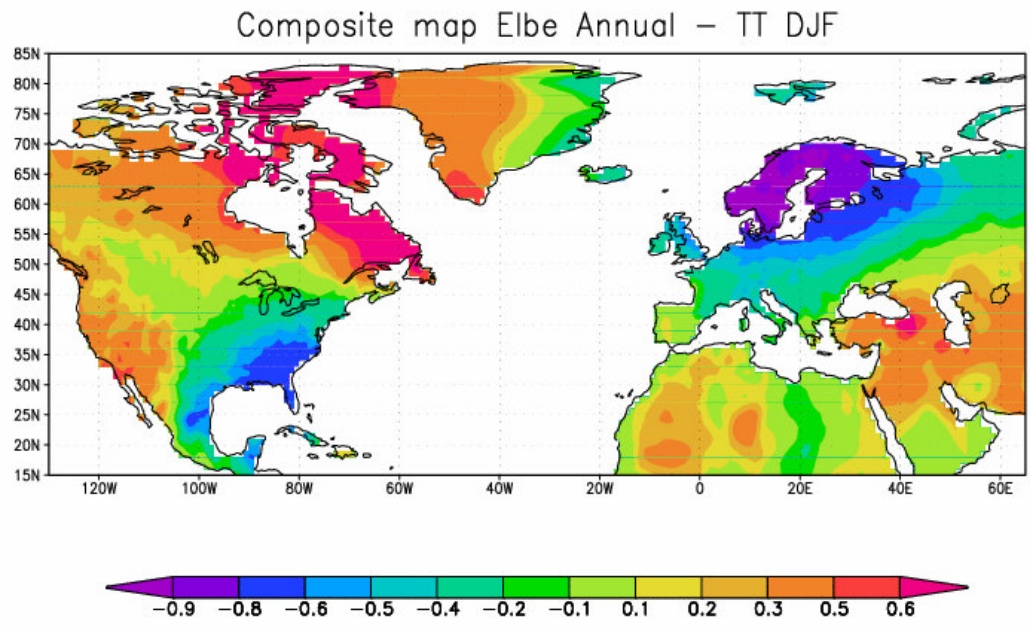

Figure 5.4 The composite map between the time series of the decadal component of annual Elbe river flow and winter TT

5.5 Relation with sea surface temperature and sea level pressure

5.5.1 Relationship with global Sea Surface Temperature

Several studies have established that large-scale SST fluctuations can be linked to atmospheric circulation that produces precipitation fluctuations (Dai et al., 1997; Latif et al., 2000). Rajagopolan et al. (1998) found evidence of significant coherence at decadal time scale between tropical South Atlantic SST and NAO, with warm SSTs associated with the positive phase of NAO. The composite map between annual flow and winter SST is shown in Figure 5.5. Positive anomalies of river flow are associated with negative SST anomalies in the central North Pacific and positive anomalies in the eastern and central tropical Pacific. This pattern resembles the SST pattern associated to the Pacific Decadal Oscillation (PDO) (Mantua et al., 1997). This result is compatible with the correlations between North Pacific SSTs and river flows over North America, tropical Africa, centre and Southern Europe identified by Dettinger and Diaz (2000) and Danube river (Rimbu et la., 2002). High flow

anomalies are also associated with a tripole-like pattern in the North Atlantic region similar to the pattern identified also by other authors (e.g. Hurrell, 1995, Desser and Blackmon, 1993).

This pattern has been found to have a quasi-decadal variation of about 12 years. The significant connection of this pattern to Elbe river flow at a similar time scale, as showed here, is consistent with these studies.

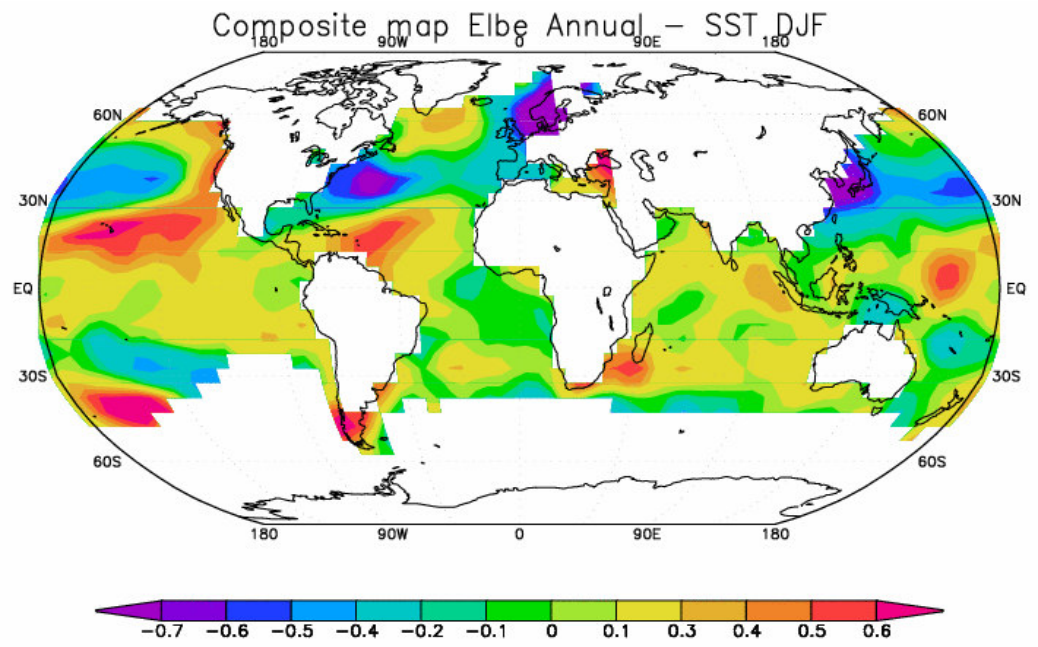

Figure 5.5 The composite map between the time series of the decadal component of annual Elbe river flow and winter SST

5.5.2 Connections with global SLP

The composite map between the time series of the Elbe river flow and SLP (Figure 5.6.a) is consistent with the patterns identified in the SST field. This pattern resembles the AO pattern, but with the Pacific centre shifted towards north. Based on this pattern we defined four SLP indexes by averaging the normalized anomalies from the centres defined in Table 5.1 (first column). An Empirical Orthogonal Function (EOF) analysis was then applied to these four indexes. The weight of each loading is given in table 5.1 (second column). The first EOF explains 57% of the total variance. The first principal component (PC1) associated to the first EOF is presented Figure 5.6.b, together with the Elbe flow and AO index.

Table 5.1. The coordinates (latitude, longitude) of the winter SLP indices used in this study (first column) and the weights of the loadings corresponding to EOF1 for each index (second column)

Latitude – Longitude	Weights of the loadings
110ºW-140°W, 30ºN-50°N	0.39
40ºW-70°W, 30ºN-45°N	0.54
20ºE-40ºE, 40ºN-50ºN	0.48
70W-5ºE, 60ºN-80ºN	-0.57

The correlation coefficient between PC1 and flow is r=-0.7, which is higher than the correlation between flow and AO index (r=-0.55). This may be due to the fact that the pattern identified in Figure 5.6.a might be the result of a superposition of different decadal modes of variability, such as AO or PDO.

a)

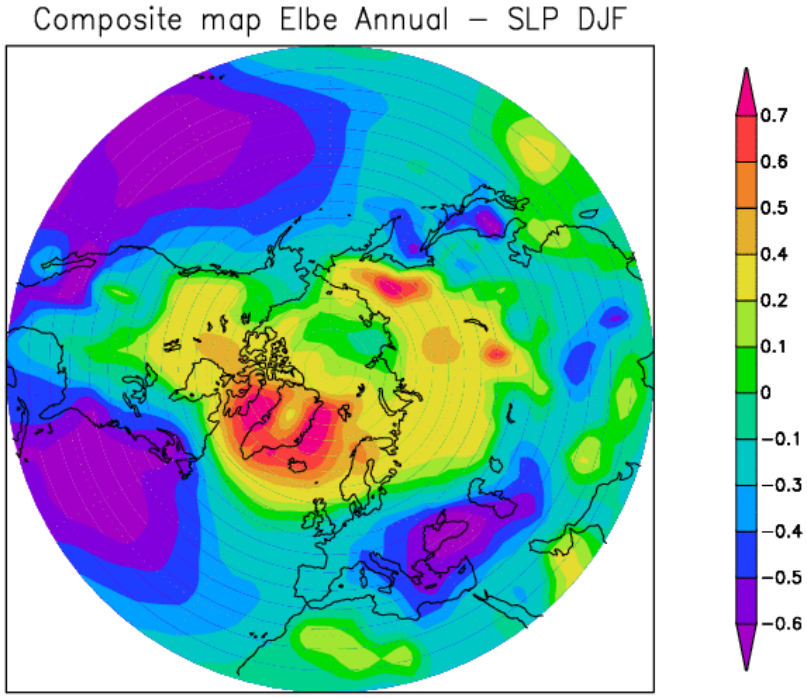

b)

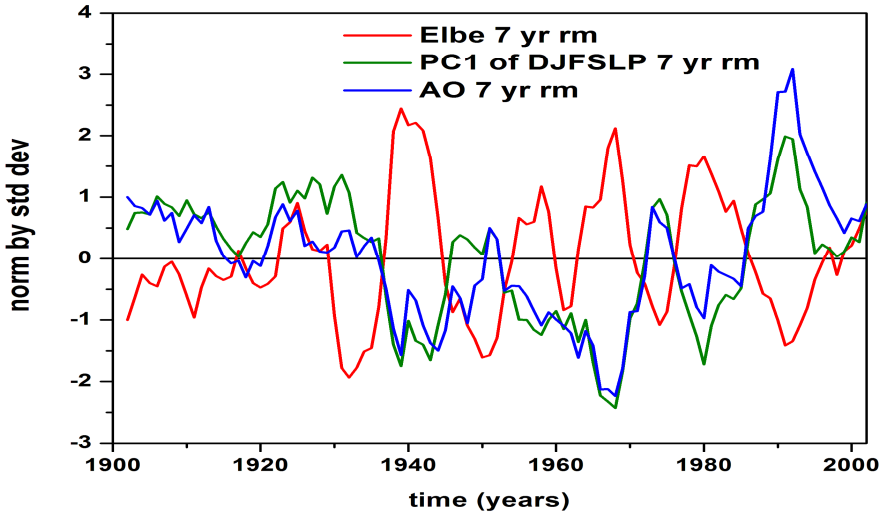

Figure 5.6 a) The composite map between the time series of the decadal component of annual Elbe river flow and winter SLP and b) The time series of normalized anomalies of Elbe river flow (red line), PC1 of DJF SLP (green line) and AO index (red line). All time series were normalized and smoothed with a 7 year running mean

5.6 Singular Spectrum Analysis

In order to identify the dominant decadal components in the flow time series we used SSA with a 40 years window length. Repeated SSAs with different window lengths show that the basic features of the identified time components remain stable and therefore are independent of the window length. For example the structure of the eigenvalue spectrum (Figure 5.7) and the approximate periods and amplitudes of the identified time components remain unchanged. Spectral peaks are associated with oscillatory pairs of eigenvectors, from which the oscillatory part of the time series can be reconstructed. A significant test of the oscillatory pairs can be made against a red noise null hypothesis using a chi-squared test or a Monte Carlo method (Allen and Smith, 1996). We used the chi-squared test for all estimates of the significance.

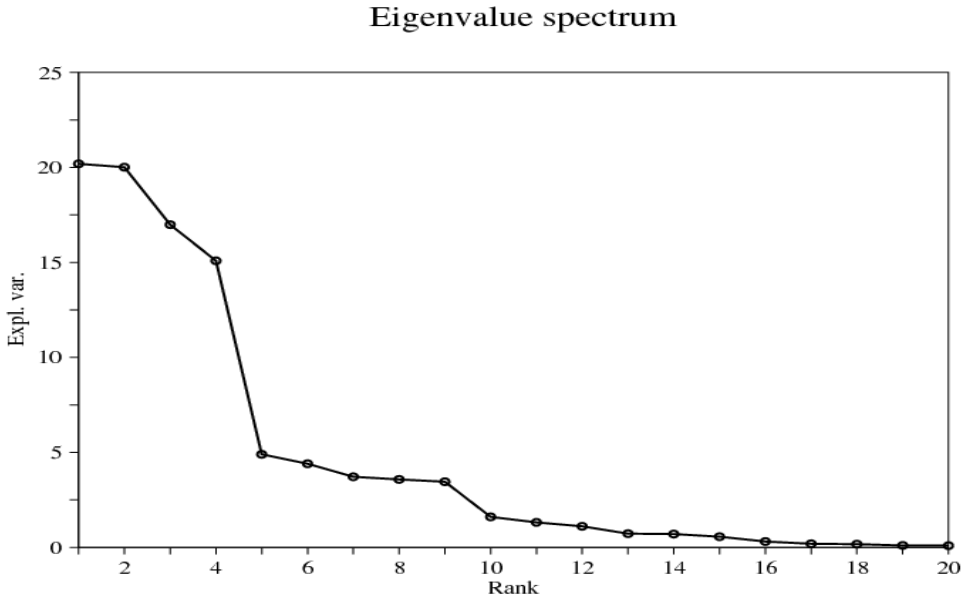

Figure 5.7 Eigenvalues derived from SSA of the annual Elbe river flow

Using a lag window of M=40 years, the two leading SSA eigenmodes (Figure 5.8) form an oscillatory pair with a dominant period of ~20 yrs, which accounts for 40% of the total variance of the time series. Using the chi-squared test, the 20 yrs SSA pair is statistically significant against a red noise null hypothesis at 95% level. A similar pattern, which is characterized by a 20-25 yrs time-scale, was identified by Dima et al (2001b), who presented observational evidence of a quasi-bidecadal mode which may be generated from a linear interaction between phenomena originating in the Pacific and Atlantic basin. They also show that an AO-like structure, resulting from inter-ocean interactions, is associated with this quasi-bidecadal mode.

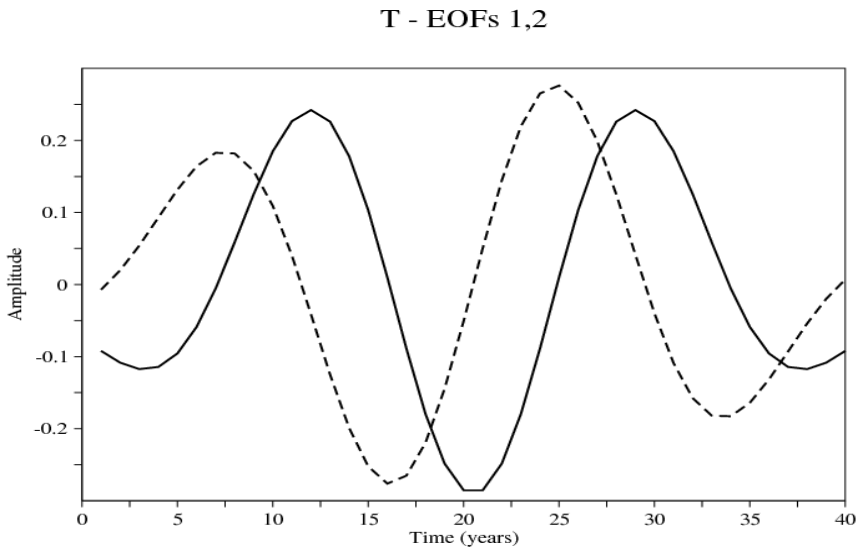

Figure 5.8 EOFs 1 and 2, explaining 40% of the total variance.
The time-EOFs of each pair are in quadrature, indicating that each of the two pairs is associated with a quasi-periodic component.

The third and fourth leading SSA eigenmodes (Figure 5.9) form an oscillatory pair with a dominant period of ~12 yrs and account for 32% of the total variance of the time series. The 12 yrs SSA pair is also statistically significant against a red noise null hypothesis at 95% level. Deser and Blackmon presented evidence for a quasi-decadal cycle in the North Atlantic. This mode is characterized by latitudinal bands of alternating polarities that extent from tropics to the North Atlantic (Deser and Blackmon, 1993; Dima et al., 2001a) and is consistent with the SST pattern from figure 5.5.

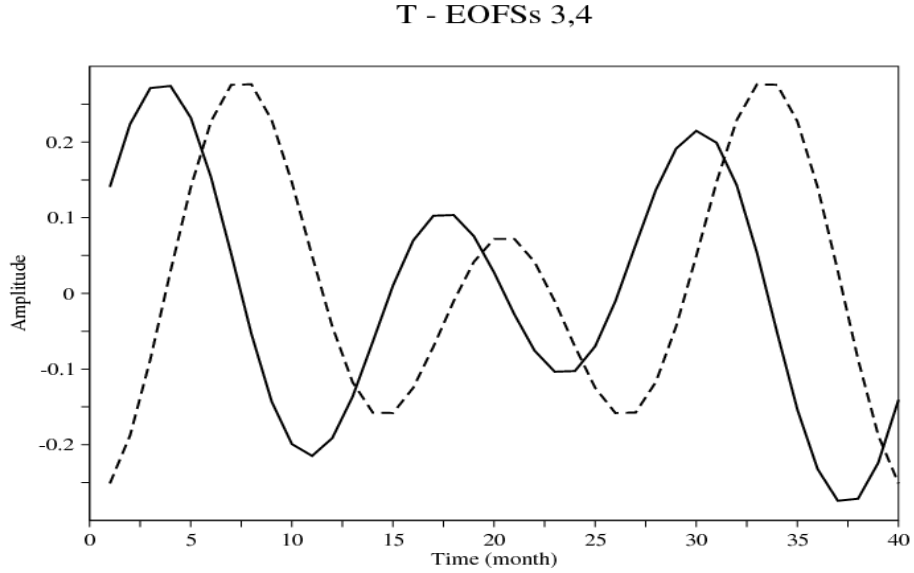

Figure 5.9 EOFs 3 and 4, explaining 32% of the total variance

5.7 Bandpass – filter analysis

In order to isolate the main frequencies identified by the SSA analysis, we have applied a bandpass-filter to Elbe annual time series and SST field, to be able to suppress all the variance outside the prescribed windows (von Stroch and Zwiers, 1999). The filtering was applied for the two main frequencies identified in the previous section: 12 years (F12, from now on) and 20 years (F20, from now on). Thus, we performed the filter for wave numbers between 6 and 9 for F12 and 4 and 5 for F20, respectively. These wave numbers represent periods of 11-15 years and 17-25 years, respectively, for our time series length of 101 years.
The second approach was to apply an EOF analysis to the SST filtered data set. For F12, the EOF analysis was applied just for the Atlantic region, since the 12 years periodicity is specific to this area. For F20, the EOF analysis was performed on global scale.
The first EOF (Figure 5.10) of bandpass-filtered SST in the range of 11-15 years explains 71.54% of the total variance. EOF1 is characterized by a tripole-like pattern in the Atlantic region. This pattern resembles the composite map between Elbe discharge and global SST identified in Figure 5.5. There is significant observational evidence for the SST variability on 10-14 years in various parts of the Atlantic Ocean, which are supposed to be part of a coherent pan-Atlantic decadal oscillation (Deser and Blackmon, 1993; Dima and Lohman, 2004).
In order to further prove that the F12 mode and Elbe river co-vary, we relate (Figure 5.11) the filtered Elbe discharge time series and the PC1 corresponding to the first EOF. Elbe time series is significantly correlated with PC1 and there is an out-of-phase relationship between them. The correlation coefficient is r=-0.81.

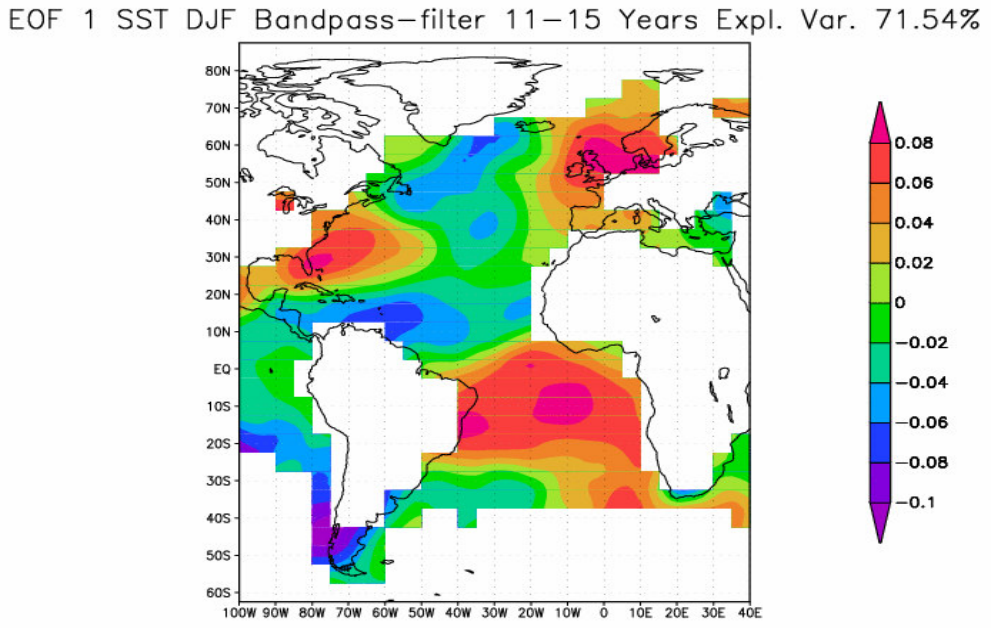

Figure 5.10 EOF1 pattern of the bandpass-filtered (*F12*) SST anomalies

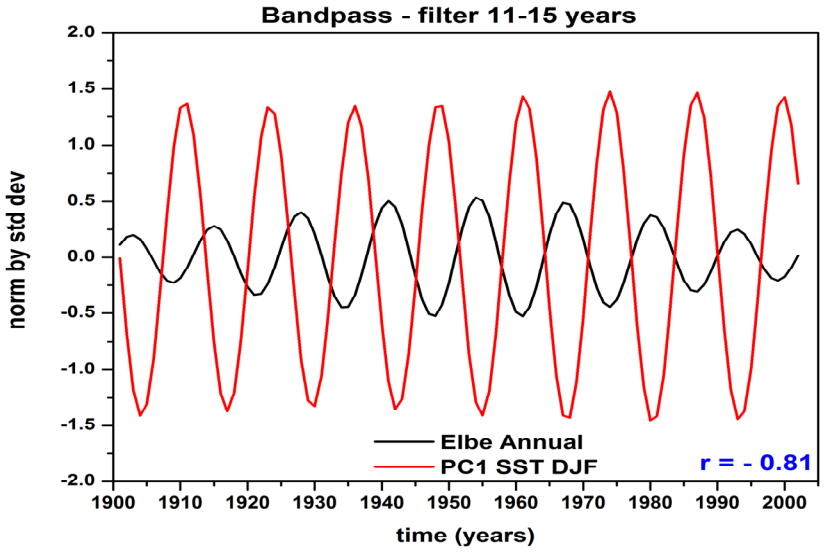

Figure 5.11 PC1 of bandpass-filtered SST (red line) and the time series of bandpass-filtered Elbe flow (black line)

The first EOF of the bandpass-filtered SST (Figure 5.12), in the range of 17-25 years, explains 66.71% of the total variance. This pattern resembles the PDO pattern described by Kaplan et al. (2000) and others (Mantua et al., 1997; Tourre et al., 2001). EOF1 is characterized by a large area of positive anomalies in the eastern equatorial Pacific that extend up to the North a South of American coasts. There is also the typical cold water tongue in the west Pacific.

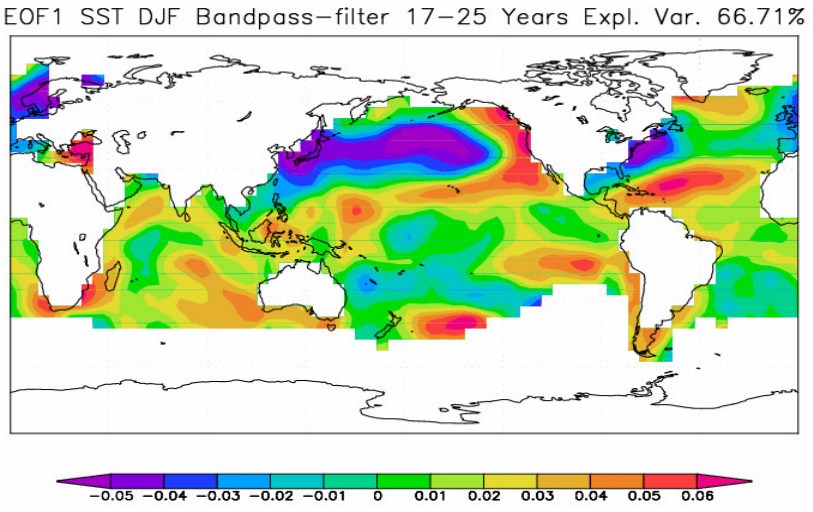

Figure 5.12 EOF1 pattern of the bandpass-filtered (*F20*) SST anomalies

The filtered time series of annual discharge and PC1, corresponding to EOF1 – F20, are strongly correlated (r=0.99) (Figure 5.13). There is a strong relationship between the two time series and the phase is identical for the whole period analyzed.

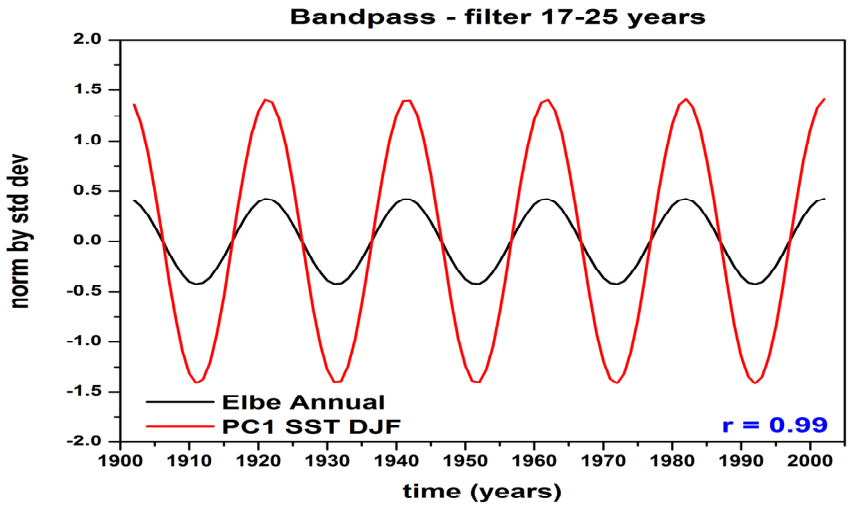

Figure 5.13 PC1 of bandpass-filtered SST (red line) and the time series of bandpass-filtered Elbe flow (black line)

5.8 Discussion and conclusions

In this chapter we have investigated the decadal variability of Elbe river flow and its connection with PP and TT in the European sector and SST and atmospheric circulation over the Northern Hemisphere, for the period 1902 - 2002.
The correlation map with PP showed that high values of PP throughout the river catchment area occur in connection with high values of Elbe flow. Elbe flow is highly positive correlated with a PP index defined as the average PP over Elbe's basin.
On decadal time scale, high flow anomalies are strongly correlated with winter TT over land. There is an out-of-phase relationship between Elbe flow and TT over Scandinavian region. High positive correlation is also found with the TT over the northern part of Canada. This pattern in the TT field is similar to the negative phase of the Arctic Oscillation.

The correlation map between Elbe river flow and SSTs shows that high flow anomalies tend to be associated with low SST anomalies in the central North Pacific and high SST anomalies in the eastern and central tropical Pacific. A tripole-like pattern in the SST files is also associated with high flow anomalies. The strong correlation of flow with the SST from Pacific and Atlantic basin can be explained via the mechanism proposed by Dima et al. (2001). They argue that there is an interaction between phenomenon originating in the Tropical Pacific, like ENSO, and the Atlantic basin, like the Atlantic quasi-decadal mode. The result of this interaction

is a coherent mode at global scale. The 20-year oscillation over the north Pacific is suspected to have a source region over the Pacific Ocean (Trenberth, 1990; Graham, 1994, Dima et al, 2001b) and is related to the PDO.

The quasi-decadal variation revealed in Atlantic SSTs is consistent with many previous studies. In addition to the Atlantic Ocean, this mode of variation has been observed in global surface air temperature (Mann and Park, 1994), US stream flow (Guetter and Georgakakos, 1993), Great Basin precipitation (Eischeid *et al.*, 1985), and the volume of the Great Salt Lake (Mann *et al.*, 1995).
In summary, we conclude that the decadal variability of Elbe river flow is driven by climate interactions at nearly global scale. These results have implications for predicting the evolution of Elbe river discharge on decadal time scales.

Chapter 6

The influence of large-scale atmospheric circulation on the variability of salinity at Helgoland Roads station

6.1. Introduction

The eastern German Bight is a zone of intensive mixing of two water bodies, the North Sea water and the coastal water which is of lower salinity and density. In addition, the water of the river Elbe leads to a strong inhomogeneity in this area which can be seen in the distribution of salinity and nutrients Goedecke (1968). During the last decade interest in the variability of hydrological (i.e. river run-off) and ecological parameters (salinity, nutrients) in connection with large-scale atmospheric circulation has markedly increased (Aebischer et al., 1990, Dippner, 1997a, b; Becker and Pauly, 1996). The interannual variability in observed ecological time series is sometimes suspected to be driven by interannual variability in climatic parameters (Fromentin and Planque, 1996).

Cushing and Dickson (1976) speculated that atmospheric circulation is responsible for a series of events that were observed in the North Sea in the last few decades. He showed that the beginning and end of an anomalously strong and long-lasting high pressure system over Greenland correspond with the so-called "Russell cycle" (Russell et al., 1971; Russell, 1973). According to his hypothesis the breakdown of this high pressure system at the end of 1960s led to changes in the wind stress and induced the Great Salinity Anomaly (GSA) (Dickson et al, 1988). The cool, low-stratified water columns of the GSA delayed the primary production (phytoplankton) and thus led to changes in the food web.

Other studies focused on the whole German Bight identified that on annual timescales, 90% of the observed salinity variability is in phase and correlated with a lag of several months to large-scale air pressure (Heyen and Dippner, 1998). Schott (1966) and Dickson (1971) revealed a connection between salinity variations in the North Sea and the atmospheric circulation, though both authors disagreed on the mechanism. While Schott (1966) found evidence that the surface salinities in the entire North Sea are dominated by large-scale atmospheric advection via precipitation, Dickson (1971) suggested that advection of haline Atlantic waters is the main cause.

The goal of this chapter is to investigate the possible relationships between the large-scale atmospheric circulation and salinity, at Helgoland Roads station (54.12ºN, 7.9ºE, Germany) for the period 1962-2000. Understanding the causes of salinity variability: (i) will help to reconstruct historical salinities in connection with the atmosphere-ocean dynamics and (ii) will allow the study of the variability of other ecological time series (i.e. nutrients) in connection with the large-scale circulation, due to the fact that salinity anomalies are supposed to coincide with observed changes in the ecosystem (Nehring, 1994; Lindeboom et al., 1995).

6.2. Data

In 1962 a long-term pelagic monitoring program observing nutrients, salinity and plankton species composition at Helgoland was initiated by the Biologische Anstalt Helgoland (Hickel et. al, 1993; Hickel, 1998). The measurements were made on a daily basis, except weekends. Helgoland Roads station (Figure 6.1) is situated approximately 60 km of the mouth of Elbe River, which is the most important source of fresh water input. In this study we used the daily salinity data from which we computed the monthly means for the period 1962-2000.
The monthly means for Elbe river discharge (see 3.2, 4.2) for the period 1962-2000. The average March discharge of Elbe river, for the period analyzed in this study, is 1024 m^3/s.

Figure 6.1 Location of Helgoland Roads station (black square)
(Source: Potsdam Institute for Climate Impact Research and River Basin Community Elbe)

In the analysis we used the following large-scale variables:

a) Monthly Sea Level Pressure (SLP) on a 5ºx5º grid from the reanalysis data of the National Centre for Atmospheric Research (NCAR) (Trenberth and Paolino, 1980), updated version.
b) Monthly Sea Surface Temperature (SST) on a 5ºx5º grid (Kaplan et. al, 1998), for the 170ºW to 170ºE and 40ºS to 90ºN area. The data set have been update to year 2000.

c) The vertically integrated water vapour transport (WVT) (eq. 1) (Peixoto and Oort, 1992) for the period 1962–2000, calculated using zonal wind (u), meridional wind (v) and specific humidity (q):

$$\vec{Q}(\lambda,\phi,t) = Q_\lambda \vec{i} + Q_\phi \vec{j} \qquad (1)$$

Where zonal (Q_λ) and meridional (Q_Φ) components of Q are given by:

$$Q_\lambda = \int_0^{p_0} qu \frac{dp}{g}$$
$$Q_\phi = \int_0^{p_0} qv \frac{dp}{g} \qquad (2)$$

For each vertical layer and each grid-point of the NCEP/NCAR data set we calculate the product between the daily values of horizontal wind and specific humidity (q) corresponding to lower and upper pressure level (p), respectively. The result is multiplied with the pressure difference corresponding to lower and upper layer and divided by gravity. The WVT is obtained by summation of water transport for all layers located between the earth's surface and 300 hPa level. Above 300 hPa the specific humidity in the NCEP/NCAR model is zero (Kalnay et al., 1996).

We also used the divergence of water vapour Q, which is in balance with the surface fresh water flux E-P (Starr and Peixoto, 1958; Peixoto and Ort, 1992):

$$\nabla \bullet \vec{Q} = E - P,$$

where ∇ denotes the two dimensional divergence operator, E evaporation and P precipitation. Regions of mean positive divergence (E-P>0) constitute source regions of water vapour, meanwhile the regions of convergence (E-P<0) are sink regions for water vapour.

d) Gridded precipitation data from the Climatic Research Unit (CRU) with 0.5ºx0.5º horizontal resolution (Mitchell et al., 2003). This data set (CRU TS 2.1) is based on precipitation observations at meteorological stations corrected for inhomogeneities in the station records. From the CRU precipitation data we defined an *index for March precipitation* which covers the Elbe river catchments area (5ºE to 20ºE and 47ºN to 53ºN), as the averaged normalized precipitation over this region.

All the data sets used in this study are for the common period 1962-2000 and have been detrended and normalized, with respect to their standard deviation, prior to the analysis.

6.3 The dominant pattern of variability in the salinity, Elbe river discharge and precipitation time series

In a first step, the correlation of Helgoland salinity and large-scale variables is calculated. Just April mean salinity was retained for this study, due to the fact that the highest correlation between salinity and large-scale circulation is found for this month (not shown) and the highest variability in the salinity time series was identified for April (Figure 6.2).

Taking into account that the cross-correlation between the river discharge and salinity is highest when Elbe leads salinity with 14-24 days (Figure 6.3) we used for our study March river discharge data.

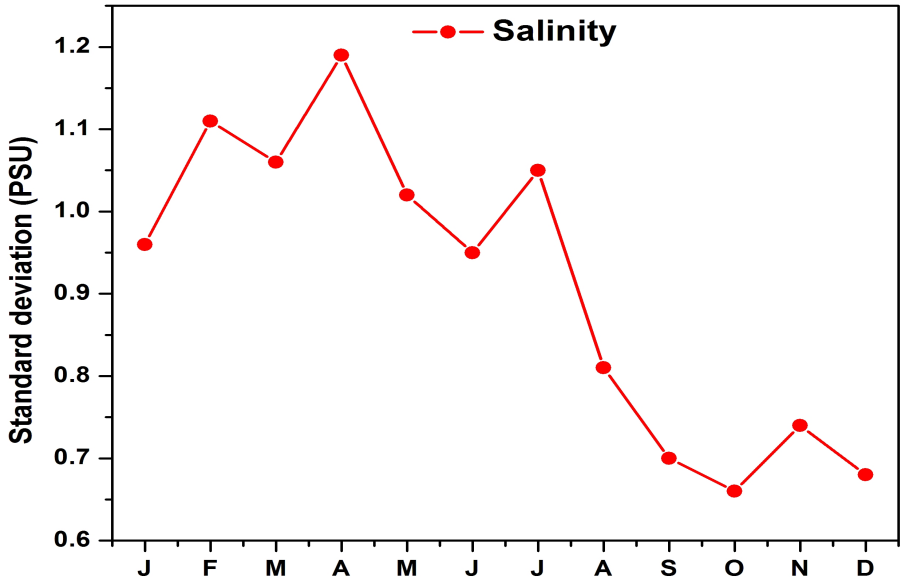

Figure 6.2 Standard deviation of salinity at Helgoland Roads station for the period 1962-2000

The dominant pattern of variability in the salinity, Elbe discharge and precipitation time series is calculated through Empirical Orthogonal Function (EOF) analysis. EOF technique (e.g.von Storch and Zwiers, 1999) aims at finding a new set of variables that capture most of the observed variance from the data through a linear combination of the original variables. The EOF method also served as a data-filtering procedure to smooth the noise in the data sets.

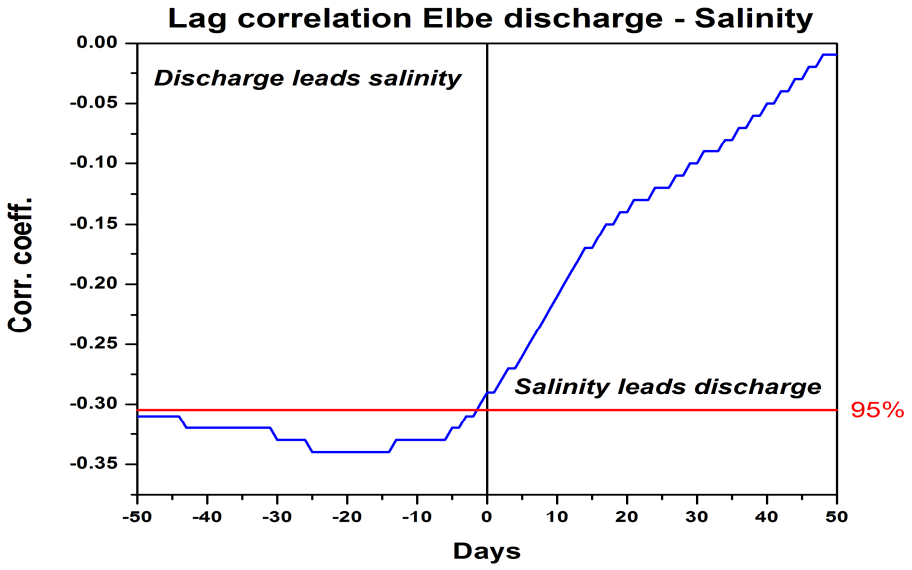

Figure 6.3 Lag-correlation between daily Elbe river discharge and salinity (the 95% significance level is indicated with the dash-dotted line)

The EOFs (see Appendix A) are constructed using the normalized and detrended time series of April salinity, March Elbe discharge and the precipitation index for the period 1962-2000. The associated time series (PC1) was normalized by its standard deviation.

The first EOF (Figure 6.4.a), which explains 71.23% of the total variance, captures an out-of phase relation between salinity and Elbe discharge and precipitation. This pattern implies that positive anomalies of salinity are associated with negative anomalies of Elbe discharge and precipitation and *vice versa*. The associated time coefficient (PC1) (Figure 6.4.b) is highly correlated with Elbe discharge and salinity time series (Table 6.1).

a)

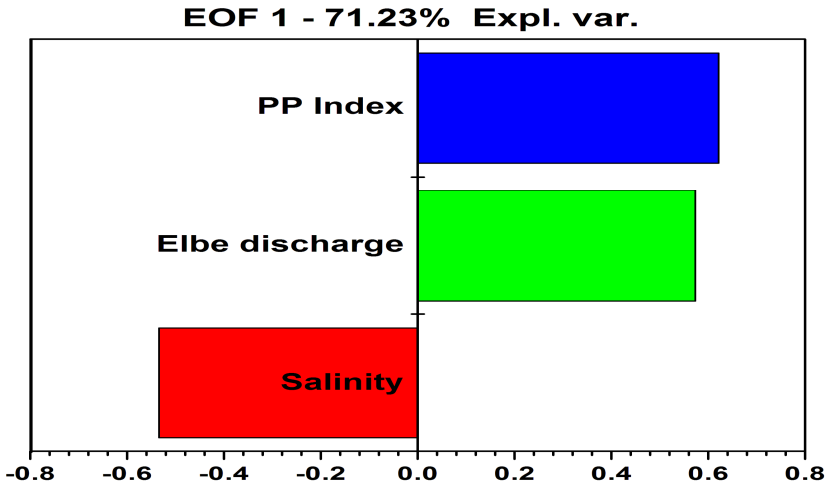

b)

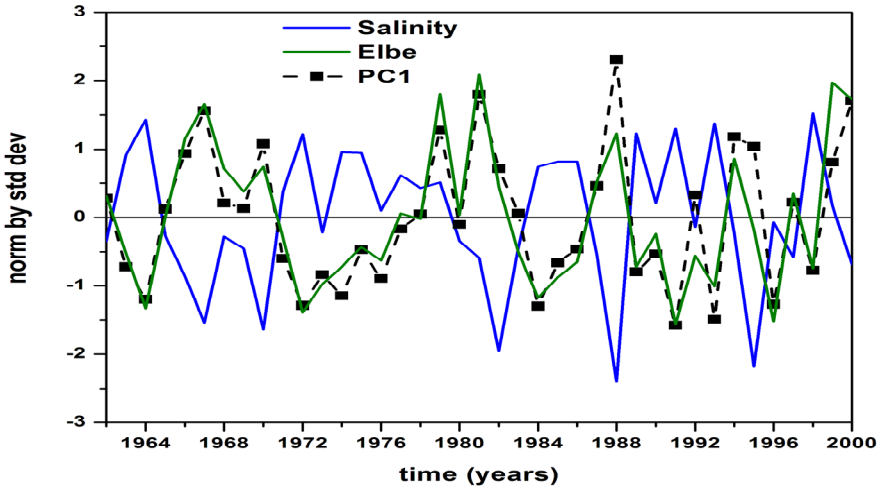

Figure 6.4 a) First EOF based on the normalized time series of April salinity, March Elbe river discharge and March PP Index and b) The corresponding coefficient time series (PC1) and salinity and discharge normalized time series

Table 6.1. Correlation coefficients between PC1 and April salinity, March Elbe discharge and March PP index

PC1	
Salinity	**-0.78**
Elbe Discharge	**0.84**
PP CRU	**0.91**

6.4 The relationship between salinity and large-scale atmospheric circulation

Given the significant relationship between the first principal component (PC1) and salinity, discharge and precipitation, we will show further just the composite maps between PC1 with SLP, SST and WVT fields.

To identify the physical mechanism responsible for the connection between PC1 and large-scale atmospheric circulation, we constructed the composite maps between PC1 and SLP for the years of high (> 0.75), respectively low (<-0.75) values of PC1. This threshold was chosen as a compromise between the strength of the climate anomalies associated to flow anomalies and the number of maps which satisfy this criteria. Further analysis has shown that the results are not sensitive to the exact threshold value used for our composite analysis.

For the years when PC1 < -0.75 (Figure 6.5.a) we obtain a tripole-like pattern with positive centres over northern Europe and the Atlantic Ocean centred at 50ºW and negative anomalies centred over the Mid-Atlantic Ocean, centred at 18ºW. This tripole pattern in the SLP field resembles the jet guide identified by Hoskins and Ambrizzi (1993). According to them by putting a forcing in the vicinity of the North Atlantic jet stream maximum (40ºN, 75ºW), will produce a propagating wave train in the North Atlantic jet with a extension in the Arabian Gulf, as well as, a Eurasian extension.

The anticyclone pattern over the northern part of Europe is consistent with low precipitation and high salinities. Anticyclonic activity over the German Bight blocks a large-scale advection of marine air to Europe and causes reduced precipitation (Heyen and Dipnner, 1998).

The tripole-like pattern in the SLP field is associated with a tripole-like pattern in the composite of PC1 with SST (Figure 6.5.b). A similar SST pattern was identified by Deser and Blackmon (1993). Positive SST anomalies over the north tropical Atlantic are associated with negative SLP anomalies and anomalous lower cyclonic circulation over the subtropical latitudes. This can be attributed to the weakening of the Hadley circulation (suppressed ascending air over the equatorial region and descending air over the sub-tropics) (Handoh et al., 2006). The associated wind anomalies weaken the prevailing easterly winds, which in turn reduces surface evaporation, maintaining a positive SST anomaly (Sutton et al., 2000; Handoh et al., 2006).

a)

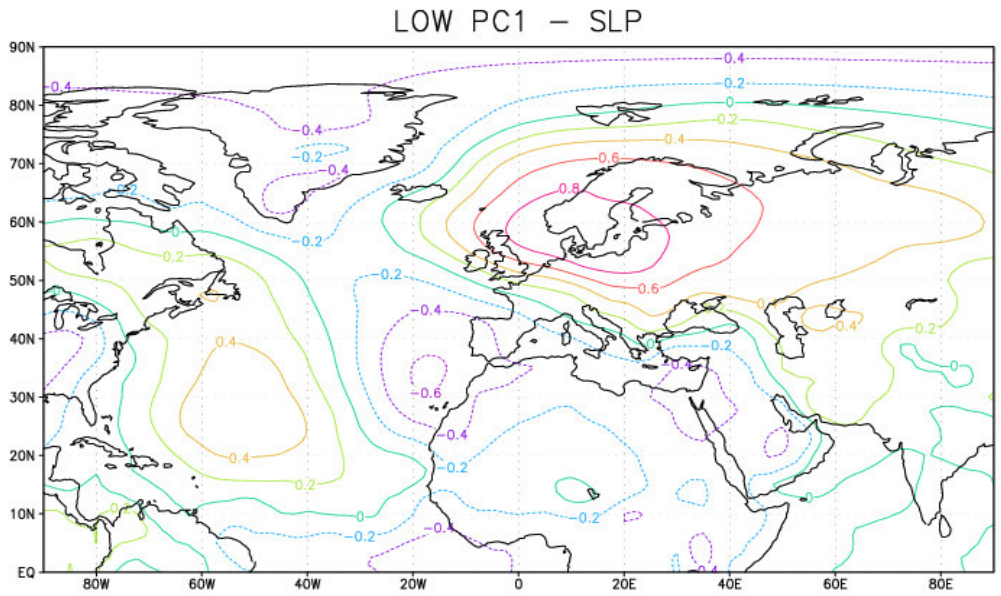

b)

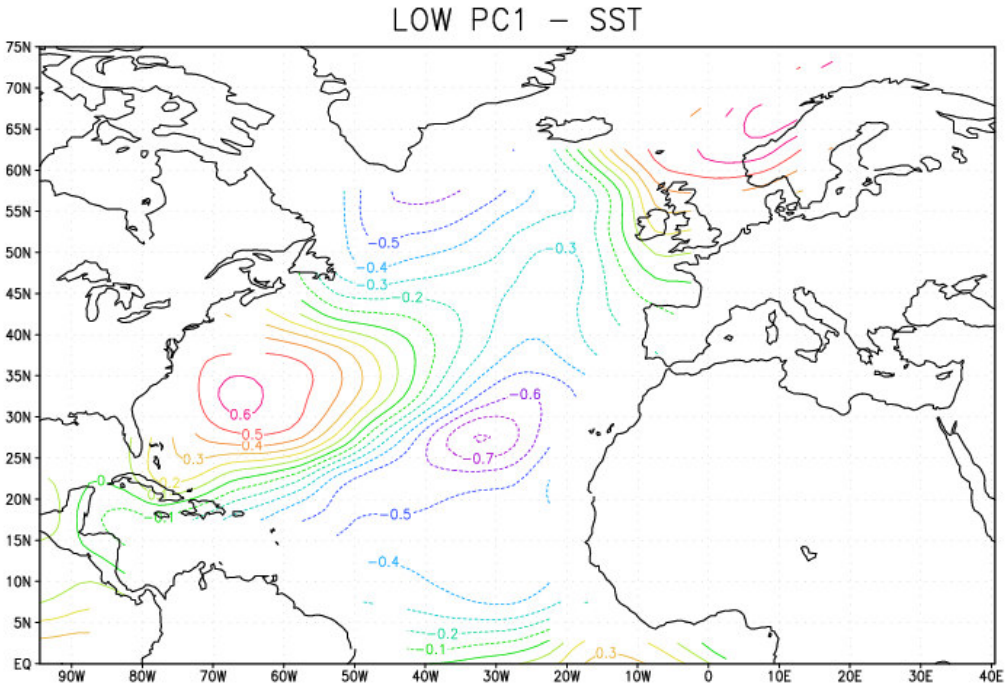

Figure 6.5 Composite map between PC1 (<-0.75) and (a) SLP, (b) SST. Units are hPa and K, respectively

For the years when PC > 0.75 we obtain a pattern like the one in Figures 6.5a, b but with opposite signs (Figures 6.6 a, b). The cyclonic pattern over the northern part of Europe induces high precipitation, high discharge and low salinity anomalies. This pattern is accompanied by westerly winds and the advection marine air, which causes intense precipitation in the western part of Europe.

a)

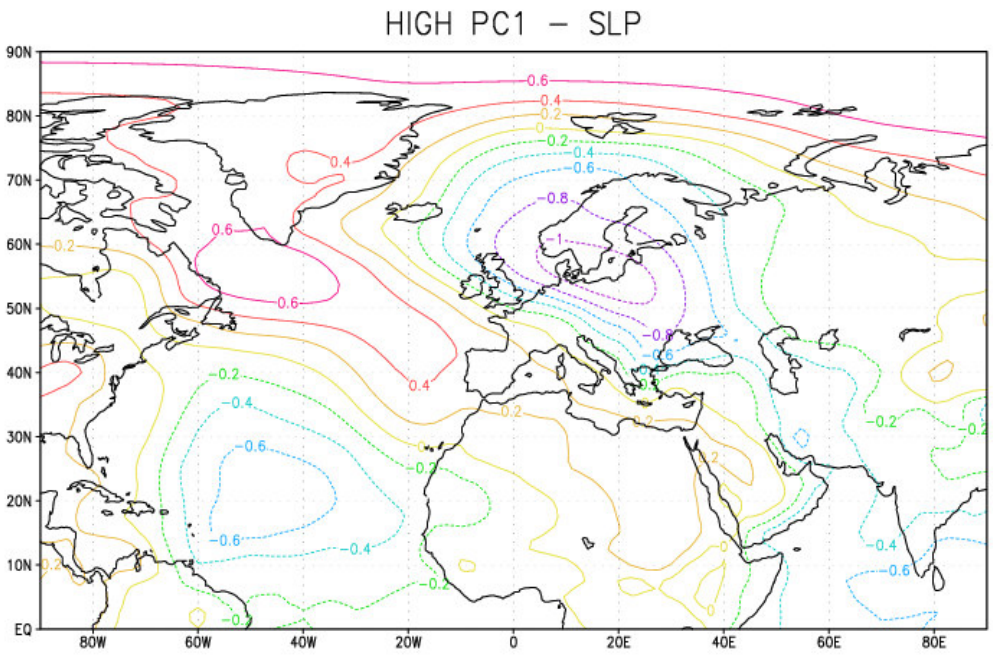

b)

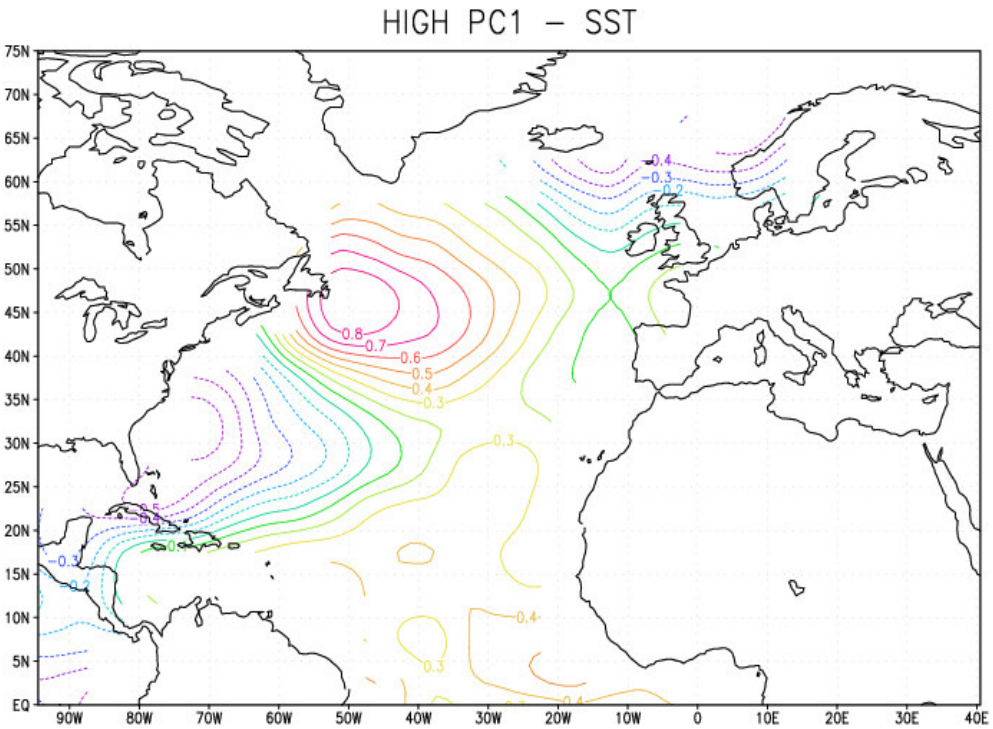

Figure 6.6 Composite map between PC1 (>-0.75) and (a) SLP, (b) SST. Units are hPa and K, respectively

To better assess the relationship between salinity variability in the Helgoland area and large-scale atmospheric circulation, we investigated the moisture transport in the North Atlantic regions for the years with PC1 > 0.75 and PC1 < -0.75 standard

deviation. Vector plots of the vertically integrated water vapour transport composites show that during years with PC1 < 0.75 (Figure 6.7.a) a significant reduction of the water vapour transport downstream the whole German Bight and a shift of the axis of water vapour transport north-west of the North Sea is obvious.

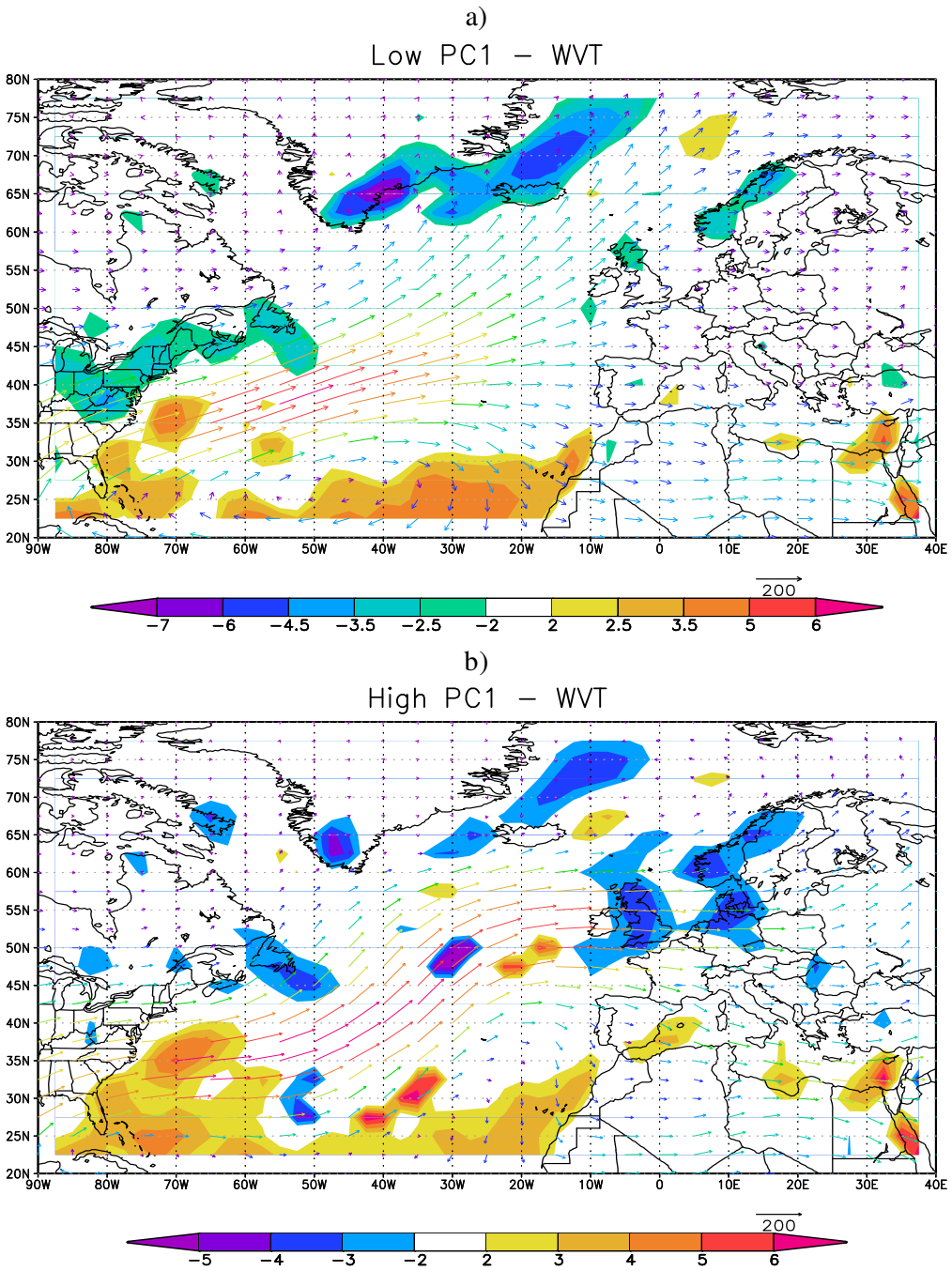

Figure 6.7 Composite maps of the vertically integrated water vapour transport for low (a) and high (b) values of PC1. Units are kg/(ms). The shaded areas indicate the distribution of the horizontal divergence of the total water vapour transport (units 10^{-6} kg/m^{2}s)

For the case when PC1 > 0.75 (Figure 6.7.b) the axis of maximum moisture transport is directed from the Atlantic to the German Bight, which causes high precipitation anomalies and low salinity anomalies over this region. An intense convergent zone can be found over the western part of Europe, including Elbe's river catchment area, which causes intense precipitation and low salinity. This convergent zone associated with the low pressure pattern identified in the SLP field, suppresses evaporation and induces intense precipitation and low salinity.

6.5 Summary and conclusions

In this study we investigated the relation between large-scale atmospheric circulation and variability of salinity and Elbe river discharge. The main features of our study can be summarized as follows. High salinities levels (low discharge anomalies) are associated with a tripole-like pattern in SLP and SST fields. The SLP pattern associated with positive salinity anomalies resemble the wave train identified by Hoskins and Ambrizzi (1993) in the North Atlantic jet stream. Positive anomalies of salinity (low discharge anomalies) are associated with an anticyclone pattern over Western Europe which causes reduced precipitation leading to higher salinity levels. Low salinity levels (high discharge anomalies) are associated with a cyclonic circulation over Western Europe which causes high precipitation. The SST pattern associated with high salinity anomalies (low discharge) has a tripole-like structure. Positive SST anomalies over northern tropical Atlantic are associated with negative SLP anomalies and anomalous lower cyclonic circulation over the subtropical latitudes that can be attributed to the weakening of the Hadley Cell circulation with suppressed ascending air over the equatorial region and descending air over the sub-tropics (Handoh et al., 2006).

The vertically integrated water vapour transport composites show that during years with high salinity anomalies (low discharge anomalies) there is a significant reduction of the moisture transport through the whole German Bight and a shift of the axis of moisture transport north-west of the North Sea and the European continent, which causes low precipitation over Western Europe. Low salinity anomalies are associated with an intense convergent zone over the western part of Europe, which induces high precipitation anomalies and suppresses evaporation.

Establishing a relationship between salinity variability, river discharge and large scale atmospheric circulation, might be a step forward in understanding the influence of climate on ecological parameters in the Helgoland area (i.e. nutrients), taking into account that most of these parameters are sensitive to changes in the salinity concentration and to the inputs from the Elbe river discharge (Nehring, 1994; Lindeboom et al., 1995; Fromentin and Planque, 1996).

Chapter 7

Conclusions and future perspectives

7.1 General summary

The objective of this study was to assess the variability and potential predictability of Elbe river streamflow and their relationship with global teleconnection patterns, from a synoptical scale and extending to decadal time scales. At the beginning of this thesis (Section 1.3) several questions have been raised and the answers to them were made throughout this study and will be summarized bellow.

How important are the seasonal fluctuations in flood frequency analysis? Are there special synoptic circulation patterns responsible for the occurrence of extreme events in Elbe catchemnt are? If yes, are these circulation patterns different from one season to another?

In the first part of this thesis the extreme events in the Elbe river catchment area and their associated main circulation patterns were analyzed on seasonal timescale. To identify the threshold, which defines an extreme event, and to fit the data to an extreme value distribution we have made use of the Peak over Threshold method associated with generalised Pareto distribution (GPD). It was found that the behaviour of Elbe daily streamflow is well statistically modelled by the GPD. The results indicate that for winter, spring and fall the times series have normal tail behaviour, meanwhile for summer the distribution has heavy-tail behaviour, summer being more exposed to the occurrence of extreme events compared to the other seasons. These findings were also confirmed by analyzing the Q-Q and P-P plots, which were almost linear for all seasons, indicating that the chosen model (GPD) fits well our data sets. Although summer is usually characterized by low flows in the case of Elbe river, the highest values for the 100 years return period were identified for this specific season. One explanation for these results might be that extreme events in summer are mostly associated with heavy rain episodes and the values of the discharge are growing rapidly, reaching very high values.
To identify which are the main circulation patterns responsible for triggering these extreme events we computed the composite maps of sea level pressure anomalies, corresponding to the days when the discharge was above the threshold, for every specific season. In winter most of the extreme discharge events are associated a dipole-like pattern with a strong negative centre over central Europe and extending over the southern part of the Atlantic Ocean and a strong positive centre over the northern part of the Atlantic Ocean. Such pattern favours a north-easterly circulation. In summer, extreme events are triggered by a blocking-like pattern over the Atlantic Ocean and a cyclonic circulation over the southern part of Europe, which carries humid air form the Baltic Sea over the northern part of Germany.

*Can we resolve the problem of non-stationarity by identifying **stable** predictors from several key regions, which can be used for the prediction of Elbe river streamflow?*

One of the most difficult issues of hydrology is how to appreciate the seasonal variability of rivers streamflow. The availability of water is greatly influenced by climate conditions that vary on seasonal, interannual to decadal time scales. On seasonal time scales, anomalous atmospheric conditions are often linked with seasonal variations in rivers streamflow, via variations in precipitation and temperature (Dettinger and Diaz, 2000; Cullen et al., 2002). Different teleconnection indices have been used as predictors for seasonal streamflow anomalies over Europe (Rimbu et al., 2005, Cullen et al, 2002, Trigo et al., 2004). However, the association between these teleconnection indices (e.g. NAO, ENSO) has proved to be non-stationary, i.e. the strength of the correlation between these two phenomena and streamflow anomalies has changed over time.
In the second part of this thesis a simple forecast scheme was developed, which is able to solve the problem of non-stationarity, by identifying stable predictors form key regions.
We show that during the period 1902-1971 the Elbe spring streamflow is stable correlated with previous winter PP anomalies from its catchment area, with TT anomalies from the Black Sea-Caspian Sea region, north-western Europe and northern Canada, as well as with SST anomalies from the tropical Pacific, the Indian Ocean and several regions of the North Pacific and the North Atlantic. Spring Elbe streamflow anomalies are related not only with regional winter climatic anomalies but also with climate anomalies from several key regions located far from Elbe region. Winter SST, TT and PP anomalies from several key regions provide a significant source of predictability for Elbe spring streamflow. Also a small, but significant potential predictability was detected for summer streamflow anomalies using previous spring SST, TT and PP anomalies from several key regions.
The correlation coefficient increases when we calculate the EOF using all the indices (SST+TT+PP), comparing to the case when we make the analysis separately on each of them.
Using this simple statistical model, it is shown that when climate indices from the key regions are used together, the forecast improves compared to the case when we used predefined teleconnection indices, like NAO and ENSO. The forecast scheme shows an improvement of about 20% when compared with climatology and persistence and major advantages than the forecast based on different predefined teleconnection patterns.

Is there any statistically significant relationship between different climatic variables (e.g. sea surface temperature, precipitation) and the seasonal to decadal variability of discharge anomalies?

Interannual to decadal variability of the atmosphere over the North Atlantic region is mainly influenced by NAO teleconnection pattern (Bjerkenss, 1964; Hurrell, 1995). On decadal time scales there are strong parallels between North Pacific temperature and NAO that reflect much coherence of the Northern Hemisphere climate (e.g. Livezey and Smith 1999). In the tropical Atlantic a cross-equatorial dipolar SST anomaly pattern with a period of 12-13 years has been identified (Allen and Smith,

1996; Mehta, 1998). River flow anomalies may be related to some of the same climatic oscillation that underlies those in SST.
The third part of this thesis aimed at find a connection between Elbe's river streamflow and large scale atmospheric circulation and SST, on decadal time scales. High values of PP throughout the river catchment area occur in connection with high values of Elbe flow. Elbe flow is highly positive correlated with a PP index defined as the average PP over Elbe's basin. On decadal time scale, high flow anomalies are also strongly correlated with winter TT over land. There is an out-of-phase relationship between Elbe flow and TT over Scandinavian region. High positive correlation is also found with the TT over the northern part of Canada. This pattern in the TT field is similar to the negative phase of the Arctic Oscillation.
The correlation map between Elbe river flow and SSTs shows that high flow anomalies tend to be associated with low SST anomalies in the central North Pacific and high SST anomalies in the eastern and central tropical Pacific. A tripole-like pattern in the SST files is also associated with high flow anomalies.
The quasi-periodic patterns of Elbe flow variability were also identified, by employing the SSA methodology. Long-term variability and detections of preferred periodic oscillatory pairs in the time series of river streamflow, may be of significant importance for water resources manages, for whom the ability to forecast water inflows is highly desirable. Two quasi-decadal variations of approximately 12 years and 20 years have been identified in the time series of Elbe river flow.

To which extent is Elbe river streamflow influencing the variability of salinity in the German Bight area?

The eastern German Bight is a zone of intensive mixing of two water bodies, the North Sea water and the coastal water which is of lower salinity and density. In addition, the water of the river Elbe leads to a strong inhomogeneity in this area which can be seen in the distribution of salinity and nutrients Goedecke (1968). The last part of this thesis focused to investigate the possible relationships between the large-scale atmospheric circulation, Elbe river streamflow and salinity at Helgoland Roads station. Establishing a relationship between salinity variability, river discharge and large scale atmospheric circulation, might be a step forward in understanding the influence of climate on ecological parameters in the Helgoland area (i.e. nutrients), taking into account that most of these parameters are sensitive to changes in the salinity concentration and to the inputs from the Elbe river discharge (Nehring, 1994; Lindeboom et al., 1995; Fromentin and Planque, 1996).
Based on this analysis it was found that high salinities levels (low discharge anomalies) are associated with a tripole-like pattern in SLP and SST fields. The SLP pattern has an anticyclonic centre over Western Europe which causes reduced precipitation leading to higher salinity levels. This SLP pattern resembles the wave train identified by Hoskins and Ambrizzi (1993) in the North Atlantic jet stream. There is also a significant reduction of the moisture transport through the whole German Bight and a shift of the axis of moisture transport north-west of the North Sea and the European continent, which causes low precipitation over Western Europe. Low salinity levels (high discharge anomalies) are associated with a cyclonic circulation over Western Europe which causes high precipitation. The SST pattern associated with high salinity anomalies (low discharge) has a tripole-like

structure. Positive SST anomalies over northern tropical Atlantic are associated with negative SLP anomalies and anomalous lower cyclonic circulation over the subtropical latitudes that can be attributed to the weakening of the Hadley Cell circulation with suppressed ascending air over the equatorial region and descending air over the sub-tropics (Handoh et al., 2006). Low salinity anomalies are also associated with an intense convergent zone over the western part of Europe, which induces high precipitation anomalies and suppresses evaporation.

7.2 Conclusions and outlook

The aim was of this thesis was to study the variability and potential predictability of Elbe river streamflow and their relationship with global teleconnections. Throughout chapters 3 to 6 it was shown that both atmosphere and ocean are valuable candidates in triggering the variability of river streamflow, starting from a synoptically point of view and ending with decadal time scales.

An important role in flood frequency analysis is to quantify and mitigate the risk of flooding that arises from the variability of extreme runoff and precipitation. Although seasonal fluctuations of these parameters are an important source of variability, the most used variable for this kind of analysis is the annual maximum (the highest value in the year). The seasonal information is most of the time overlooked, when considering and evaluating flood risk. For example the term "1 in 100 years flood" doesn't specify weather a given extreme value is more likely to come from one season over another (Leonard, 2008). One of the aims of this thesis was to deal with this problem and to model the behavior of Elbe river streamflow based on daily seasonal values. By applying the theory of extreme values it has been found that the most sensitive season to extreme events it is summer. One explanation for these results might be that extreme events in summer are mostly associated with heavy rain episodes (e.g. convective precipitation) and the values of the discharge are growing rapidly, reaching very high values in a very short period of time.
The circulation patterns associated with these extreme events were also analyzed. Again the influence of the seasonality has been emphasized, taking into account that the extreme events in Elbe's catchment area are triggered by different circulation patterns in every specific season.
One weak point of this analysis might have been the use of k-mean cluster analysis to identify the circulation patterns associated with the extreme events in Elbe's catchment area. Although the aim was not to find the best clustering methods and the optimal number of clusters, we have to take into account this problem when defining the number of clusters to split the data and the clustering methods employed. One way to resolve this problem will be to perform the same analysis using other clustering methods, such as SANDRA method (Philipp et al., 2006). Nevertheless, it is not necessary that other methods will perform better than k-means algorithm.
Also it will be useful to take into account more variables (e.g. geopotential height) to study the synoptic situations related to extreme discharge events. Another important issue which should be taken into account in further studies is the evolution of these extreme events under different climate change scenarios.
From a seasonal point of view is very important for water managers to be able to predict in advance the evolution of the streamflow anomalies. The forecast model

developed in this thesis is a simple statistical model which tries to eliminate the non-stationarity problems in forecasting based on predefined teleconnection indices. Although the skill of the forecast based on this model improved with about 20% when compared to climatology or persistence, to improve our definition of the model skill, more testing of the observed relationships could be performed. For example, we have calibrated our model for the period 1902-1970 and validate the skill of the model for the period 1979-2002. But how will the skill of the model change if we choose another calibration and validation period?

A further and logical step will be to test forecast scheme for other rivers that lie under different atmospheric and geomorphologic influences. The forecast scheme will be applied also to rivers with smaller catchment areas, in order to test the influence of the size of the catchment to the memory of the river. Also, new predictors will be tried (e.g. SLP, snow cover), to see if the forecast scheme improves much further.

The issue of predictability can be taken into account also when speaking about decadal time scales. This might be done by studying the variability of the streamflow on decadal time scales (> 7 years) and the relationship with different global teleconeections patterns and by identifying preferred periodic oscillatory pairs in the time series of the river streamflow. In this study we have shown that Elbe river streamflow is influenced by different atmospheric modes which are over imposed one over the other, but it is not yet clear which mode drives the other and which accounts for the highest variability in triggering the streamflow variability. Am improvement could be achieved by modeling studies with coupled GCMs, which could provide more information about the physical mechanism which drive the streamflow variability on decadal time scales.

Appendix A
Empirical Orthogonal Function Analysis

Empirical Orthogonal Function (EOF) analysis seeks structures that explain the maximum amount of variance in a two dimensional data set. One dimension in the data set represents the dimension in which we are seeking to find structure, and the other dimension represents the dimension in which realizations of this structure are sampled.

In seeking characteristic spatial structures that vary with time, for example, we would use space as the structure dimension and time as the sampling dimension. The analysis produces a set of structures in the first dimension, which we call the EOF's, and which we can think of as being the structures in the spatial dimension. The complementary set of structures in the sampling dimension (e.g. time) we can call the Principal Components (PC's), and they are related one-to-one to the EOF's. Both sets of structures are orthogonal in their own dimension. Sometimes it is helpful to sacrifice one or both of these orthogonalities to produce more compact or physically appealing structures, a process called rotation of EOF's.

The EOF analysis provides a convenient method for studying the spatial and temporal variability of time series which cover large areas. This method splits the temporal variance of the data into orthogonal spatial patterns called empirical eigenvectors.

This technique enables one to identify a set of orthogonal spatial modes, such that, when ordered, each successive eigenvector explains the maximum amount possible of the remaining variance in the data. Each eigenvector is associated with a series of time coefficients that describe the temporal evolution of the particular spatial mode. The eigenvector patterns that account for a large fraction of variance are, in general, considered to be physically meaningful and connected with the main centres of action.

Lets consider a climatological field *f(x,t)* defined simultaneously at *M* positions denoted as *x* with *N* observations at times *t*. This can be seen as an ensemble of *N* instantaneous observations of a scalar field *f(x,t)* defined at *M* stations.

We can assume that each sample *n* constitutes a map with *M* elements that can be organized in an *M* X 1 array of data represented by a column vector $\mathbf{f}_n$ (Peixoto and Oort, 1992):

$$(\mathbf{f}_n) = \begin{bmatrix} f_{1n} \\ f_{2n} \\ \cdot \\ \cdot \\ \cdot \\ f_{Mn} \end{bmatrix} \qquad \text{A.1}$$

where n=1,…,N. When we consider all N maps together, we obtain an array of N column vectors forming an M X N rectangular matrix. The matrix element f_{mn} represents the observation made at station m at time n.

The set of the N vectors can be represented in an M-dimensional linear vector space spanned by an arbitrary unit basis $\{\mathbf{u}_1, \mathbf{u}_2, ..., \mathbf{u}_M\}$. The N data vectors are

directed from the origin to a point in the *M* space. If there is some correlation between the *N* vectors we expect that the distribution of their extremities will be organized in clusters or along some preferred directions.

The problem that needs to be resolved is to find an orthogonal basis in the vector space $\{\mathbf{e}_1, \mathbf{e}_2, ..., \mathbf{e}_M\}$ instead of the original basis such that each vector $\mathbf{e}_m$ best represents the cluster of the original data vectors $\mathbf{f}_n$ with n=1,…,N. This is equivalent to finding a set of M vectors, $\mathbf{e}_m$, whose orientation is such that the sum of squares of the projection of all *N* observations vectors $\mathbf{f}_n$ onto each $\mathbf{e}_m$ is maximized sequentially. We assume that the vectors of the set $\{\mathbf{e}\}$ are mutually orthonormal so that by definition the inner product:

$$(\mathbf{e}_m \cdot \mathbf{e}_j) = \mathbf{e}_m^T \mathbf{e}_j = \begin{cases} 1 \text{ for } m = j \\ 0 \text{ for } m \neq j \end{cases},$$

where $\mathbf{e}_m^T$ is the transpose of $\mathbf{e}_m$. The set of vectors $\{\mathbf{e}\}$ are called the empirical orthogonal functions (EOF's). In mathematical terms this means that we have to maximize the expression:

$$\frac{1}{N}\sum_{n=1}^{N}[\mathbf{f}_n \cdot \mathbf{e}_m]^2 \qquad \text{A.2}$$

for m=1,2,…, M subject to the conditions:

$\mathbf{e}_m^T \mathbf{e}_m = 1$ and $\mathbf{e}_m^T \mathbf{e}_j = 0$ for all $j \neq m$. A.3

Expression A.2 can be written in matrix form:

$$\frac{1}{N}\sum_{n=1}^{N}[\mathbf{f}_n \cdot \mathbf{e}_m]^2 = \frac{1}{N}[\mathbf{e}_m^T \mathbf{F}\mathbf{F}^T \mathbf{e}_m] = \mathbf{e}_m^T \mathbf{R}\mathbf{e}_m \qquad \text{A.4}$$

where $\mathbf{R}$ is the matrix defined by $\mathbf{R} = \frac{1}{N}\mathbf{F}\mathbf{F}^T$. This is an *M* X *M* real symmetric matrix and is the covariance matrix of the data. Its elements are given by: $r_{mj} = \frac{1}{N}\sum_{n=1}^{N} f_{mn} f_{jn}$ and the diagonal elements are the variances $r_{mn} = \left(\sum_{n=1}^{N} f_{mn} f_{mn}\right) / N$.

The maximizing of $[\mathbf{e}_m^T \mathbf{R}\mathbf{e}_m]$ subject to the conditions A.3 constitutes a variational problem leading to an eigenvalue problem. Thus, we can obtain an equation of the form:

$$\mathbf{R}\mathbf{e}_m = \lambda_m \mathbf{e}_m$$

or

$$(\mathbf{R} - \lambda I)\,\mathbf{e}_m = 0 \qquad \text{A.5}$$

where the vector $\mathbf{e}_m$ is the characteristic vector associated with the characteristic value λ_m of the matrix $\mathbf{R}$, and *I* is the unit matrix of order *M*. The matrix $\mathbf{L} = \lambda I$ is a diagonal matrix with the eigenvalues λ_m as diagonal elements.

Equation A.5 leads to homogenous system of *M* linear equations of *M* unknows. This homogenous system possesses nontrivial solutions if and only if the determinant of the coefficients of the matrix $\mathbf{R} - \lambda I$ vanishes, i.e., if:

$$|\mathbf{R}-\lambda I| \equiv \begin{vmatrix} r_{11}-\lambda & r_{12} & \cdots & r_{1M} \\ r_{21} & r_{22}-\lambda & \cdots & r_{2M} \\ \cdots & \cdots & \cdots & \cdots \\ r_{M1} & r_{M2} & \cdots & r_{MM}-\lambda \end{vmatrix} = 0 \qquad \text{A.6}$$

This leads to an algebric equation of degree M in λ, known as characteristic equation of **R**. The M solutions $\lambda_1, \lambda_2, \ldots, \lambda_M$ are real and positive, because **R** is symmetric and positive definite. Since **R** is symmetric, its trace is invariant under a basis transformation and, thus, is equal to the sum of the eigenvalues $\sum_{m=1}^{M} r_{mm} = \sum_{m=1}^{M} \lambda_m$.

This means that each value λ_m explains a fraction of the total explained variance, i.e.,

$$\lambda_m \Big/ \sum_{i=1}^{M} \lambda_i \qquad \text{A.7}$$

For each value $\lambda_m (m = 1, \ldots, M)$ equation A.6 leads to a vector solution $\mathbf{e}_m$ which is the eigenvector associated with λ_m. Any two eigenvectors associated with different eigenvalues are orthonormal, so that the inverse of the matrix **E**, euqals the transpose. The eigenvalues in the **L** matrix are arranged in decreasing order of magnitude so that $\lambda_1 \geq \lambda_2 \geq \cdots \geq \lambda_M$. Thus, the first mode $\mathbf{e_1}$ associated with λ_1 explains the largest fraction of the total variance.

The set of M independent and mutually orthogonal eigenvectors, each scaled to have length 1, can be taken as an ordered orthonormal basis $\{\mathbf{e}_1, \mathbf{e}_2, \ldots, \mathbf{e}_M\}$ in the M-vector space. This gives theoptimum represenation of the set of the observation data vectors, $\mathbf{f}_n$.

Thus, any observation vector $\mathbf{f}_n$ can be expressed as a linear combination of the M eigenvectors, $\mathbf{e}_m$:

$$\mathbf{f}_n = \sum_{m=1}^{M} c_{mn} \mathbf{e}_m \qquad \text{A.8}$$

where the coefficients c_{mn} are the components or the projections of $\mathbf{f}_n$ on $\mathbf{e}_m$ $(m = 1, \ldots, M)$ so that:

$$c_{mn} = \mathbf{e}_m^T \mathbf{f}_n \qquad \text{A.9}$$

These coefficients represent the weight of a certain mode $\mathbf{e}_m$ in describing the observations $\mathbf{f}_n$. Furthermore, the coefficients c_{mn} are the elements of an M X N matrix **C**, such that:

$$\mathbf{C} = \mathbf{E}^T \mathbf{F} \qquad \text{A.10}$$

with

$$\mathbf{F} = \mathbf{E}\,\mathbf{C} \qquad \text{A.11}$$

Because the N refer to different times, the elements of a row vector $[c_{m1}, c_{m2}, \ldots, c_{mN}]$ give the values of the coefficients associated with a given eigenvector $\mathbf{e}_m$. It is important to note that the row vectors $\mathbf{c}_m$ are also mutually orthogonal. Noting that:

$$\sum_{n=1}^{N} \mathbf{f}_n \cdot \mathbf{f}_n = \sum_{n=1}^{N} \left(\sum_{m=1}^{M} c_{mn}\, \mathbf{e}_m \right) \left(\sum_{j=1}^{M} c_{jn}\, \mathbf{e}_j \right) = \sum_{m=1}^{M} \sum_{n=1}^{N} c_{mn}^2$$

and

$$\sum_{n=1}^{N} \mathbf{f}_n \cdot \mathbf{f}_n = N \sum_{m=1}^{M} \lambda_m$$

we find

$$N^{-1} \sum_{n=1}^{N} c_{mn}^2 = \lambda_m$$

Thus, the eigenvalues are the mean-square values of the expansion coefficients of the various modes. The magnitude of the correlations is described completely by the set (λ_m) of the eigenvalues.

Appendix B
Software

The statistical modelling of the extreme events in Chapter 3 have been performed with the statistical software R, which can be found at http://www.r-project.org

For the extreme value analysis the package extRemes by Eric Gilleland and Richard Katz has been applied. This package and more information can be found at http://www.isse.ucar.edu/extremevalues/evtk.html .

The composite and correlation maps in this thesis were made with The Grid Analysis and Display System (GrADS), which is an interactive desktop tool that is used for easy access, manipulation, and visualization of earth science data. More information about the software can be obtained from: http://www.iges.org/grads/.

Bibliography

Ansell, T.J., Jones, P.D., Allan, R.J., Lister, D. , Parker, D.E., Brunet, M., Moberg, A., Jacobeit, J., Brohan, P., Rayner, N.A., Aguilar, E., Alexandersson, H., Barriendos, M., Brandsma, T., Cox, N.J., Della-Marta, P.M., Drebs, A., Founda, D., Gerstengarbe, F., Hickey, K., Jónsson, T., Luterbacher, J., Nordli, Ø., Oesterle, H., Petrakis, M., Philipp, A., Rodwell, M.J., Saladie, O., Sigro, J., Slonosky, V., Srnec, L., Swail, V., García-Suárez, A.M., Tuomenvirta, H., Wang, X., Wanner, H., Werner, P., Wheeler, D. and Xoplaki, E. 2006. Daily Mean Sea Level Pressure Reconstructions for the European – North Atlantic Region for the Period 1950-2003, *J. Climate*, 19, 2717-2742.

Aebischer, N.J., Coulson, J.C. and Colebrook, J.M. 1990. Parallel long-term trends across four marine trophic levels and weather. *Nature,* 347, 753–755.

Allen, M.R. and Smith, L.A. 1996. Monte Carlo SSA: detecting irregular oscillations in the presence of coloured noise, *International Journal of Climatology,* 9**,** 3373–3404.

Arnell, N.W., Krasovskaia, I. and Gottschalk, L. 1993. River flow regimes in Europe. In *Flow Regimes from International Experimental and Network Data (FRIEND), vol. 1. Hydrological Studies*, Gustard A (ed.). Institute of Hydrology: Wallingford, Oxfordshire, UK, 112-121.

Arnell, N.W. 1995. Scenarios for hydrological climate change impact studies. In The Role of Water and the Hydrological Cycle in Global Change, Oliver HR, Oliver S (eds). NATO ASI Series 1, *Springer-Verlag: Berlin*, Heidelberg, vol. 31, 393–396.

Arnell, N.W. 1999. The effect of climate change on hydrological regimes in Europe: a continental perspective. *Global Environmental Change,* 9, 5–23.

Arnell, N.W. and Reynard, N.S. 1996. The effects of climate change due to global warming on river flows in Great Britain. *J. Hydrol.,* 183, 397–424.

Barnston, A.G. and Livezey, R.E. 1987. Classification, seasonality and persistence of low frequency atmospheric circulation patterns. *Mon. Wea. Rev.*, 115, 1083–1126.

Becker, G.A. and Pauly, M. 1996. Sea surface temperature changes in the North Sea and their causes, *ICES J. Mar. Sci.* 53, 887–898.

Bednorz, E. 2007. Synoptic reasons for heavy snowfalls in the Polish – German lowlands, *Theor. Appl. Climatol.*, 92, 133-140.

Bjerknes, J. 1964. Atlantic air-sea interactions. *Advances in Geophysics,* 10, 1-82.

Branković, C., Palmer, T.N. and Ferranti, L. 1994. Predictability of seasonal atmospheric variation. *J. Climate,* **7**, 217–237.

Brankovic, C. and Palmer, T. N. 2000. Seasonal skill and predictability of ECMWF PROVOST ensembles. *Q. J. R. Meteorol. Soc*., 126, 2035-2067.

Brönnimann, S. 2007. Impact of El Niño–Southern Oscillation on European climate. *Rev. Geophys.*, 45, RG3003, doi:10.1029/2006RG000199.

Brönnimann, S., Luterbacher, J., Staehelin, J., Svenby, T.M., Hansen, G. and Svenoe, T. 2004. Extreme climate of the global troposphere and stratosphere 1940-1942 related to El Nino. *Nature*, 431, 971-974.

Bronstert, A., Ghazi, A., Hladny, J., Kundzewicz, Z. and Menzel, L. 1998. The Odra/Oder flood in summer 1997 (Proc. European Expert Meeting, Potsdam, Germany, 18 May 1998). *PIK report,* 48, Potsdam, Germany.

Brunetti, M., Maugeri, M. and Nanni, T. 2002. Atmospheric circulation and precipitation in Italy for the last 50 years, *Int J Climatol*, 22(12), 1455–1471.

Cassou, C., Terray, L., Hurrell, J. W. and Deser, C. 2004. North Atlantic winter climate regimes: Spatial asymmetry, stationarity with time, and oceanic forcing. *J. Climate*, 17, 1055–1068.

Cassou, C., Terray, L. and Phillips, A. 2005. Tropical Atlantic influence on European heat waves, *J. Climate*, 18, 2805–2811.

Climate Prediction Centre (CPC). 2005. Northern hemisphere teleconnection patterns. (http://www.cpc.ncep.noaa.gov/data/teledoc/telecontents.shtml).

Coles, S. 2001. An Introduction to Statistical Modelling of Extreme Values. Springer Series in Statistics. Springer-Verlag. Berlin. Germany.

Colman, A. 1997. Prediction of summer Central England Temperature from preceding North Atlantic winter sea surface temperature. *Intl. J. Climatol.,* 17, 1285–1300.

Colman, A., and Davey, M. 1999. Prediction of summer temperature, precipitation and pressure in Europe from preceding winter North Atlantic Ocean temperature. *Intl. J. Climatol.*, 19, 513–536.

Corti, S., Molteni, F. and Palmer, T. N. 1999. Signature of recent climate change in frequencies of natural atmospheric circulation regimes, *Nature*, 398, 799–802.

Croley T.E. II and Luukkonen, C.L. 2003. Potential Effects of Climate Change on Ground Water in Lansing, Michigan, *Journal of the American Water Resources Association,* 39, 149-163.

Croley, T.E. II. 2003. Great Lakes climate change hydrologic impact assessment I.J.C. Lake Ontario-St. Lawrence River Regulation Study. NOAA Technical Memorandum GLERL, 126, 77 pp.

Cullen, H.M., Kaplan, A., Arkin, P. and DeMenocal, P.B. 2002. Impact of the North Atlantic Oscillation on Middle Eastern climate and streamflow. *Clim. Change*, 55, 315– 338.

Cushing, D.H. and Dickson, R.R. 1976. The biological response in the sea to climate change. *Adv. Mar. Biol.,* 14, 1–122

Dai, A.G., Fung, I.Y. and DelGenio, A.D. 1997. Surface observed global land precipitation variations during 1900-1988. *Journal of Climate,* 10, 2943-2962

Deser, C. and Blackmon, M.L. 1993. Surface Climate Variations over the North Atlantic Ocean during Winter: 1900-1989. *Journal of Climate,* 6, 1743-1753.

Deser, C. 2000. On the teleconnectivity of the "Arctic Oscillation". *Geophys. Res. Lett.*, 27 , 779–782

Dettinger, M.D., Cayan, D.R., McCabe, G.J. and Marengo, J.A. 2000. Multiscale streamflow variability associated with El Niño/Southern Oscillation, *El Niño and the Southern Oscillation-Multiscale Variability and Global and Regional Impacts*. Cambridge Univ. Press, 113-146.

Dettinger, M.D. and Diaz, H.F. 2000. Global characteristics of streamflow seasonality. *J. Hydrometeor.*, 1, 289– 310.

Dickson, R. R. 1971. A recurrent and persistent pressure-anomaly pattern as the principle cause of intermediatescale hydrographic variation in the European shelf-seas. *Dt. Hydrogr. Zt.*, 24, 97–119.

Dickson, R. R., Meincke, J., Malmberg, S.A. and Lee, A.J. 1988. The “Great salinity anomaly” in the Northern Atlantic 1968-1982, *Prog. Oceanog.,* 20, 103-151.

Dima, M., Rimbu, N., Stefan, S. and Dima, I. 2001a. Quasi-decadal variability in the Atlantic Basin involving tropics-midlatitudes and ocean–atmosphere interactions. *Journal of Climate,* 14, 823–832.

Dima, M., Stefan, S., Dima, V. and Borsan, D. 2001b. Interdecadal variability generated by interactions between Pacific and Atlantic Oceans, *Geophysical Research Letters,* 28, 4459-4461.

Dippner, J.W. 1997a. Recruitment success of different fish stocks in the North Sea in relation to climate variability. *Dtsch. Hydrogr. Zt.,* 49, 277–293.

Dippner, J.W., 1997b. A note on SST anomalies in the North Sea in relation to the North Atlantic Oscillation and the potential influence on the theoretical spawning time of fish. *Dt. Hydrogr. Zt.,* 49, 267–275.

Easterling, D.R., Evans, L.G., Grosiman, P.Y., Karl, T.R., Kunkel, K.E. and Ambenje, P. 2000. Observed variability and trends in extreme climate events: a brief review, *Bull Amer Meteor Soc*, 3, 417-425.

Eischeid, I.K., Bradley, R.S. and Shao, X. 1985. Secular climatic fluctuations in the Great Salt Lake basin. In *Problems and Prospects for of Prediction Great Salt Lake Le6els*, Kay P, Diaz HF (eds). Center for Public Affairs and Administration, University of Utah:Salt Lake City, UT; 111–122.

Ekström, M., Fowler, H.J., Kilsby, C.G. and Jones, P.D. 2005. New estimates of future changes in extreme rainfall across the UK using regional climate model integrations. 2, Future estimates and use in impact studies, *J Hydrol*, 300, 234-251.

European Environment Agency, 2003. Mapping the impacts of recent natural disasters and technological accidents in Europe, Environmental issue report No 35, EEA, Copenhagen

Fischer, E. M., Seneviratne, S. I., Lüthi, D. and Schär, C. 2007. Contribution of land-atmosphere coupling to recent European summer heat waves, *Geophys. Res. Lett.*, 34, L06707, doi:10.1029/2006GL029068.

Fragoso, M. and Tildes Gomes, P. 2008. Classification of daily abundant rainfall patterns and associated large-scale atmospheric circulation types in Southern Portugal, *International Journal of Climatology*, 28 (4), 537-544, DOI: 10.1002/joc.1564.

Fromentin, J.M. and Planque, B. 1996. *Calanus* and environment in the eastern North Atlantic. II. Influence of the North Atlantic Oscillation on *C. finmarchicus* and *C. helgolandicus*. *Mar. Ecol. Prog. Ser.,* 134,111–118.

Ghil, M. and Mo, K. 1991. Intraseasonal oscillations in the global atmosphere. Part 1: Northern Hemisphere and tropics. *Journal of Atmospheric Science,* 48, 752–779.

Ghil, M. and Vautard, R. 1991. Interdecadal oscillations and the warming trend in global temperature time series. *Nature,* 350, 324–327.

Goedecke, E. 1968. Über die hydrographische Struktur der Deutschen Bucht im Hinblick auf die Verschmutzung in der Konvergenzzone. Helgoländer wissenschaftliche Meeresuntersuchungen, 17**,** 108–125 (in German).

Gong, D.Y., Pan, Y.Z. and Wang, J.A. 2004. Changes in extreme daily temperatures in summer in eastern Chinan during 1955-2000, *Theor. Appl. Climatol.,* 77, 25-37.

Goodess, C.M. and P.D. Jones, 2002. Links between circulation and changes in the characteristics of Iberian rainfall. *Intl. J. Climatol.*, 22, 1593-1615.

Graham, N.E. 1994. Decadal-scale climate variability in the 1970s and 1980s: observations and model results. *Climate Dynamics*, 10, 135-159.

Grantz, K., Rajagopalan, B., Clark, M. and Zagona, E. 2005 A technique for incorporating large-scale climate information in basin-scale ensemble streamflow forecasts, *Water Resour. Res.*, 41, W10410, doi:10.1029/2004WR003467

Guetter, A.K. and Georgakakos, K.P. 1993. River outflow of the conterminous United States, 1939–1988. *Bulletin of the American Meteorological Society,* 74, 1873–1891.

Gumbel, E. J. 1960. Distributions des Valeurs Extremes en Plusiers Dimensions. *Publications de L'lnstitute de Statistique*, 9, 171–173.

Handoh, I.C., Matthews, A.J., Bigg, G.R. and Stevens, D.P. 2006. Interannual variability of the tropical Atlantic independent of and associated with ENSO: Part I. The North Tropical Atlantic. *International Journal of Climatology,* 26**,** 1937-1956.

Hartigan, J. A. and Wong, M. A. 1979. A K-means clustering algorithm., *Appl. Statist.*, 28, 100–108.

Heyen, H. and Dippner, J. W. 1998. Salinity in the southern German Bight estimated from large-scale climate data. *Tellus,* 50A**,** 545–556.

Hickel, W. 1998. Temporal variability of micro and nanoplankton in the German Bight in relation to hydrographic structure and nutrient changes. *ICES J. Mar. Sci.,* **19**, 600-609.

Hickel, W., Mangelsdorf, P. and Berg, J. 1993. The human impact on the German Bight: Eutrophication during three decades (1962–1991). *Helgoländer Meeresunters,* 47, 243–263.

Hoskins, B. J. and Ambrizzi, T. 1993. Rossby wave propagation on a realistic longitudinally varying flow. *J. Atmos. Sci*., 54, 1661–1671.

Hughes, D.A., 2004. Incorporating groundwater recharge and discharge functions into an existing monthly rainfall- runoff model. Hydrological Sciences-Journal- des Sciences Hydrologiques, 49(2), 297-311.

Hurrell, J.W. 1995. Decadal trends in the North Atlantic oscillation: regional temperatures and precipitation. *Science,* 269, 676-679.

Hurrell, J.W and van Loon, H. 1997. Decadal variations in climate associated with the North Atlantic oscillation. *Climatic Change,* 36, 301-306.

Hurrell, J.W. 2003. *The North Atlantic Oscillation: Climatic significance and environmental effect*. EOS 84, No. 8, 25 February 2003, 73.

IPCC, 2007: *Climate Change 2007: The Physical Science Basis. Contribution of Working Group I to the Fourth Assessment Report of the Intergovernmental Panel on Climate Change* [Solomon, S., D. Qin, M. Manning, Z. Chen, M. Marquis, K.B. Averyt, M.Tignor and H.L. Miller (eds.)]. Cambridge University Press, Cambridge, United Kingdom and New York, NY, USA.

Jacobeit, J., Glaser, R., Luterbacher, J. and Wanner, H. 2003. Links between flood events in Central Europe since AD 1500 and large-scale atmospheric circulation modes, *Geophys. Res. Lett.*, 30, 1172-1175, DOI 10.1029/2002GLO16433.

Jacobeit, J., Philipp, A. and Nonnenmacher, M. 2006. Atmospheric circulation dynamics linked with prominent discharge events in Central Europe, *Hydrological Sciences Journal*, 51, 946-965.

Jones, P.D., T. Jonsson, and D. Wheeler, 1997. Extension to the North Atlantic Oscillation using early instrumental pressure observations from Gibraltar and South-West Iceland. *Intl. J. Climatol.*, 17, 1433– 1450.

Kalnay, E., Kanamitsu, M., Kistler, R., Collins, W., Deaven, D., Gandin, L., Iredell, M., Saha, S., White, G., Woollen, J., Zhu, Y., Chelliah, M., Ebisuzaki, W., Higgins, W., Janowiak, J., Mo, K. C., Ropelewski, C., Wang, J., Leetmaa, A., Reynolds, R., Jenne, R. and Joseph, D.1996. The NMC/NCAR 40-Year Reanalysis Project. *Bull. Amer. Meteor. Soc.* **77**, 437-471.

Kaplan, A., Cane, M.A., Kushnir, Y., Clement, A.C., Blumenthal, M.B. and Rajagopolan, B. 1998. Analysis of global sea surface temperature 1856-1991, *Journal of Geophysical Research,* 103, 567-589.

Kaplan, A., Kushnir, Y. and Kane, M.A. 2000. Reduced Space Optimal Interpolation of Historical Marine Sea Level Pressure: 1854-1992. Journal of Climate, 13(16), 2987-3002.

Katz, R., Parlange, M. and Naveau, P. 2002. Statistics of extremes in hydrology, *Adv. Water Res.*, 25, 1287–1304.

Kiladis, G.N. and Diaz, H.F. 1989. Global climatic anomalies associated with extremes in the Southern Oscillation. *J. Climate,* 2, 1069–1090.

Kingston, D. G., McGregor, G. R., Hannah, D. M. and Lawler, D. M. 2006. River flow teleconnections across the northern North Atlantic region, *Geophys. Res. Lett.*, 33, L14705, doi:10.1029/2006GL026574.

Klemes, V. 2000. Tall tales about tales of hydrological distribution, *J. Hydrol. Eng*., 5(3), 227–239.

Knippertz, P., U. Ulbrich, F. Marques, and Corte-Real, J. 2003. Decadal changes in the link between El Niño and spring North Atlantic oscillation and European-North African rainfall. *Intl. J. Climatol.*, 23, 1293– 1311.

Knox, J.C. 2000. Sensitivity of modern and Holocene floods to climate change, *Quatern. Science Rev.*, 19, 439-457.

Kushnir, Y. 1994. Interdecadal variations in the North Atlantic sea surface temperature and associated atmospheric conditions. *Journal of Climate,* **7**, 141-157

Kyselý, J. and Beranová, R. 2008. Climate change effects on extreme precipitation in central Europe: uncertainties of scenarios based on regional climate models, *Theoretical and Applied Climatology*, doi: 10.1007/s00704-008-0014-8 (in press).

Latif, M., Arpe, K. and Roeckner, E. 2000. Oceanic control of decadal North Atlantic sea level pressure variability in winter. *Geophysical Research Letters,* 27, 727-730.

Leonard, M., Metcalfe, A. and Lambert, M. 2008. Frequency analysis of rainfall and streamflow extremes accounting for seasonal and climatic partitions, *Journal of Hydrology*, **348**, 135-147.

Lindeboom, H., van Raaphorst, W., Beukema, J., Cadebae, G. and Swennen, C. 1995. Sudden changes in the North Sea and Wadden Sea: Oceanic influences underestimated? *Dt. Hdrogr. Zt.* (suppl. 2), 87–100.

Livezey, R.E. and Smith, T.M. 1999. Covariability of aspects of North American climate with global sea surface temperatures on interannual to interdecadal timescales. *Journal of Climate,* 12, 289-302.

Lloyd-Hughes, B. and Saunders, M.A. 2002. Seasonal prediction of European spring precipitation from ENSO and local sea surface temperatures. *Intl. J. Climatol.,* 22**,** 1–14.

Lohmann, G., Rimbu, N. and Dima, M. 2005. Where can the Arctic Oscillation be reconstructed? Towards a reconstruction of climate modes based on stable teleconnections. *Clim. Past Disc*., 1, 17–56.

Mann, M.E., Lall, U. and Saltzman, B. 1995. Decadal-to-centennial-scale climate variability: insights into the rise and fall of the Great Salt Lake. *Geophysical Research Letters,* 22, 937–940.

Mann, M.E. and Park, J. 1994. Global-scale modes of surface temperature variability on interannual to century timescales. *Journal of Geophysical Research,* 99, 25819–25833.

Mantua, N.J., Hare, S.J., Zhang, Y., Wallace, J.M. and Francis, R.C. 1997. A Pacific interdecadal climate oscillation with impacts on salmon production. *Bulletin of the American Meteorological Society,* 78, 1069-1079.

Marengo, J.A. 1992. Interannual variability of surface climate in the Amazon basin. *Intl. J. Climatol.,* 12, 853–863.

Mares, C., Mares, I. and Stanciu, A., 2008. Extreme value analysis in the Danube lower basin discharge time series in the 20th century, *Theoretical and Applied Climatology*, doi: 10.1007/s00704-008-0001-0 (in press).

Mariotti, A., N. Zeng, and Lau, K.M. 2002. Euro-Mediterranean rainfall and ENSO - A seasonally varying relationship. *Geophys. Res. Lett.*, 29(12), 1621, doi:10.1029/2001GL014248.

Martin, M.L., Luna M.Y., Morata A. and Valero F. 2004. North Atlantic teleconnection patterns of low-frequency variability and their links with springtime precipitation in the western Mediterranean. *Intl. J. Climatol.*, 24, 213-230.

Maurer, E. P., Lettenmaier, D. P. and Mantua, N. J. 2004. Variability and potential sources of predictability of North American runoff, *Water Resour. Res.*, 40, W09306, doi:10.1029/2003WR002789

Maurer, E.P. and Lettenmaier, D.P. 2003. Predictability of seasonal runoff in the Mississippi River basin, *J. Geophys. Res.* 108 (D16) 8607 doi:10.1029/2002JD002555

McCabe, G.J. and Dettinger, M.D. 2002. Primary modes and predictability of year-to-year snowpack variation n the Western United States from teleconnections with Pacific Ocean Climate. *J. Hydrometeor.*, 3, 13-25.

Mehta, V. 1998. Variability of the tropical ocean surface temperatures at decadal–multidecadal timescales. Part I: The Atlantic Ocean. *Journal of Climate,* 11, 2351–2375

Merkel, U. and Latif, M. 2002. A high resolution AGCM study of El Niño impact on the North Atlantic/European sector. *Geophys. Res. Lett.*, 29(9), doi: 10.1029/2001GL013726

Michelangeli, P. A., Vautard, R. and Legras, B. 1995. Weather regimes: Recurrence and quasi stationarity, *J. Atmos. Sci.*, 52, 1237–1256.

Mitchell, T.D., Carter, T.R., Jones, P.D., Hulme, M. and New, M. 2003. A comprehensive set of high-resolution grids of monthly climate for Europe and the globe: The observed record (1901-2000) and 16 scenarios (2001-2100). *Tyndall Center Working Paper*, 55

Mudelsee, M., Börngen, M., Tetzlaff, G. and Grünewald, U. 2003. No upward trends in the occurrence of extreme floods in central Europe, *Nature*, 425, 166–169.

Naveau, P., Nogaj, M., Amman, C., Yiou, P., Cooley, D. and Jomelli, V. 2005. Statisctical methods for the analysis of climate extremes, *C.R. Geosci*, 337**,** 1013-1022.

Nehring, S. 1994. Gymnodinium catenatum Graham (Dinophyceae) in Europe: A growing problem?. *J. Plankton Res.,* 17, 85–102.

Palutikof, J.P., Barbson, B.B., Lister, D.H. and Adcock, S.T. 1999. A review of methods to calculate extreme wind speeds, *Meteorol. Appl.,* 6, 119–132.

Peixoto, J. P., and Oort, A. H. 1992. Physics of Climate, 520 pp., Springer, New York.

Philipp, A., Della-Marta, P.M. , Jacobeit, J., Fereday, D.R., Jones, P.D., Moberg, A. and Wanner, H. 2007. Long-Term Variability of Daily North Atlantic–European Pressure Patterns since 1850 Classified by Simulated Annealing Clustering. *J. Climate*, 20, 4065–4095.

Pickands, J., 1975. Statistical inference using extreme order statistics. *Annals of Statistics,* 3, pp. 119–131.

Pitman, W.V., 1973. A mathematical model for generating river flows from meteorological data in South Africa. Report no. 2/73, Hydrological Research Unit, University of the Witwatersrand, Johannesburg, South Africa.

Power, S., Casey, T., Folland, C., Colman, A. and Mehta, V. 1999. Inter-decadal modulation of the impact of ENSO on Australia. *Climate Dyn.,* 15**,** 319–324.

Plaut, G. and Vautard, R. 1994. Spells of low-frequency oscillations and weather regimes in the Northern Hemisphere. *Journal of Atmospheric Science,* 51, 210–236.

Pozo-Vázquez, D., Gamiz-Fortis, S.R., Tovar-Pescador, J., Esteban-Parra, M.J. and Castro-Diez, Y. 2005. El Niño-Southern Oscillation events and associated European winter precipitation anomalies. *Intl. J. Climatol.,* 25, 17–31.

Quadrelli, R. and Wallace, J. M. 2004. A simplified linear framework for interpreting patterns of Northern Hemisphere wintertime climate variability, *J. Clim.*, 17, 3728–3744

Rajagopalan, B., Kushnir, Y. and Tourre, Y.M. 1998. Observed decadal midlatitude and tropical Atlantic climate variability, *Geophysical Research Letters*, 25, 3967-3970

Rimbu, N., Boroneant, C., Buta, C. and Dima, M. 2002. Decadal variability of the Danube river flow in the lower basin and its relation with the North Atlantic Oscillation. *International Journal of Climatology*, 22, 1169-1179.

Rimbu, N., Dima, M., Lohmann, G. and Musat, I. 2005. Seasonal prediction of Danube flow variability based on stable teleconnection with sea surface temperature. *Geophys. Res. Lett.*, 32, L21704, doi:10.1029/2005GL024241.

Rimbu, N., Dima, M., Lohmann, G. and Stefan, S. 2004. Impacts on the North Atlantic Oscillation and the El Niño-Southern Oscillation on Danube river flow variability. *Geophys. Res. Lett.,* 31, L23203, doi:10.1029/2004GL020559.

Rodríguez-Puebla, C., Encinas, A.H. and Sáenz, J. 2001. Winter precipitation over the Iberian peninsula and its relationships to circulation indices. *Hydrology and Earth System Sciences,* 5, 233-244.

Ronchail, J., Cochonneau, G., Molinier, M., Guyot, J. L., Gorreti, A., Guimarães, V. andDe Oliveira, E. 2002. Interannual rainfall variability in the Amazon Basin and sea surface temperatures in the equatorial Pacific and the tropical Atlantic Oceans. *Int. J. Climatol*., 22**,** 1663–1686.

Russel, F.S. 1973. A summary of the observations on the occurrence of planktonic stages of fish off Plymouth 1924-1972. *Journal of the Marine Biological Association of the United Kingdom,* 53, 347-355.

Russel, F.S., Southward, A.J., Boalch, G.T. and Butler, E.I. 1971. Changes in biological conditions in the English Channel off Plymouth during the last half century. *Nature,* 234, 468-470.

Salinger, M.J., Renwick, J.A. and Mullan, A.B. 2001. Interdecadal Pacific Oscillation and South Pacific Climate. *International Journal of Climatology* 21, 1705–1721.

Schott, F. 1966. Der Oberflächensalzgehalt in der Nordsee. *Dt. Hydrogr. Zt.* (suppl. A9),1–58.

Shorthouse, C., Arnell, N.W. 1997. Spatial and temporal variability in European river flows and the North Atlantic oscillation. In *FRIEND'97 - Regional Hydrology: Concepts and Models for Sustainable Water Resource Management*, Gustard A , Blazkova S , Brilly M , Demuth S , Dixon J , van Lanen H , Llasat C , Mkhandi S , Servat E (eds). *IAHS Publication* No. 246. IAHS: Walling Ford, 77-85.

Slonosky., V.C., Jones, P.D. and Davies, T.D. 2001. Atmospheric circulation and surface temperature in Europe from the 18th century to 1995. *Int. J. Climatol*., 21, 63-75.

Smith, R.L. 2003. Statistics of extremes, with applications in environment, insurance and finance. Chapter 1 of *Extreme Values in Finance, Telecommunications and the Environment*, edited by B. Finkenstadt and H. Rootzen, Chapman and Hall/CRC Press, London, pp. 1-78.

Sobolowski, S., Gong, G. and Ting, M. 2007. Northern Hemisphere winter climate variability: Response to North American snow cover anomalies and orography. *Geophys. Res. Lett.*, 34, L16825, doi:10.1029/2007GL030573.

Souza, F. and Lall, U. 2003: Seasonal to interannual ensemble streamflow forecasts for Ceara, Brazil: applications of a multivariate, semiparametric algorithm. *Water Resour. Res.,* 39, 1–13.

Stanciu, P., Nedelcu, G. and Nicula, G. 2005. Hazardurile hidrologice din Romania. *Natural and anthropogenic hazards*, 5(23),11-17.

Starr, V. and Peixoto, J. 1958. On the global water vapour and the hydrology o deserts. *Tellus,* 10, 189-194.

Sutton, R.T., Jewson, S.P. and Rowell, D.P. 2000. The elements of climate variability in the tropical Atlantic region. *Journal of Climate,* 13, 3261-3284.

Tallaksen, L.M., 1995. A review of baseflow recession analysis. Journal of Hydrology,165, 349-370.

Thompson, D.W.J. and Wallace, J.M. 2000. Annular modes in the extratropical circulation. Part I: Month-to-month variability. *Journal of Climate,* 13, 1000-1016.

Tourre, Y. M., Kushnir, M. and White, W. B. 2001. Patterns of coherent decadal and interdecadal climate signals in the Pacific basin during the 20th century. *Geophys. Res. Lett.*, 28, 2069–2072.

Trenberth, K.E. 1990. Recent interdecadal climate changes observed in the Northern Hemisphere. *Bulletin of the American Meteorological Society,* 71, 988–993.

Trenberth, K.E. and Hurrell, J.W. 1994: Decadal atmosphere-ocean variations in the Pacific. Clim. Dyn., 9, 303-319.

Trenberth, K. E. and Paolino, D. A. 1980. The Northern Hemisphere sea-level pressure data set: Trends, errors and discontinuities. *Mon. Wea. Rev.,* 108, 855-872.

Trenberth, K. E., Hurrell, J. W. and Stepaniak, D. P. 2005b. The Asian Monsoon: Global Perspectives. Chapter 2 of "Asian Monsoon" B. Wang (Ed.) Praxis publishing Ltd. pp 67-87 and color section 9-19. ISBN 35040406107.

Trigo, R.M. 2006. Relations between variability in the Mediterranean region and mid-latitude variability. In *Mediterranean Climate Variability; Developments in Earth & Environmental Sciences* 4, Elsevier, pp 179-226.

Trigo, R.M., Pozo-Vázquez, D., Osborn, T.J., Castro-Diez, Y., Gamiz-Fortis, S. and Esteban-Parra, M.J. 2004. North Atlantic Oscillation influence on precipitation, river flow and water resources in the Iberian Peninsula. *Int. J. Climatol*., 24, 925–944.

Ulbrich, U., Brücher, T., Fink, A.H., Leckebusch, G.C., Krüger, A. and Pinto, J.G. 2003b. The central European floods of August 2002: Part 2 – Synoptic causes and considerations with respect to climatic changes, *Weather*, 58(10), 434-441.

Ulbrich, U., Brücher, T., Fink, A.H., Leckebusch, G.C., Krüger, A. and Pinto, J.G. 2003a. The central European floods of August 2002: Part 1 – Rainfall periods and flood development, *Weather*, 58(10), 371-377.

Van Loon, H. and Rogers, J.C. 1978. The seesaw in winter temperatures between Greenland and Northern Europe. Part I: general description. *Monthly Weather Review,* 106, 296-310.

Van Loon, H. and Madden, R. 1981. The Southern Oscillation. Part I: Global associations with pressure and temperature in northern winter. *Mon. Wea. Rev.,* 109, 1150–1162.

Van Oldenborgh, G.J., Burgers, G. and Klein Tank, A. 2000. On the El Niño teleconnection to spring precipitation in Europe. *Int. J. Climatol*., 20, 565–574.

Vautard, R., Yiou, P. and Ghil, M. 1992. Singular-spectrum analysis: A toolkit for short, noisy chaotic signals. *Physica D,* 58, 95–126.

von Storch, H. and Zwiers, F. W. 1999. Statistical Analysis in Climate Research, 494 pp., *Cambridge Univ. Press*, New York.

Wallace, J. M., and Gutzler, D. S. 1981. Teleconnections in the geopotential height field during the Northern Hemisphere winter. *Mon. Wea. Rev*., 109, 784-812.

Wang, W. 2006. Stochasticity, Nonlinearity and Forecasting of Streamflow Processes PhD Thesis. Hohai University.

Wang, W., van Gelder, P.H.A.J.M., Vrijling, J.K., and Ma, J. 2004. Predictability of streamflow processes of the Yellow River. *In: Proceedings of the 6th International Conference on Hydroinformatics*. Singapore : World Scientific, pp.1261-1268.

Wibig, J. 1999. Precipitation in Europe in relation to circulation patterns at the 500 hPa level, *Int. J. Climatol.*, 19, 253-269.

Wilby, R.L., 2001. Downscaling summer rainfall in the UK from North Atlantic Ocean temperatures. *Hydrology and Earth Systems Sciences,* 5, 245–257.

Wilks, D.S., 1995. Statistical Methods in the Atmospheric Sciences. *International Geophysics Series*, 59, Academic Press, San Diego, pp. 464.

Yiou, P. and Nogaj, M. 2004. Extreme climatic events and weather regimes over the North Atlantic: When and where?, *Geophys. Res. Lett.*, 31, L07202, doi:10.1029/2003GL019119

Yiou, P., Ribereau, P., Naveau, P., Nogaj, M. and Brazdil, R. 2006. Statistical analysis of floods in Bohemia (Czech Republic) since 1825, *Hydrol. Sci. J.*, 51, 930–945.

Yiou, P., Goubanova, K., Li, Z. X. and Nogaj, M. 2008. Weather regime dependence of extreme value statistics for summer temperature and precipitation, *Nonlin. Processes Geophys.*, 15, 365-378.

Acknowledgements

First and most sincerely I want to give my most gratefulness to my PhD advisor Prof. Dr. Gerrit Lohmann, for his continuous support, valuable guidance throughout my PhD study period and his expert advice.

Many thanks to Dr. Norel Rimbu for his advices, struggling times and support and for his willingness to review my thesis. My discussions with Dr. Rimbu were very helpful in deciding the final topic of my thesis. I am also grateful to Dr. Mihai Dima for encouraging me to follow my ideas, for believing in me and for the fruitful discussions we had.

I want to thank Deutscher Akademischer Austausch Dienst (DAAD) for providing the funding and support for this study. I am very grateful that I had the pleasure to be a PhD student at Alfred Wegener Institute, which gave me the opportunity to work independently on my own research ideas and to attend many interesting conferences and summer schools.

Many thanks to Andrea for correcting my english mistakes, both for my thesis and my articles. Thanks are also due to my colleague Axel for the fruitful discussion we had and for accepting to be in my thesis Committee. I am also grateful to Dr. Martin Werner for his willingness to read my thesis and for the comments and suggestions he made.

I am very grateful to Dr. Constanta Boroneant, Prof. Dr. Sabina Stefan, Dr. Liana Cazacioc and Dr. Aristita Busuioc for introducing me to the topic of climate research, helping me with their advices and sharing their knowledge. My sincerely gratitude to my physics teacher, Prof. Ecaterina Benedict, for introducing to the topic of physics and for encouraging me to follow this path.

Many thanks to my beloved friends, in particular Elena, Claudia and Florinela, for their constant encouragement and for the good times we had.

This thesis would have never been completed without the continuous moral support, patience and love of my parents, my sister, Silvia and Patrick. This PhD thesis is dedicated to them.